Self-Assembled Monolayers Protecting Metal Nanoparticles

3-D SAMs

Outline

- **Introduction to nanoparticles**
- **Monolayer-Protectected Metal nanoparticles**
  synthesis, characterizations
  properties and packing of the monolayer
- **Functional Nanoparticles**
  Methods of synthesis. Mixed-monolayers
  Monovalent- and divalent metal nanoparicles
- **Nanoparticles of different size and shape**
- **Applications of nanoparticles in different fields**

NANOPARTICLES

books

Colloidal Gold. Principles. Methods, and Applications
M. A. Hayat, 3 volumi, Academic Press, 1989

Nanoparticles. From Theory to Application Edited by Günter Schmid
Wiley-VCH, 2004

Metal Nanoparticles: Synthesis, Characterization, and Applications.
Edited by D. L. Feldheim and C. A. Foss; M. Dekker, Inc., 2002.

reviews

Self-Assembled Monolayers of Thiolates on Metals as a Form of Nanotechnology
J. C. Love, L. A. Estroff, J. K. Kriebel, R. G. Nuzzo, G. M. Whitesides, *Chem. Rev.* **2005**, *105*, 1103.

Large Clusters and Colloids. Metals in the Embryonic State
G. Schmid, *Chem. Rev.* **1992**, *92*, 1709.

Chemistry Change with Size
C. N. R. Rao, G. U. Kulkarni, P. J. Thomas, P. P. Edwards, *Chem. Eur. J.* **2002**, *8*, 29.

On the development of colloidal nanoparticles towards multifunctional structures and their possible use for biological applications
T. Pellegrino, S. Kudera, T. Liedl, A. Muñoz Javier, L. Manna, W. J. Parak, *Small*, **2005**, *1*, 48.

…….and thousands of papers

NANOPARTICLES

publications on nanoparticles

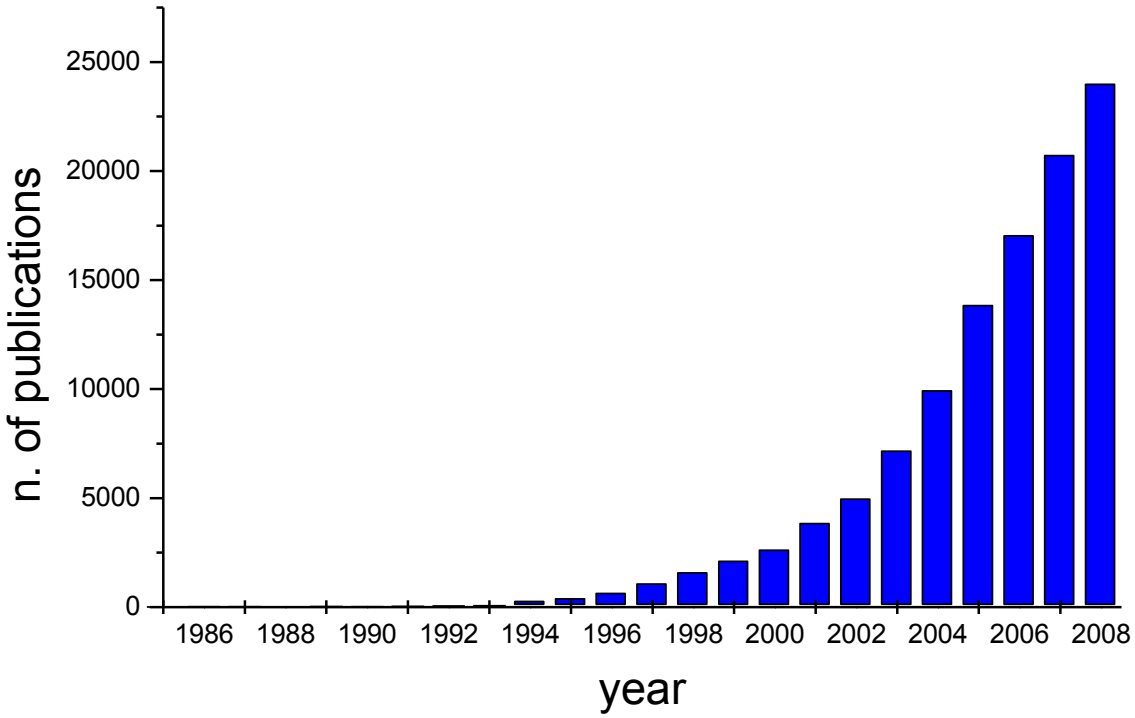

A brief historical background

- gold nanoparticles are known since ancient time, 5º - 4º millenium B.C. (China, Egypt). We believe that ancient Egyptian known how to prepare "soluble" gold and they were used these solutions as "elisir".

- colloidal gold sols are used to obtain red glass

- around 1600 Paracelso (1493-1541) described the preparation of "aurum potable, oleum auri: quinta essentia auri" by reduction of acid tetrachloroauric using an alcoholic extract of plants.

  At that time medical doctors believed that "drinkable gold" exert curative properties for several diseases.

A brief historical background

The roman industry of IV century A.D., developed a sophisticated use of metal NPs, they were able to produce colored glass with particular optical properties.
For example the addition of Ag and Au compounds, enable to produce glass which appear to be green under reflected light and red under trasmitted light.
The famous "Licurgus cup" has been realized with this technique.

day light (reflected light) trasmitted light

40 ppm of Au and 300 ppm of Ag

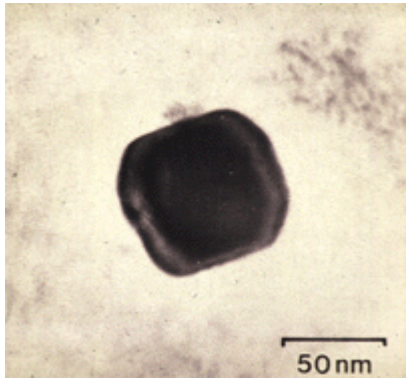

TEM image

Nanoparticles - hystorical background

- in 1857 Michael Faraday reported the first scientific studies on preparations of colloidal gold solutions, M. Faraday, *Phil.Trans.Roy. Soc.* **1857**, *147*, 145.
- around the half of 19th century the italian physician Enrico Selmi write a description of "colloids", not very different from the actual definition.
- in 1861 the term "**colloid**" (from the greek *kolla)* was conied by the Scottish chemist Thomas Graham

$(AuCl_4)^-$ —white phosphorous, reduction on CS_2, two phase system→ solution of colloids

diameter of 3 ÷ 30 nm

Nanoscale Materials

Florence - Santa Croce

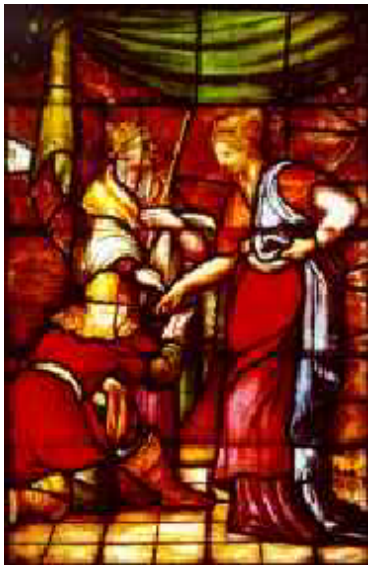

Milan - Duomo

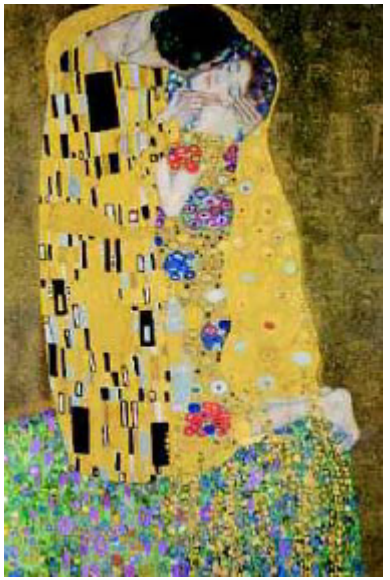

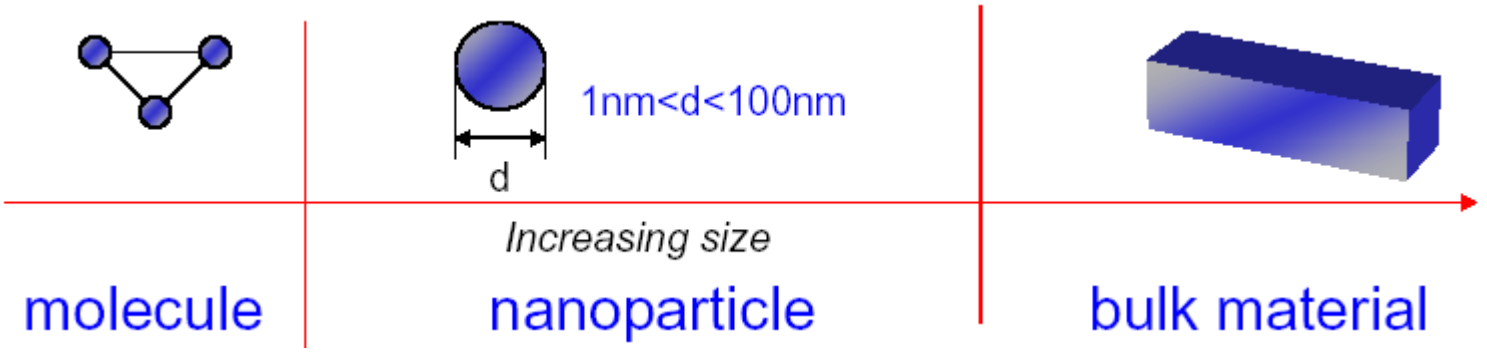

Nanoscale materials have different properties when compared to their bulk counterparts!

Nanoscale Materials

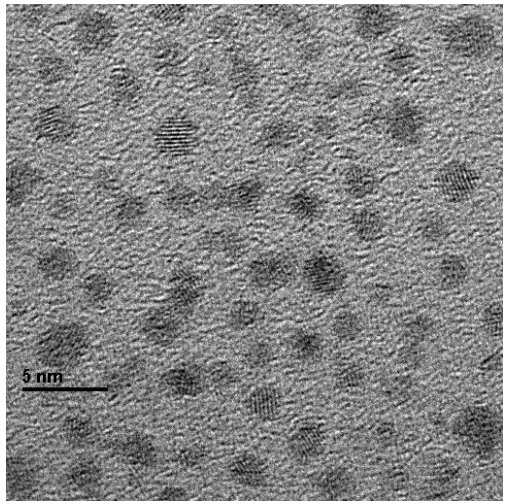

Nanoparticles - quantum dots

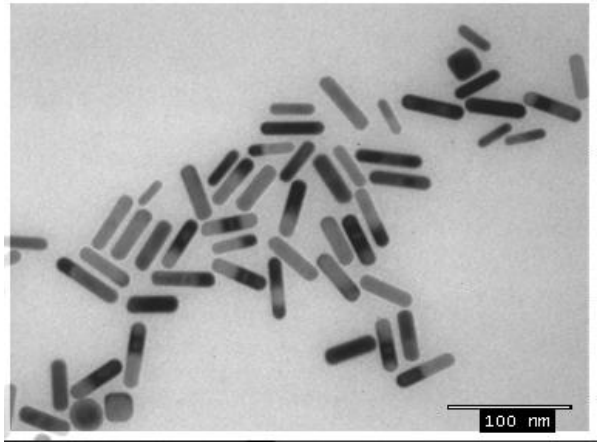

nanorods

0 dimensional nanomaterials:
unique properties due to
quantum confinement
and very high surface/volume ratio

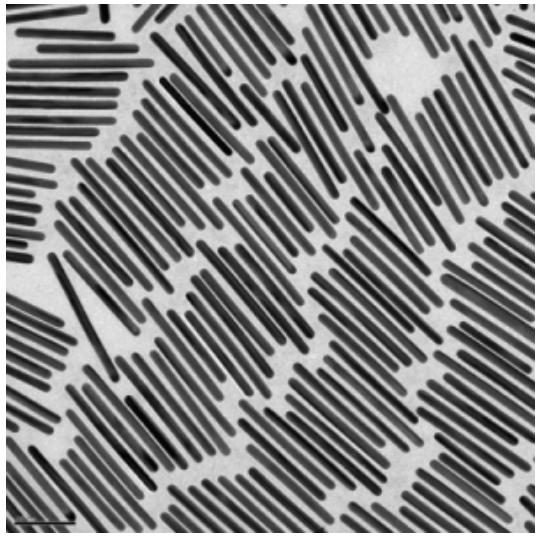

nanowires

1 dimensional nanomaterials:
extremely efficient
classical properties

These ultra-long devices exhibit tremendous photothermal properties, converting up to 90% of incident light energy to heat.

Properties of Metal Nanoparticles

Optical Properties

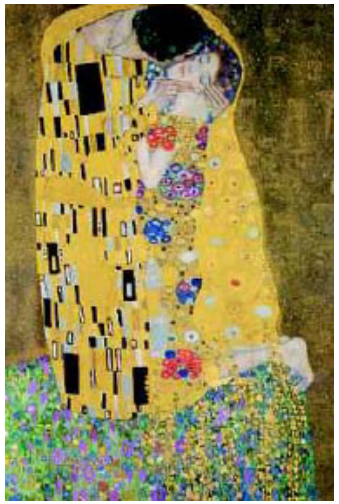

Electronic Properties

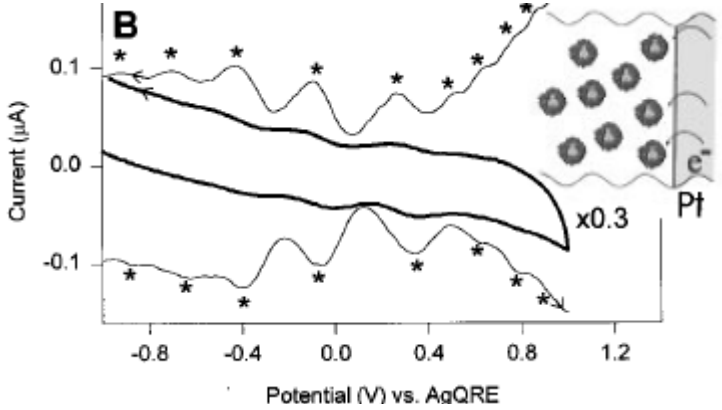

Nanoscale Materials Have Different Properties when compared to their bulk counterparts!

Nanoscale Materials

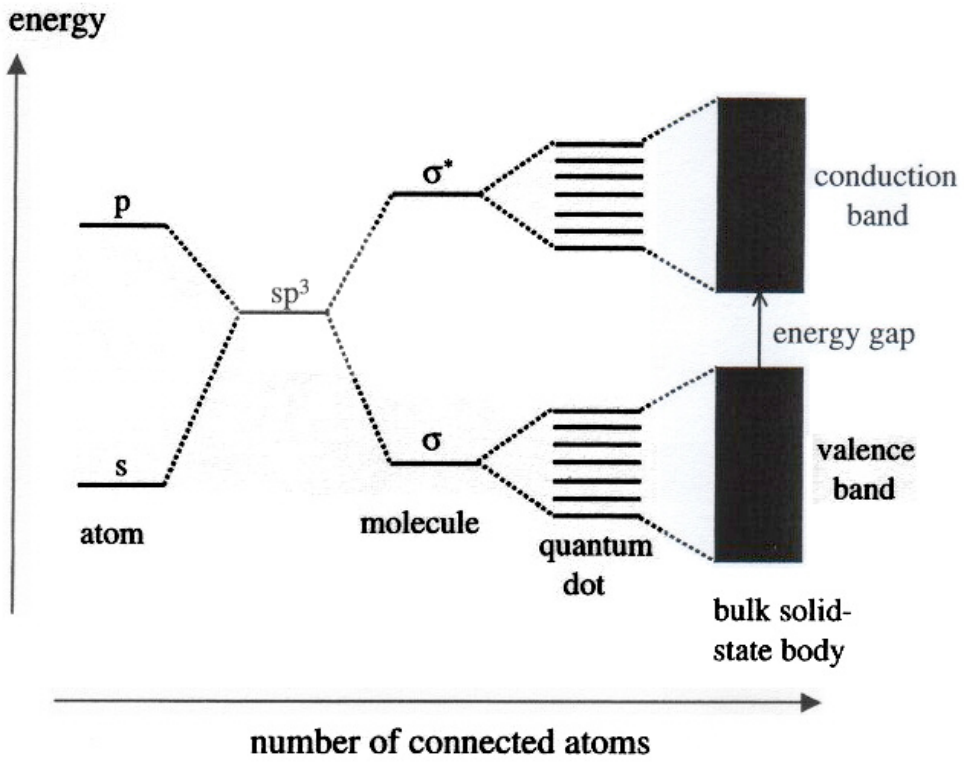

Fig. 2-1 Electronic energy levels depending on the number of bound atoms. By binding more and more atoms together, the discrete energy levels of the atomic orbitals merge into energy bands (here shown for a semiconducting material) [16]. Therefore semiconducting nanocrystals (quantum dots) can be regarded as a hybrid between small molecules and bulk material.

Synthesis of metal nanoparticles

PVD *(physical vapor deposition)*
formation of clusters in the gas phase - Au metal as strating material
for example, the nanoparticles are formed from bulk metal by irradiating it with a laser beam.
At low laser flux, the material is heated by the absorbed laser energy and evaporates
or sublimates and deposited over a solid support, under UHV condition.

es. cathodic arc deposition, sputter deposition, electron beam physical vapor deposition, laser ablation

CVD *(chemical vapor deposition)*
organometallic compounds as starting material
In a typical CVD process, the wafer (substrate) is exposed to one or more volatile precursors,
which react and/or decompose on the substrate surface to produce the desired deposit.
Frequently, volatile by-products are also produced, which are removed by gas flow through
the reaction chamber.

problem: control of the NP size

Synthesis of metal nanoparticles

- control of size, shape and composition with synthetic methodologies that allows to produce significative quantities of NPs.

- **molecular approach to colloidal metals**: use of molecular precursors

- many of the known methods are applicabile to different metallic elements of the periodic table, for exemple the reduction with hydrides.

- colloidal NPs are unstable and aggragate if not stibilized

Synthesis of metal nanoparticles

Two methods against aggregation:

- **electrostatic stabilization**
- **steric stabilization**

- 12-64 nm J. Turkevitch, P. C. Stevenson, J. Hillier, *Disc. Farady Soc.* **1951**, *11*, 55.

Reduction with **sodium citrate** developped by Frens in 1973:
this is the most used method for the preparation of gold colloids.

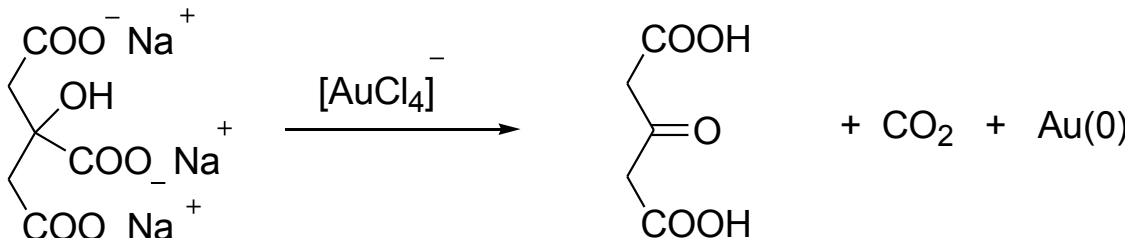

it is easy
•it requires only water
•it requires skills
•has reproducibility issues

NPs size may increases using more diluted solutions.

Synthesis of metal nanoparticles

Electrostatic stabilization: the electrical double layer

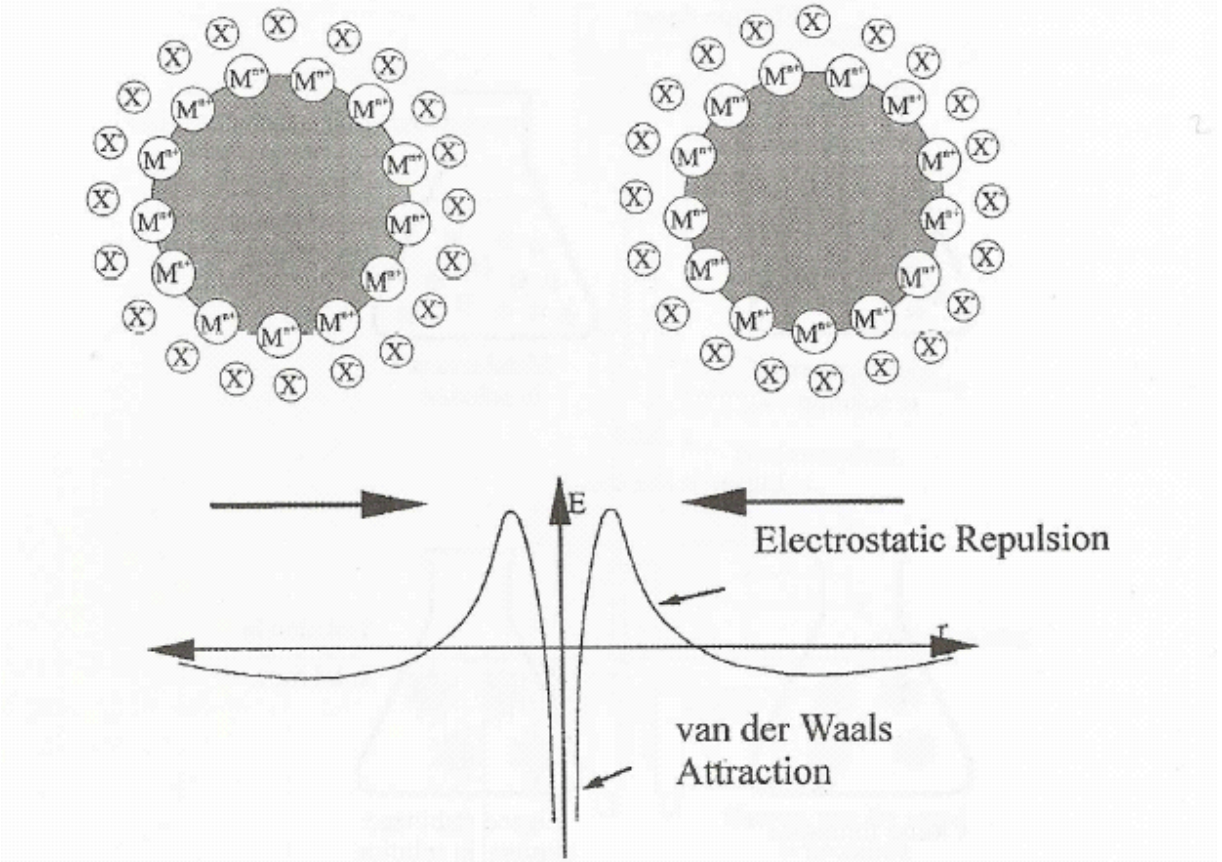

FIGURE 2.24 Electrostatic stabilization of metal colloids. Van der Waals attraction and electrostatic repulsion compete with each other.[27]

the energetic maximum can be easily overtake increasing for example the ionic strength or by increasing the thermal movement of the NPs.

Synthesis of metal nanoparticles

reduction of $HAuCl_4$ with different reducing agents

- 3-4 nm sodium borohydride ($NaBH_4$)
- 12 nm

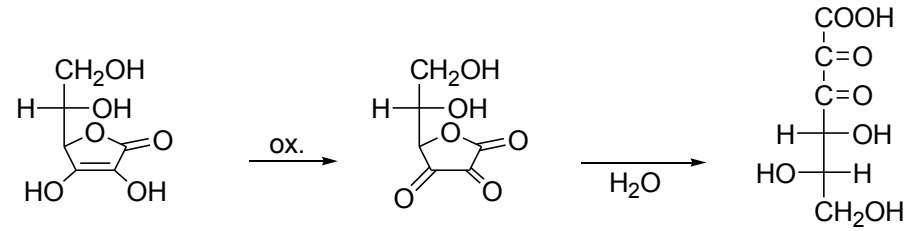

ascorbic acid

- 12-64 nm

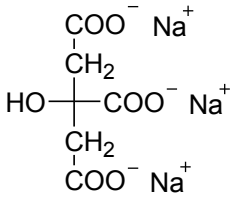

sodium citrate

Synthesis of metal nanoparticles

- the strength of the reducing agent determine the NP size
- the reaction conditions are also very important in determining the average diameter
  - the size may be reduced by: increasing reductant
    decreasing volume
    increasing stirring
    increasing temperature

Synthesis of metal nanoparticles

Steric stabilization

polymers, surfactants, and legands may be used to form a protective monolayer

polymers: they should present specific groups that bound to the NPs surface

Gold Number: quntity of polymer that stabilize 1 g of a solution of
50 mg/L of colloidal gold against aggregation in the presence of NaCl 1%

PVP [poly(vinylpyrrolidone)] and **PVA**, poly(vinyl alcohol) o
CTAB (cetyltrimethilammonium bromide)

These polymers have been used also to stabilize Pt and Ag NPs

Synthesis of metal nanoparticles

reduction of transition metals salts

- by using solvents that may easily be oxidized as alcohols that are oxidized to aldehydes or ketones

- Hirai and Toshima, “alcohol reduction process” and polymers for the stabilization

$$RhCl_3 + 3/2\ R_1R_2CHOH \longrightarrow Rh(0) + 3/2\ R_1R_2C{=}O + 3\ HCl$$

Other reducing agents:

Ascorbic acid, hydrogen, formaldehyde, hydrazine

Characterization of NPs

TEM *(transmission electron microscopy): give information about structure Dimension, dispersion, shape, and composition of the metal core*

HRTEM si ottengono informazioni sulle distanzi interplanari, TEM in alta risoluzione.

HAADF-STEM high-angle annular dark-field imaging in the scanning electron microscope è una tomografia elettronica adatta ad analizzare nanomateriali cristallini

X-ray diffraction

XRD

SAXS small-angle X-ray scattering (down to 1 nm)
anomalous SAXS (synchrotron radiatio)

WAXS wide-angle X-ray scattering

EXAFS extended X-ray absorption fine structure

XPS X-ray photoelectron spectroscopy

Mössbauer spectroscopy

XANES X-ray absorption near-edge structure

STS *scanning-tunneling spectroscopy*

Transmission Electron Microscope (TEM)

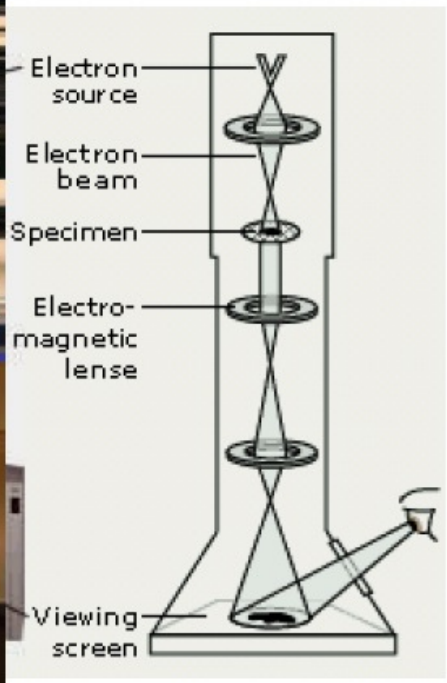

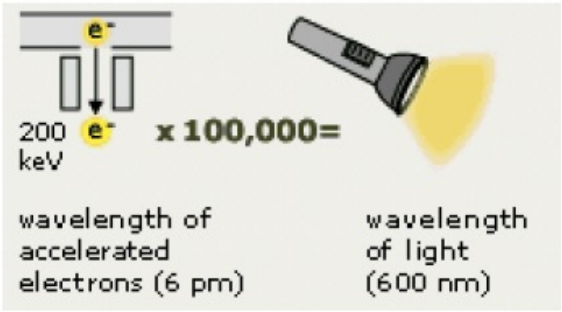

	Optical	TEM
Radiation	*Light*	*Electrons*
Lenses	*Glas*	*Magnetic fields*
Wavelength	*ca. 0,5 μm*	*ca. 2 picometer*
Resolution	*ca. 0,5 μm*	*0,1 - 0,2 nm*
Sample thickness	*ca. 25 - 50 μm*	*ca. 10 - 200 nm*

TEM
Copenhagen - 200 kV

- Å resolution
- *Transmission*,
  ie only thin slices

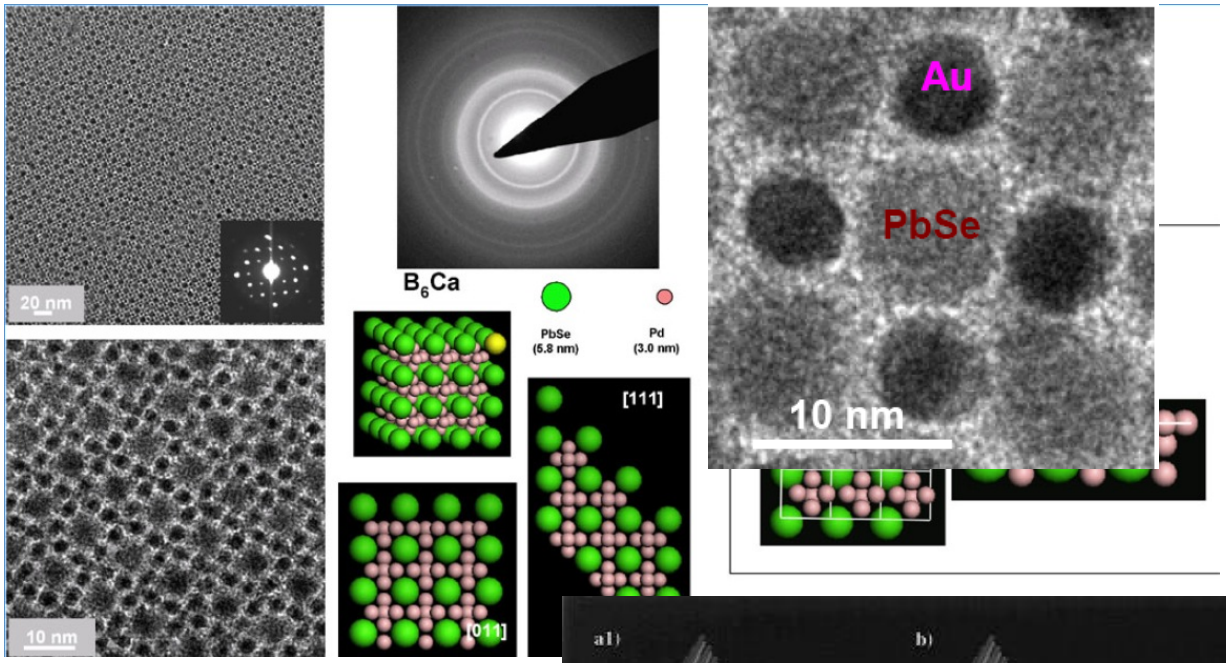
20 nm
10 nm
B6Ca
PbSe
(5.8 nm)
Pd
(3.0 nm)
[111]
[011]
Au
PbSe
10 nm

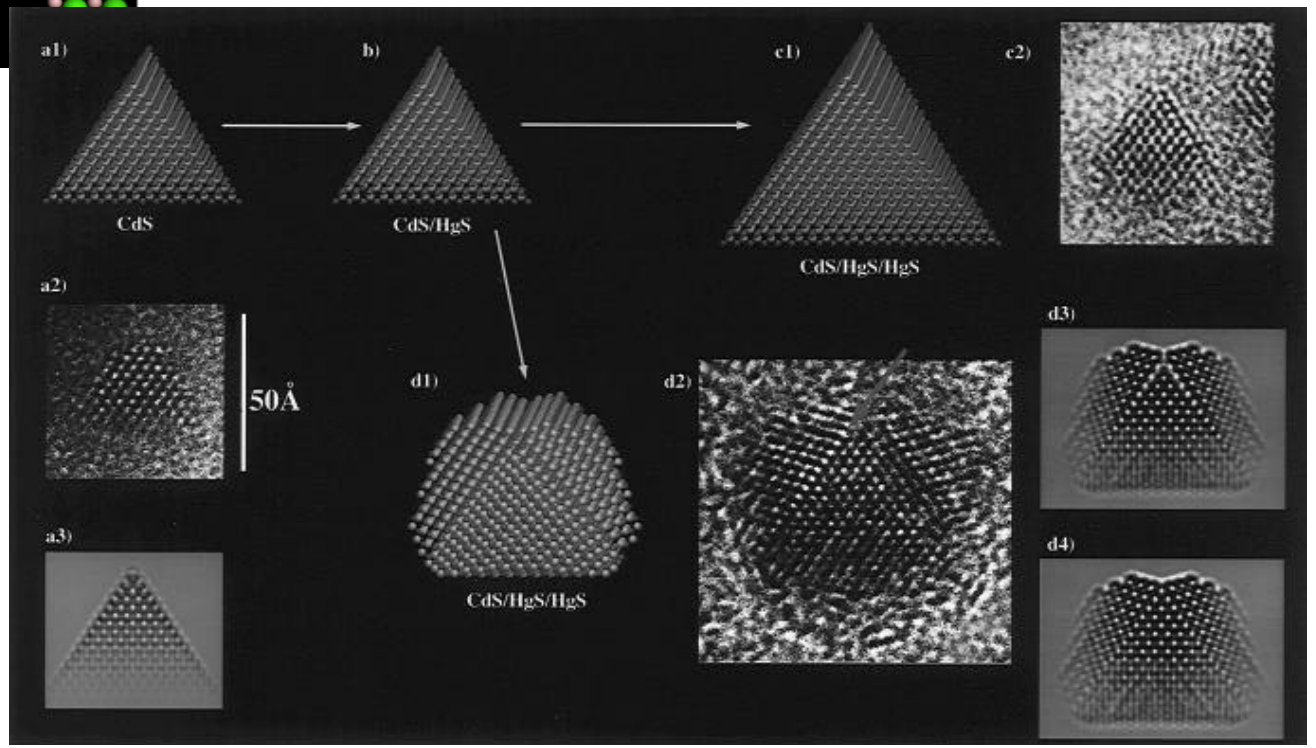
a1)
b)
c1)
c2)
CdS
CdS/HgS
CdS/HgS/HgS
a2)
50Å
d1)
d2)
d3)
a3)
CdS/HgS/HgS
d4)

NANOPARTICELLE - SINTESI

Au, Pd, Pt,

full-shell clusters: clusters are like onions, each atom like to complete his coordination

for metals the coordination number is 12

the first full-shell cluster is composed of 1+12 = 13 atoms

the shell *n*th includes $10n^2 + 2$ atoms

***n* shell**	1	2	3	4	5	6	7	8	9	10
n. atoms last shell	12	42	92	162	252	362	492	642	812	1002
n. total atoms	13	55	147	309	561	923	1415	2057	2869	3871
% surface atoms	92.3	76.4	62.6	52.4	44.9	39.2	34.8	31.2	28.3	25.8
average d (nm)		1.4	1.9	2.0	2.8	3.0			4.4	4.6

UNDECAGOLD

Step 1. $HAuCl_4 + 2PPh_3 + H_2O \xrightarrow[\text{or THF}]{\text{EtOH}} Ph_3PAuCl + Ph_3PO + 3HCl$

Step 2. $Ph_3PAuCl + NaBH_4 \xrightarrow[\text{or THF}]{\text{EtOH}} Au_{11}(PPh_3)_7Cl_3$

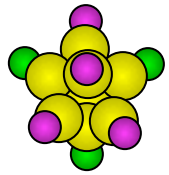

Step 3. $Au_{11}(PPh_3)_7Cl_3 + \sim 30CH_3(CH_2)_{11}SH \xrightarrow{\text{THF}} Au_{11\text{-}13}(PPh_3)_x(SC12)_yCl_z$

Step 4. Column chromatography to remove PPh_3O, Ph_3PAuCl, $[CH_3(CH_2)_{11}S]_2$

"undecagold" derivatives have been widely used as markers of biological compounds and for histochemical analysis

P. A. Bartlett, B. Bauer, S. J. Singer, *J. Am. Chem. Soc.* **1978**, *100*, 5085.
F. Cariati, L. Naldini, *Inorg. Chim. Acta*, **1971**, *5*, 172.

UNDECAGOLD

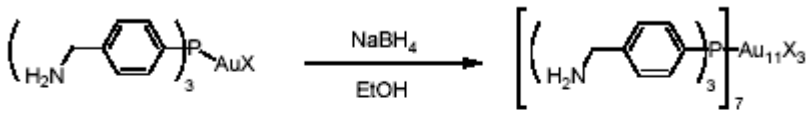

2a X = I
2b X = CN

3a X = I
3b X = CN

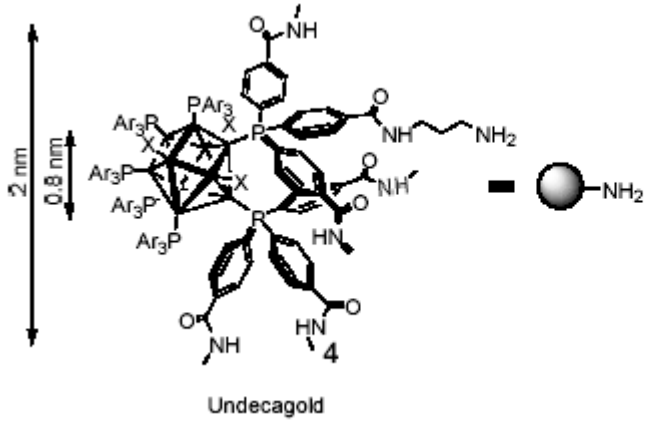

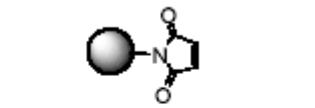

to bound thiols

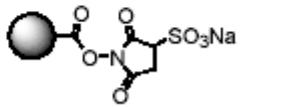

it reacts with amines

H. Yang, P. A. Frey, *Biochemistry*, **1984**, *23*, 3849, 3857, 3863.

- conjugates of peptide, ATP, nucleic acids, lipids, phospholipidis, carbohydrates, antibodies, etc. have been prepared.

Au_{55}

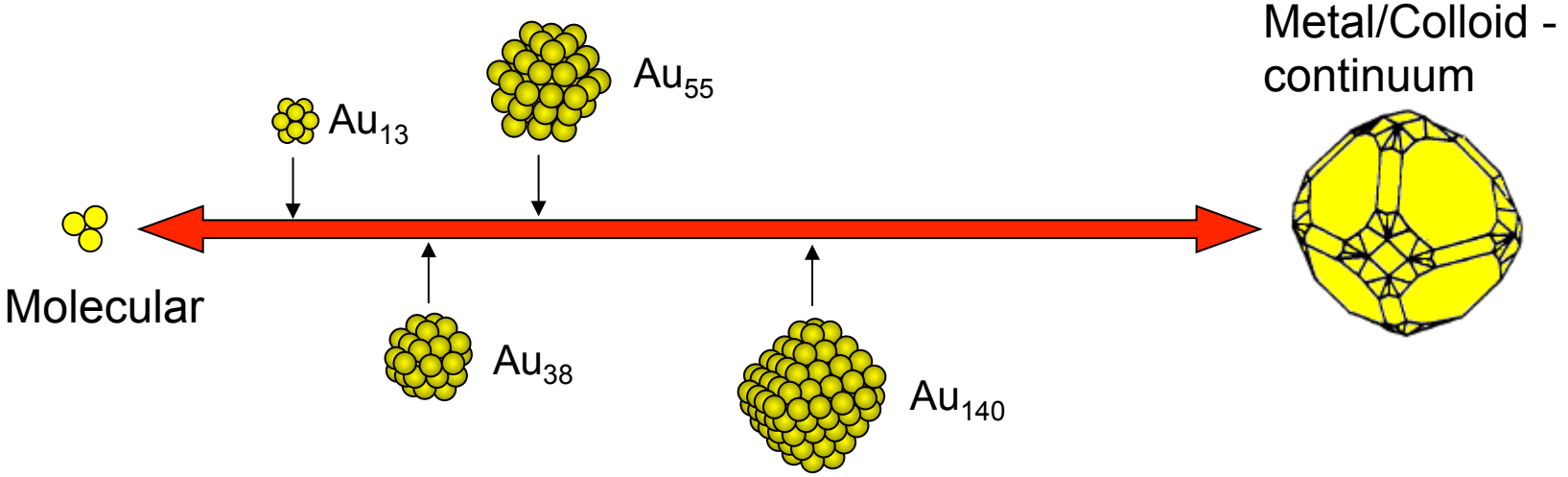

$Au_{55}(PPh_3)_{12}Cl_6$ is the most studied full-shell cluster since it represent a transition between molecular and colloidal behaviour

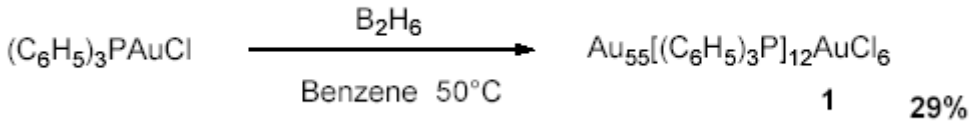

the syntheic method enable one to obtain a monodispersed cluster and because of this it could be used in the formation of fcc 3D crystals .

G. Schmid, P. Pfeil, R. Boese, F. Bandermann, S. Meyer, G. H. M. Calis, J. W. A. van der Velden, *Chem. Ber.* **1981**, *114*, 3634.

Au_{55}

Chromatographic Isolation of "Missing" Au55 Clusters Protected by Alkanethiolates

Hironori Tsunoyama,† Yuichi Negishi,† and Tatsuya Tsukuda*,†,‡

J. Am. Chem. Soc. **2006**, *128*, 6036.

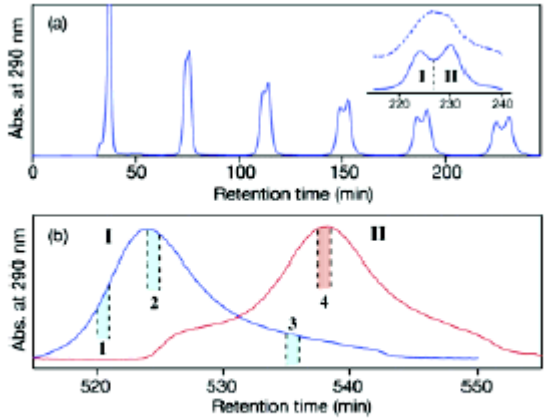

Figure 1. (a) Chromatogram of recycling GPC of the Au:SC_{18} clusters. Dotted curve in the inset is the data for the sample without etching treatment. (b) Recycling chromatograms of two fractions **I** and **II**.

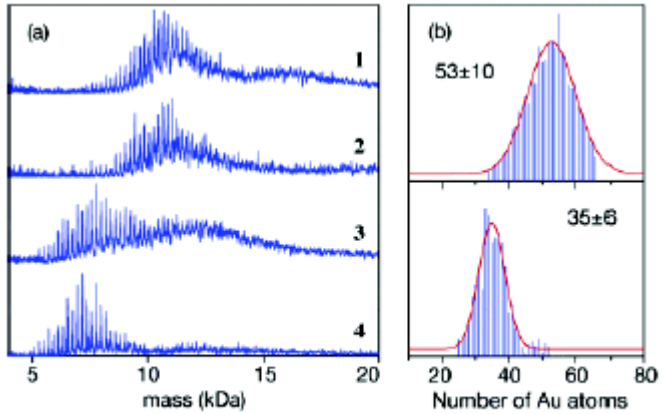

Figure 2. (a) LDI mass spectra of fractions **1**−**4** in the positive ion mode. (b) Histograms of the core numbers for fractions **2** and **4**.

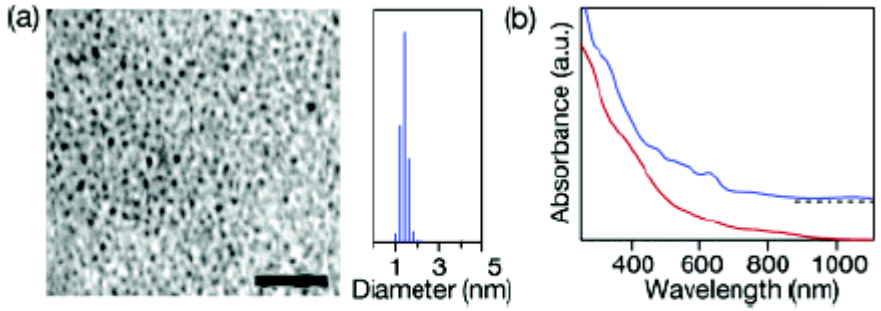

Figure 3. (a) TEM image and core-size distribution of Au_{55}:SC_{18}. The scale bar represents 20 nm. (b) Optical absorption spectra of Au_{55}:SC_{18} (red) and the 8 kDa clusters (blue).

Monolayer protected clusters MPCs

J. CHEM. SOC., CHEM. COMMUN., 1994

Synthesis of Thiol-derivatised Gold Nanoparticles in a Two-phase Liquid–Liquid System

Mathias Brust, Merryl Walker, Donald Bethell, David J. Schiffrin and Robin Whyman

Department of Chemistry, The University of Liverpool, PO Box 147, Liverpool, UK L69 3BX

Using two-phase (water–toluene) reduction of $AuCl_4^-$ by sodium borohydride in the presence of an alkanethiol, solutions of 1–3 nm gold particles bearing a surface coating of thiol have been prepared and characterised; this novel material can be handled as a simple chemical compound.

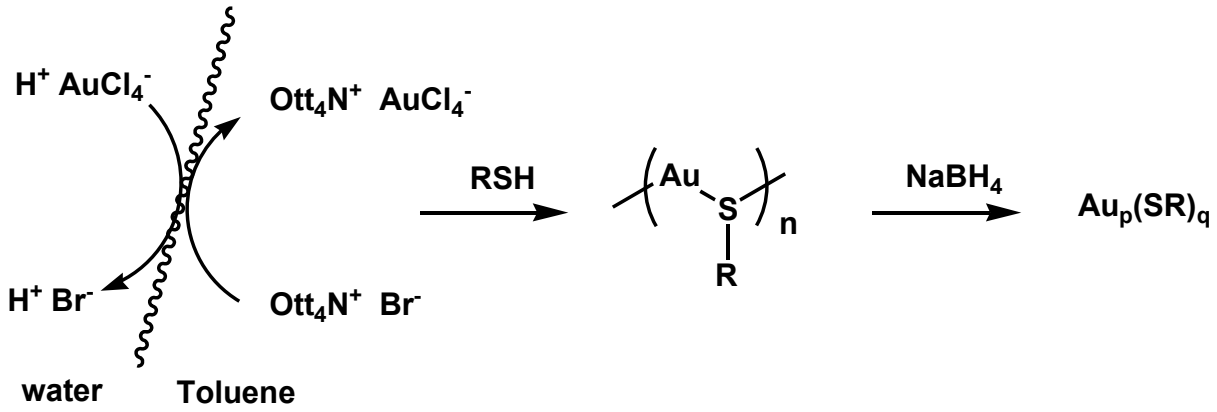

➡ MPCs OF DIFFERENT SIZE MAY BE OBTAINED USING DIFFEREN REACTION CONDITIONS:

- RATIO RSH/Au
- REDUCTION RATE
- TEMPERATURE

Nanoparticles – Au_{140}

the core

Au_{140}

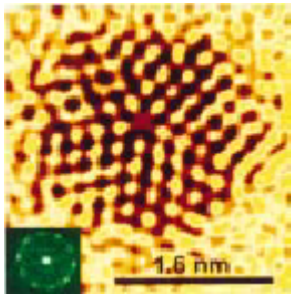

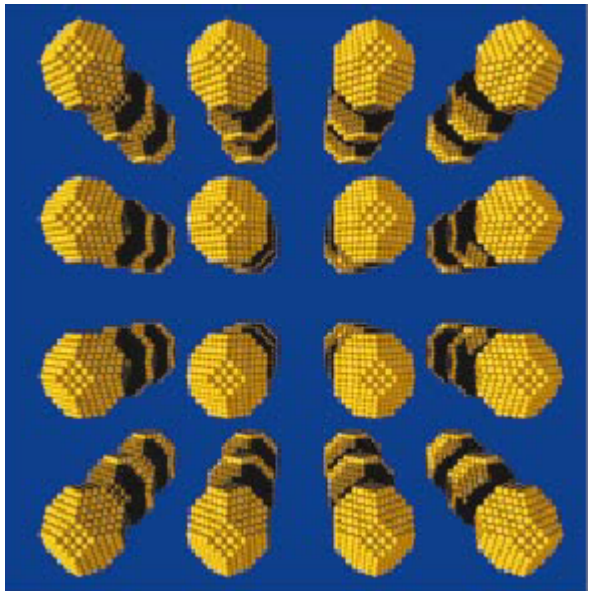

Whetten, R. L. et al. *Acc. Chem. Res.* **1999**, *32*, 397

Nanoparticles – the core

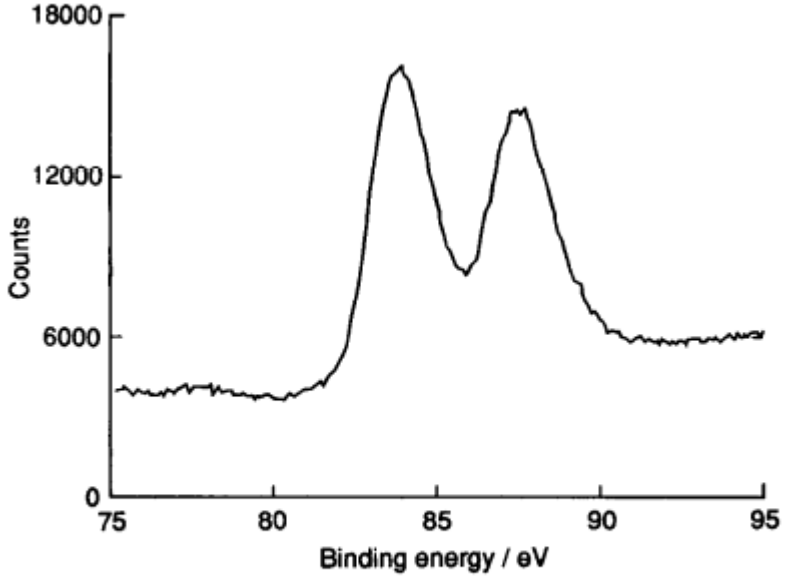

Fig. 3 XPS spectrum of the nanoparticles showing the Au $4f_{7/2}$ and $4f_{5/2}$ doublet with binding energies of 83.8 and 87.5 eV respectively. These are typical values for Au^0.

Nanoparticles - the monolayer

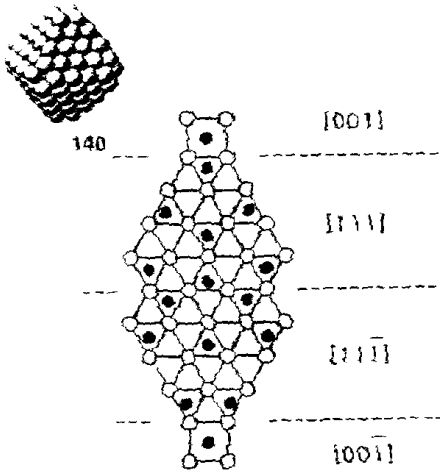

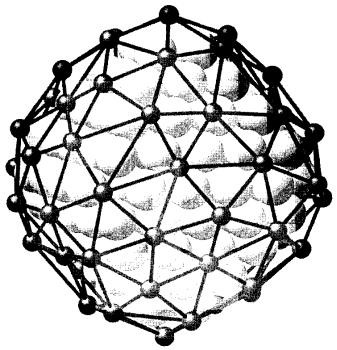

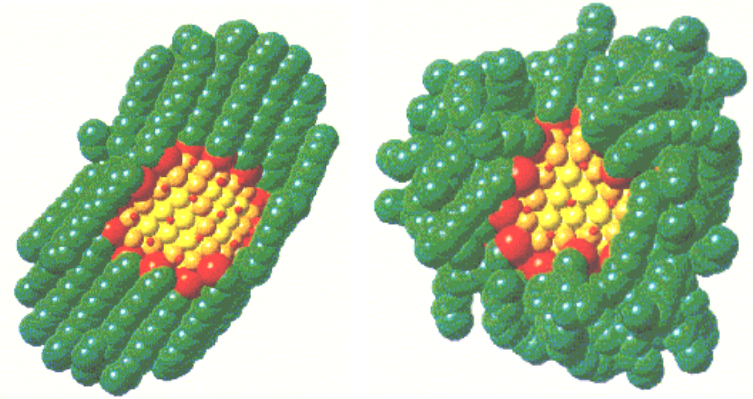

200 K 350 K

$Au_{140}(C_{12}H_{25}S)_{62}$

W. D. Luedtke, U. Landman *J. Phys. Chem.* **1996**, *100*, 13323; *J. Phys. Chem. B* **1998**, *102*, 6566

Au-NPs

Structure of a Thiol Monolayer–Protected Gold Nanoparticle at 1.1 Å Resolution

Science **2007**, *318*, 430.

Pablo D. Jadzinsky,[1,2]* Guillermo Calero,[1]* Christopher J. Ackerson,[1]†
David A. Bushnell,[1] Roger D. Kornberg[1]‡

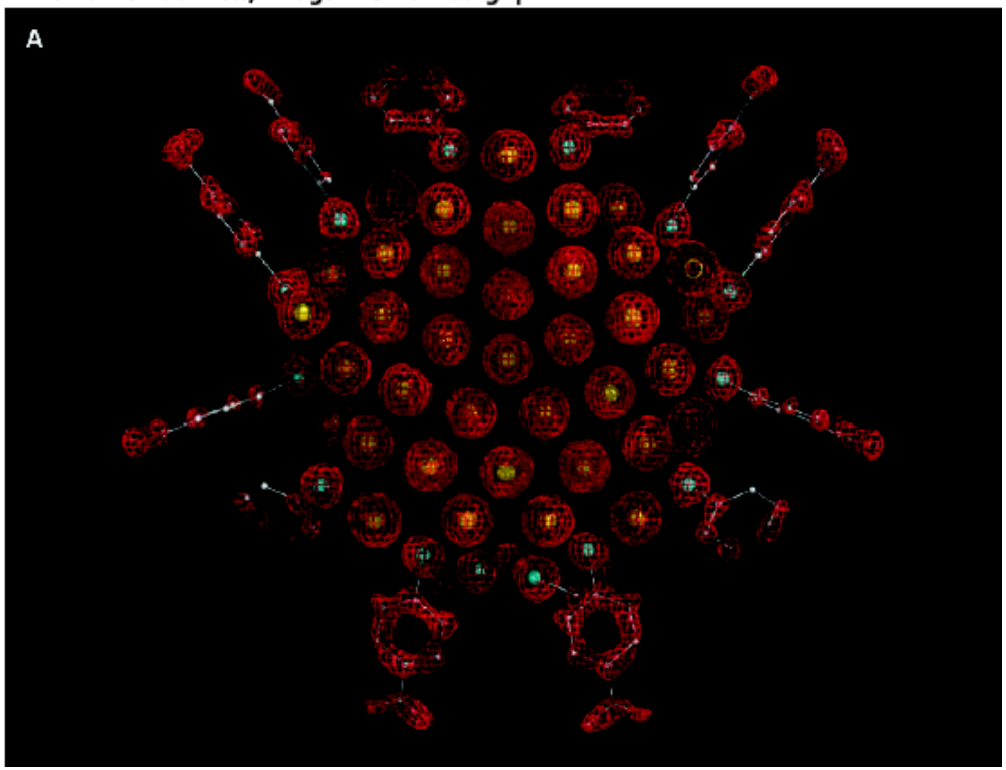

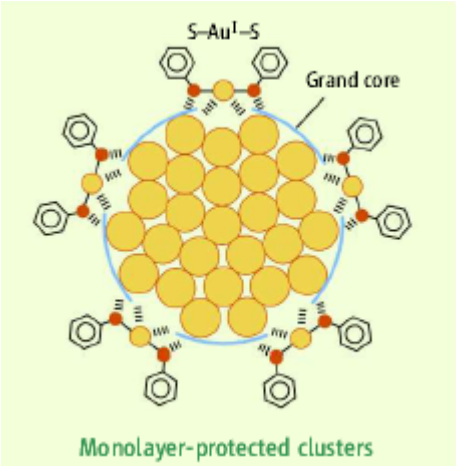

Fig. 1. X-ray crystal structure determination of the Au102(p-MBA)44 nanoparticle. (A) Electron density map(redmesh)andatomic structure (gold atoms depicted as yellow spheres, and p-MBA shown as framework and with small spheres [sulfur in cyan, carbon in gray, and oxygen in red]).

Au-NPs

Structure of a Thiol Monolayer–Protected Gold Nanoparticle at 1.1 Å Resolution

Science **2007**, *318*, 430.

Pablo D. Jadzinsky,[1,2]* Guillermo Calero,[1]* Christopher J. Ackerson,[1]†
David A. Bushnell,[1] Roger D. Kornberg[1]‡

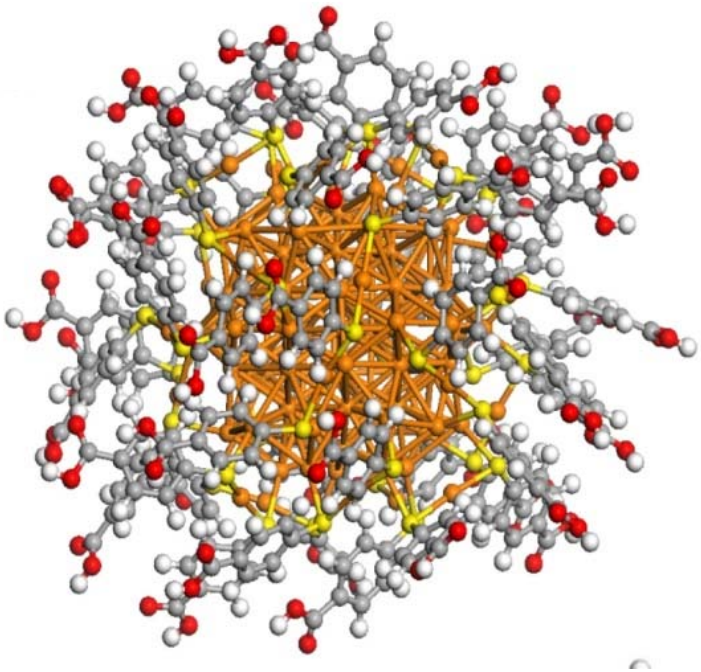

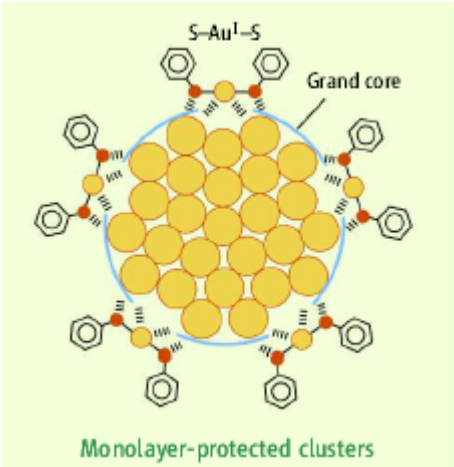

Fig. 1. X-ray crystal structure determination of the Au102(p-MBA)44 nanoparticle. (A) Electron density map(redmesh)andatomic structure (gold atoms depicted as yellow spheres, and p-MBA shown as framework and with small spheres [sulfur in cyan, carbon in gray, and oxygen in red]).

Structure of a thiol monolayer-protected Gold Nanoparticle at 1.1 Å resolution

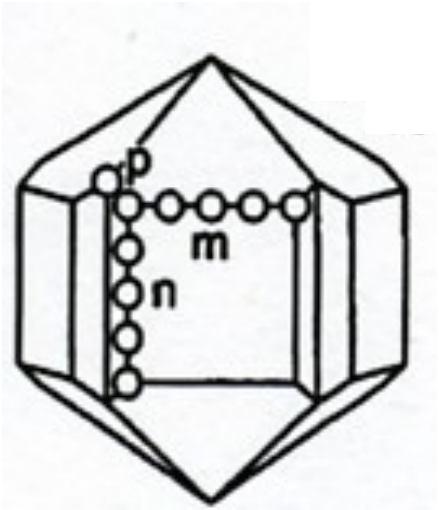

MD (m,n,p)

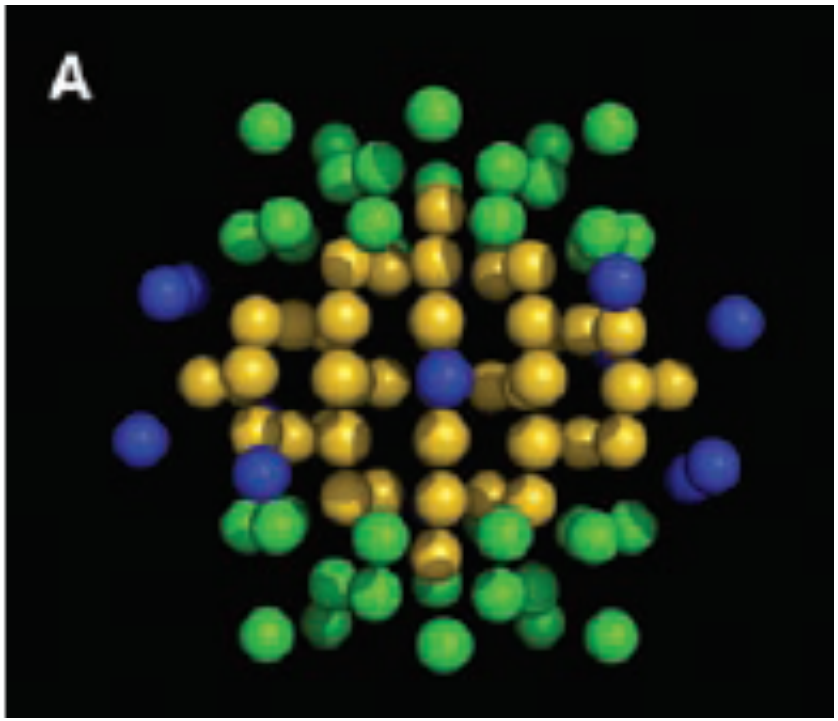

Fig.A: Packing of gold atoms in the nanoparticle. (A) MD (2,1,2) in yellow, two 20-atom“caps” at the poles in green, and the 13-atom equatorial band in blue.

Structure of a thiol monolayer-protected Gold Nanoparticle at 1.1 Å resolution

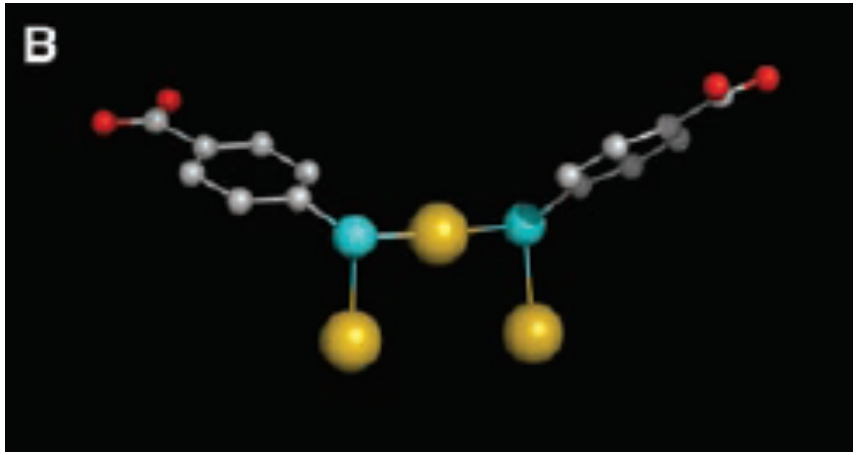

Example of two p-MBAs interacting with three gold atoms in a bridge conformation, here termed a staple motif. Gold atoms are yellow, sulfur atoms are cyan, oxygen atoms are red, and carbon atoms are gray.

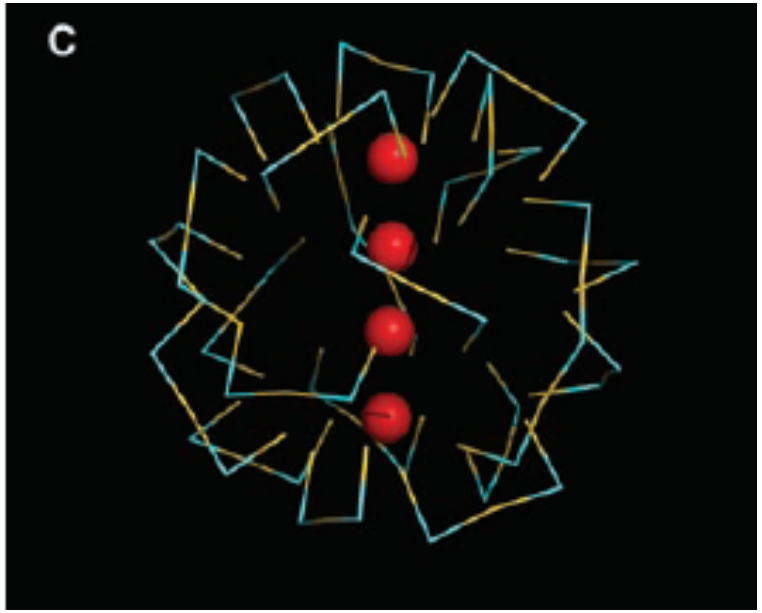

Distribution of staple motifs in the surface of the nanoparticle. Staple motifs are depicted symbolically, with gold in yellow and sulfur in cyan. Only the gold atoms on the axis of the MD are shown (in red).

Structure of a thiol monolayer-protected Gold Nanoparticle at 1.1 Å resolution

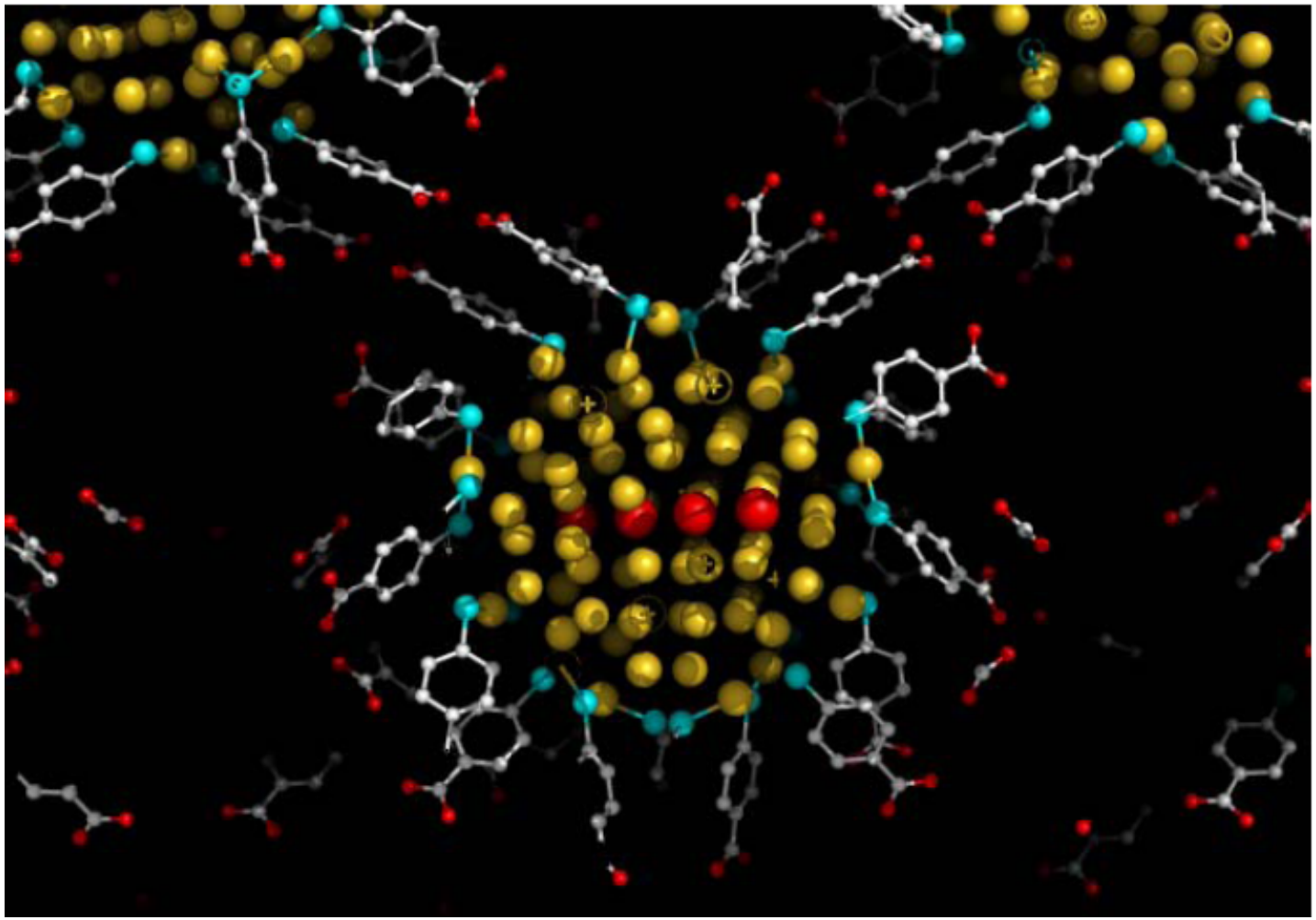

View of the crystal structure showing interparticle interaction mediated throughhydrogen bonding between carboxylic acids.

Structure of a thiol monolayer-protected Gold Nanoparticle at 1.1 Å resolution

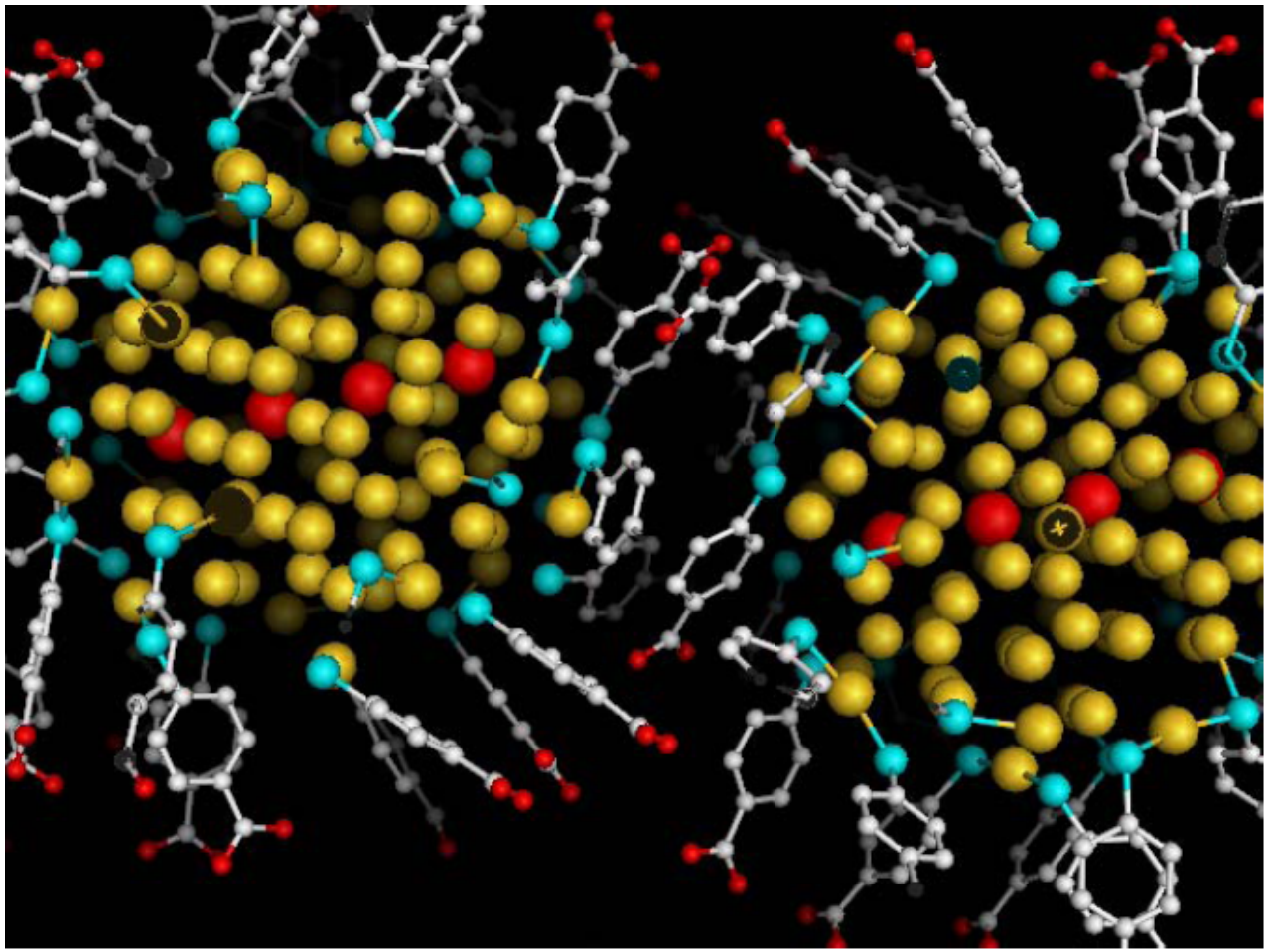

View of the crystal structure showing interparticle interactions mediated between stacked phenyl rings.

Crystal Structure of the Gold Nanoparticle [N(C8H17)4][Au25(SCH2CH2Ph)18]

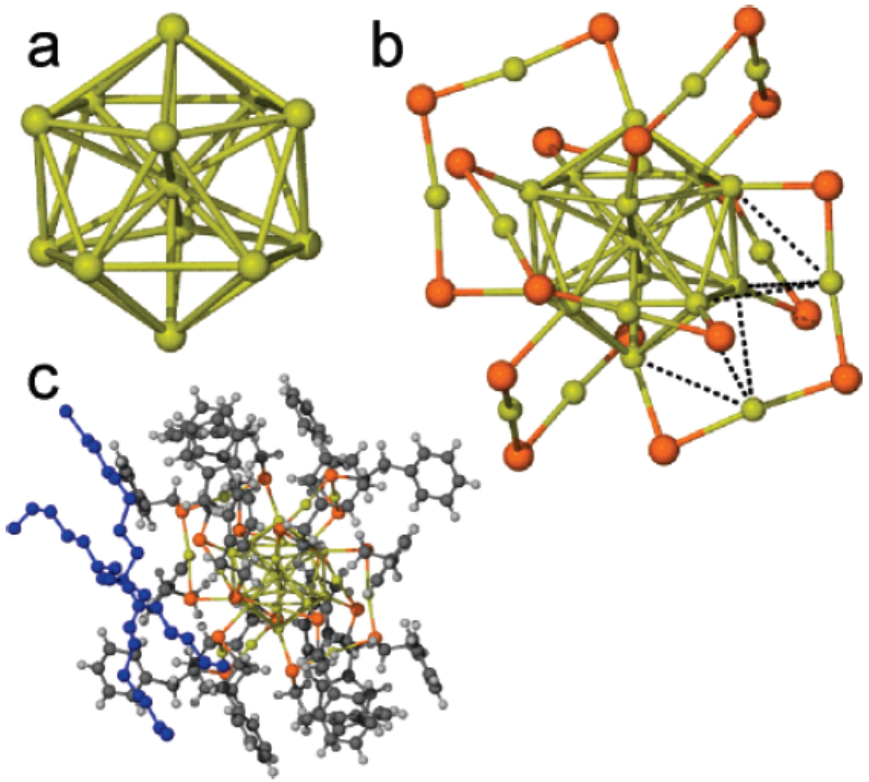

Figure 1. Breakdown of X-ray crystal structure of $[TOA^+][Au_{25}(SCH_2CH_2Ph)_{18}^-]$ as seen from [001]. (a) Arrangement of the Au_{13} core with 12 atoms on the vertices of an icosahedron and one in the center. (b) Depiction of gold and sulfur atoms, showing six orthogonal $-Au_2(SCH_2CH_2Ph)_3-$ "staples" surrounding the Au_{13} core (two examples of possible aurophilic bonding shown as dashed lines). (c) $[TOA^+][Au_{25}(SCH_2CH_2Ph)_{18}^-]$ structure with the ligands and TOA^+ cation (depicted in blue) (Legend: Gold = yellow; Sulfur = orange; Carbon = gray; Hydrogen = off-white; the TOA^+ counterion is over two positions with one removed for clarity).

M. W. Heaven, A. Dass, P. S. White, K. M. Holt, R. W. Murray **J. AM. CHEM. SOC. 2008**, 130, 3754-3755

Nanoparticles - spontaneous ordering

when monodispersed....

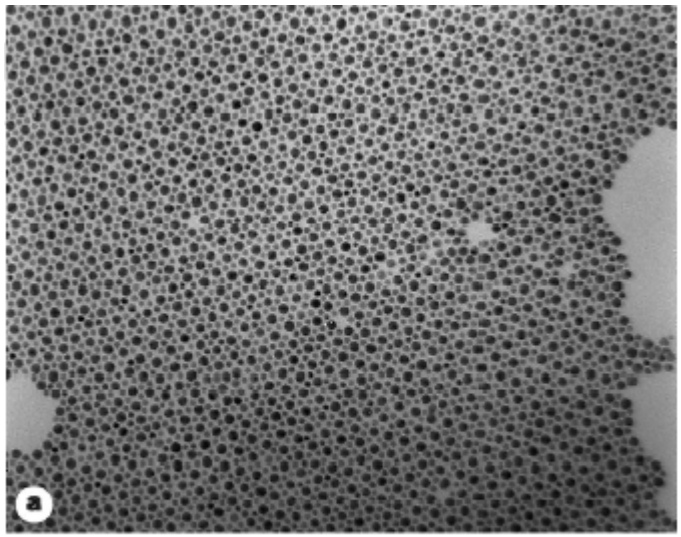

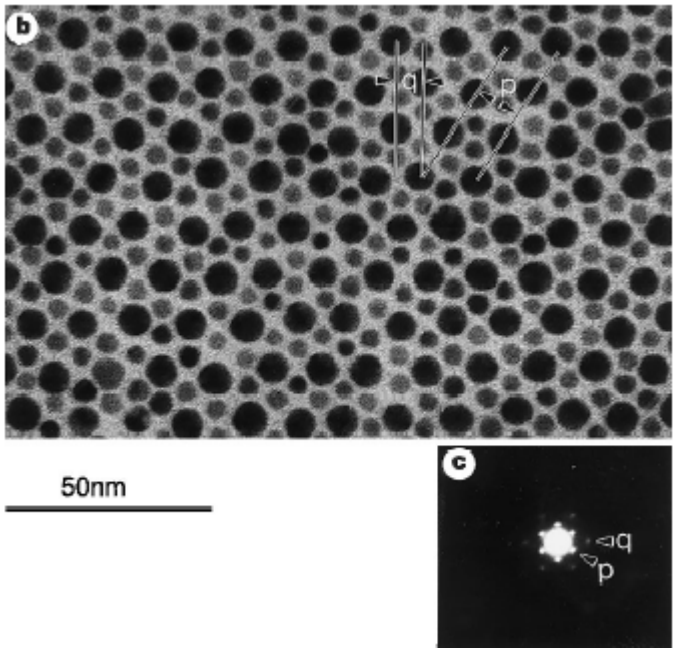

An ordered raft comprising Au nanoparticles of two distinct sizes with R_B/R_A < 0:58. Shown are electron micrographs at low (a) and higher (b) magnification. c, The low-angle superlattice electron diffraction pattern obtained from this bimodal raft structure.

C. J. Kiely, J. Fink,M. Brust, D. Bethell, D. J. Schiffrin, *Nature*, **1998**, *396*, 444.

3D alkanethiolate monolayers

Scheme 1. A Schematic 2D Representation of the RS/Au Nanoparticle Packing Structure in the Solid State[a]

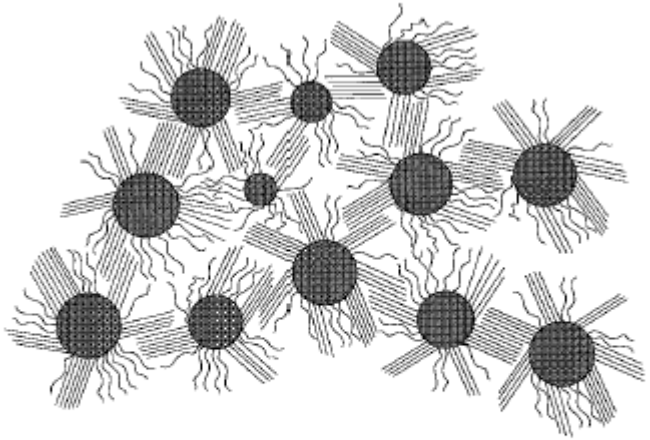

[a] In this description, *domains* or *bundles* of ordered alkylthiolate chains on a given Au particle will interdigitate into the chain domains of neighboring particles in order to compensate for the substantial decrease in the chain density which occurs toward the methyl chain end. Chains with large populations of *gauche* bonds may arise from (i) those which occupy interstitial regions in the particle lattice and cannot efficiently overlap with adjacent chains or from (ii) chains residing at domain boundaries.

Scheme 2. The Types of Chain Dynamic Processes Suggested by the ^{2}H NMR Line Shapes of the Deuterated $C_{18}S$/Au Nanoparticles[a]

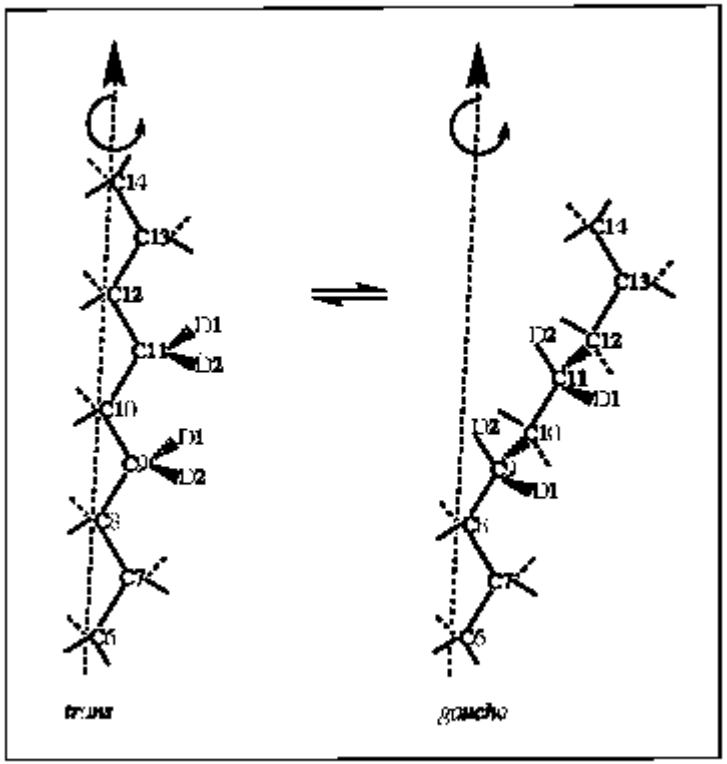

[a] These processes involve *trans-gauche* bond isomerization and pseudorotational motion of individual chain segments about the long axis of the alkanethiolate molecule.

A. Badia, L. Cuccia, L. Demers, F. Morin, B. R. Lennox, *J. Am. Chem. Soc.*, **1997**, *119*, 2682.

3D alkanethiolate monolayers

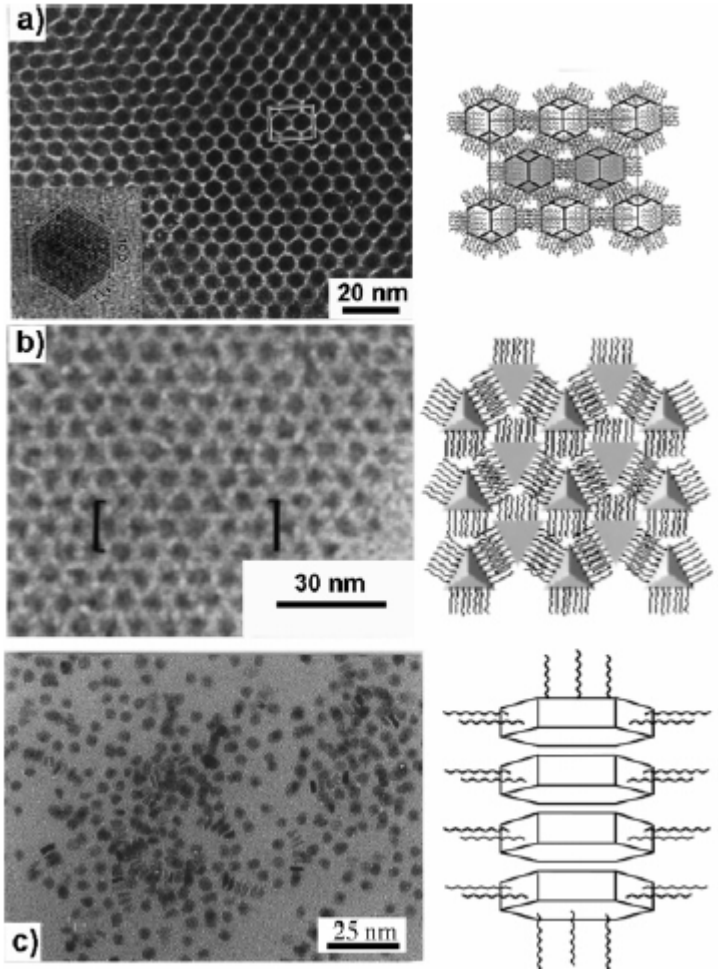

Figure 11. (a) (Left) TEM image of a face-centered, cubicpacked, array of silver nanoparticles, passivated with a dodecanethiolate monolayer, with a truncated octahedral morphology (see inset). (Right) Representation of the proposed packing of the particles via interdigitation of the bundled alkyl chains on each face. (b) (Left) TEM image of a monolayer of self-assembled silver tetrahedra passivated with dodecanethiolates. The bracketed area most closely matches the proposed model.

Langmuir **1998**, *14*, 17−30

Alkanethiolate Gold Cluster Molecules with Core Diameters from 1.5 to 5.2 nm: Core and Monolayer Properties as a Function of Core Size

Michael J. Hostetler,[†] Julia E. Wingate,[†] Chuan-Jian Zhong,[‡] Jay E. Harris,[†] Richard W. Vachet,[†] Michael R. Clark,[†] J. David Londono,[§] Stephen J. Green,[†] Jennifer J. Stokes,[†] George D. Wignall,[§] Gary L. Glish,[†] Marc D. Porter,[‡] Neal D. Evans,[∥] and Royce W. Murray*,[†]

Table 1. Size and Composition Results for Different Cluster Preparations

preparation conditions[a]	SAXS[b] R_G, nm, max/min	SAXS[c] R_{POROD}, nm	HRTEM[d] R_{TEM}, nm	TGA[e] % organic	NMR[f] CH_3, ν_{FWHM} Hz
−78°,2X,sd	1.7/0.91	0.76	—	30.7	16
0°,2X,fd	—	—	1.1	28.8	21
0°,2X,md	—	—	—	26.7	22.5
0°,2X,sd	1.7/1.0	0.89	1.1	26.2	25.5
RT,1X,fd	1.7/1.2	1.0	—	25.6	24.5
RT,4X,fd	1.7/1.1	0.94	—	24.9	26
RT,2X,sd	1.6/1.2	0.96	—	24.5	27
RT,2X,fd	—	—	—	23.7	25.5
60°,2X,sd	1.4/1.2	0.98	—	24.1	29
90°,2X,sd	—	—	1.1	23.2	32
RT,1/2X,fd	1.6/1.4	1.2	1.2	19.4	37
RT,1/3X,fd	1.8/1.6	1.4	1.4	16.9	45
RT,1/4X,fd	2.1/2.0	1.7	2.0	12.8	53
RT,1/6X,fd	2.9/2.5	2.2	2.2	9.3	126[g]
RT,1/8X,fd	—	—	—	10.4	124[g]
RT,1/10X,fd	—	—	2.4	6.2	144[g]
RT,1/12X,fd	—	—	2.6	11.9	163[g]

[a] Code for preparation conditions: (*a*,*b*,*c*), where *a* represents the temperature at which the reduction was carried out, *b* represents the RSH:$AuCl_4^-$ molar ratio before reduction, and *c* represents the rate of reductant addition (fd, 10 s; md, 2 m; sd, 15 m). [b] SAXS results for Au core radius determined from Guinier plot. [c] SAXS results from Porod plot. [d] HRTEM results, average Au core size from analysis of histogram of HRTEM images. [e] TGA for thermal loss of alkanethiolate fraction of clusters. [f] Proton NMR linewidths. [g] CH_3 ^1H NMR signal obscured; the CH_2 resonance was used instead for these clusters.

Nanoparticles - caracterization

TEM

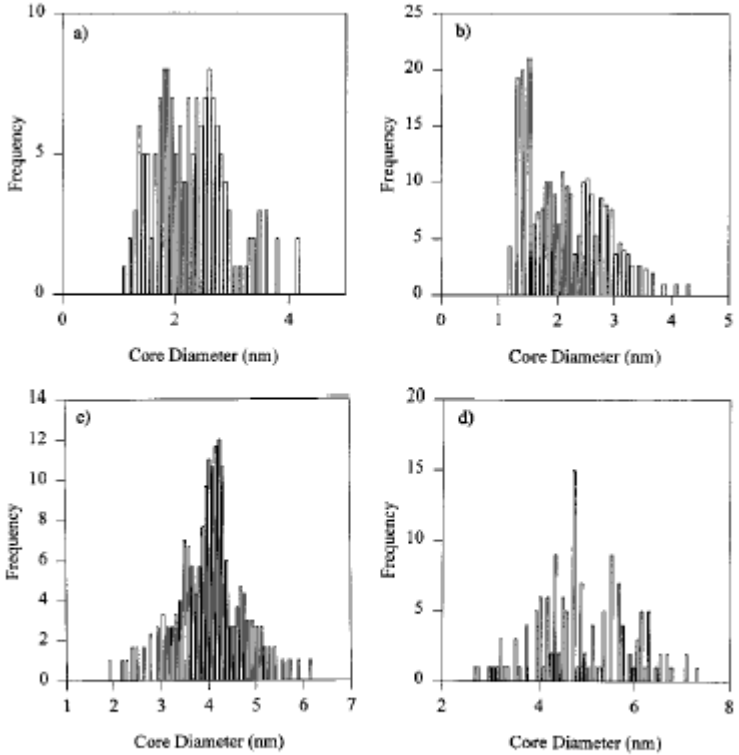

Figure 2. Size histograms (a and d are for films shown in Figure 1): (a) (0°,2X,fd); (b) (0°,2X,sd); (c) (RT,1/4X,fd); (d) (RT, 1/6X,fd).

NANOPARTICELLE - characterization

Table 2. Results from Modeling of Gold Core Sizes, Shapes, and Alkanethiolate Coverages, and of Size-Dependent T_2 Broadening of Proton NMR of CH_3 Resonances

#atoms (shape)[a]	R_{CORE}, nm	#surface atoms/ %defect/area nm^2	calc TGA %organic/ %coverage/#chains	calc R_{TOTAL}, nm	calc NMR ν_{FWHM}, Hz
79 (TO^+)	0.65	60/60%/8.30	33.0/63%/38	2.6	15
116 (TO^-)	0.71	78/61%/11.36	31.8/68%/53	2.6	16
140 (TO^+)	0.81	96/50%/11.43	27.9/55%/53	2.7	17
201 (TO)	0.87	128/47%/15.22	26.5/55%/71	2.8	18
225 (TO^+)	0.98	140/43%/15.19	24.4/51%/71	2.9	19
309 (CO)	1.1	162/52%/19.64	23.3/57%/92	3.0	22
314 (TO^+)	1.0	174/41%/19.46	22.9/52%/91	3.0	20
459 (TO^+)	1.2	234/36%/24.34	20.2/49%/114	3.1	23
586 (TO)	1.2	272/35%/28.94	19.1/50%/135	3.2	24
807 (TO^+)	1.4	348/31%/34.86	17.1/47%/163	3.3	27
976 (TO^-)	1.5	390/31%/40.02	16.4/48%/187	3.4	28
1289 (TO)	1.6	482/27%/47.22	14.9/46%/221	3.5	32
2406 (TO)	2.0	752/22%/69.86	12.2/43%/326	3.9	42
2951 (TO^+)	2.2	876/21%/79.44	11.4/42%/371	4.1	47; 94[b]
4033 (TO)	2.4	1082/19%/97.00	10.3/42%/453	4.3	55; 110[b]
4794 (TO^+)	2.6	1230/18%/108.28	9.7/41%/506	4.4	61; 122[b]
6266 (TO)	2.8	1472/16%/128.66	8.9/41%/601	4.7	70; 140[b]

[a] CO = cuboctahedron; TO = ideal truncoctahedron (all sides equal); TO^+ = truncoctahedron in which $(0 < n - m \leq 4)$, where n is the number of atoms between (111) facets and m is the number of atoms between (111) and (100) facets; TO^- = truncoctahedron in which $(-4 \leq n - m < 0, m > 1)$. [b] The second value is the calculated linewidth for the methylene peak.

NANOPARTICELLE - characterization

NMR

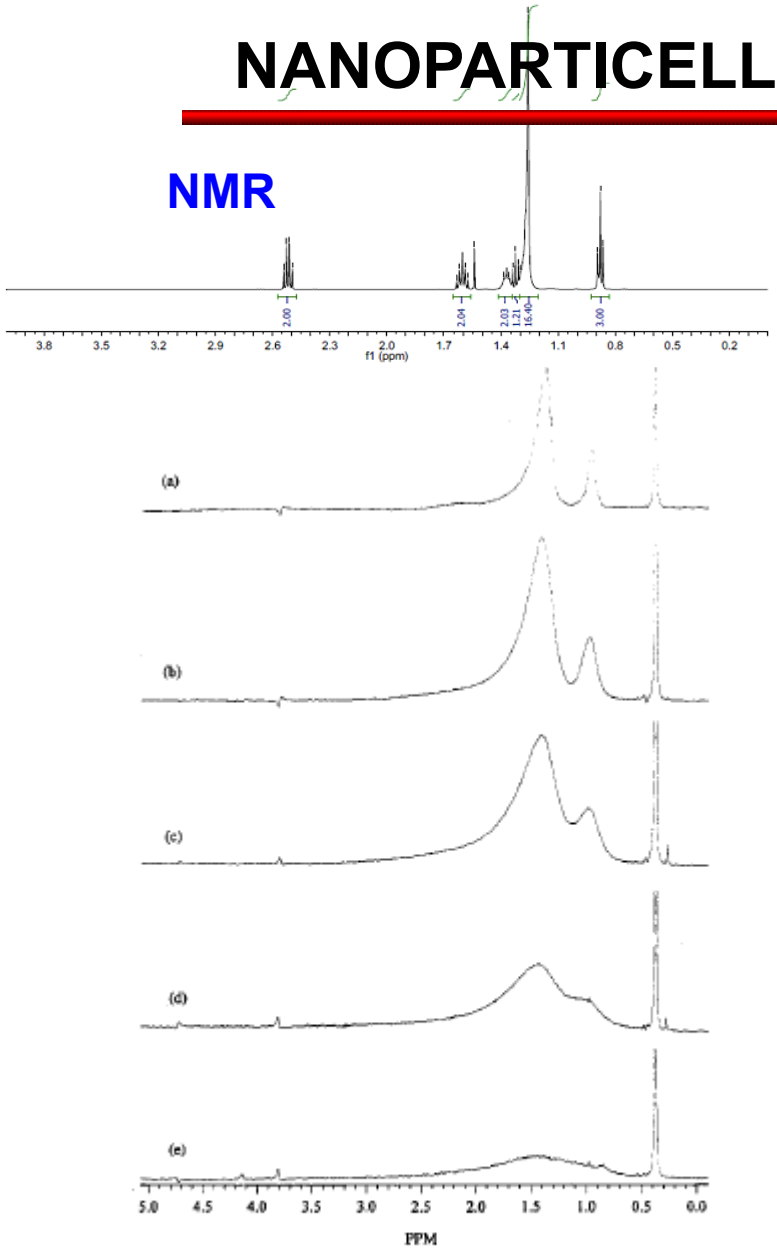

Figure 5. The ^{1}H NMR spectra (C_6D_6) of dodecanethiolate-protected Au clusters. Each spectrum was Fourier transformed using a line broadening of 1 Hz: (a) (−78°,2X,sd); (b) (90°,2X,sd); (c) (RT,1/3X,fd); (d) (RT,1/4X,fd); (e) (RT,1/12X,fd).

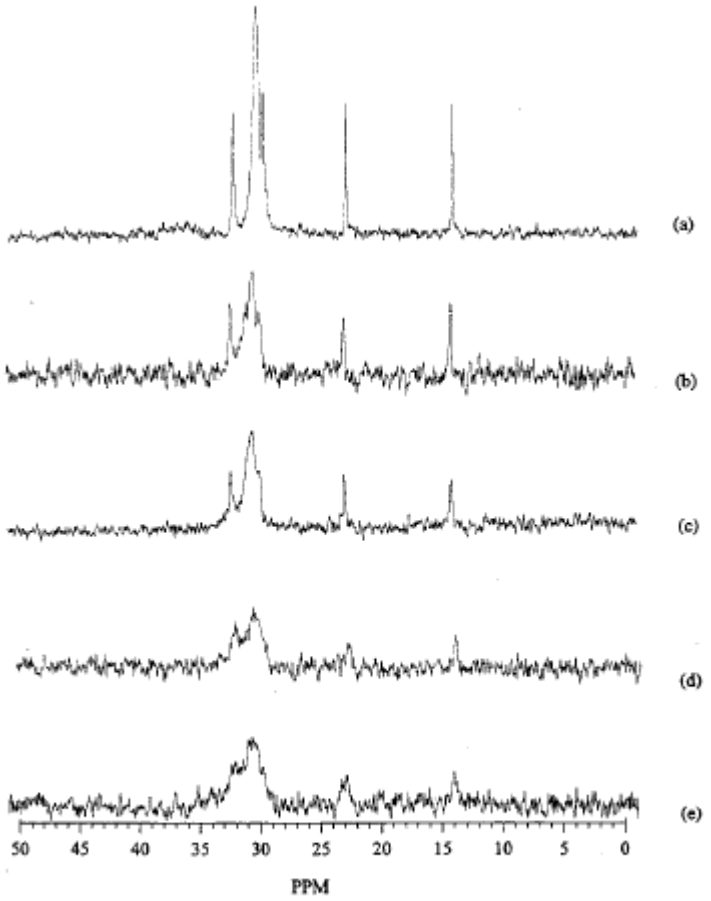

Figure 4. The ^{13}C NMR spectra (C_6D_6) of dodecanethiolate-protected Au clusters. Each spectrum was Fourier transformed using a line broadening of 3 Hz: (a) (−78°,2X,sd); (b) (90°,2X,sd); (c) (RT,1/3X,fd); (d) (RT,1/4X,fd); (e) (RT,1/6X,fd).

NANOPARTICELLE - characterization

UV-Vis

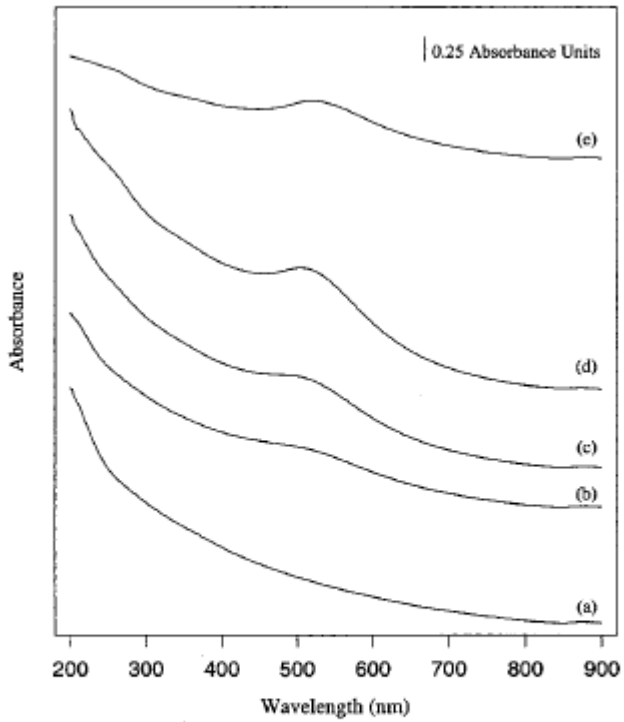

Figure 7. The UV/vis spectra (hexane) of dodecanethiolate-protected Au clusters: (a) (−78°,2X,sd), C = 3×10^{-6} M, MW = 3.4×10^{4} amu; (b) (90°,2X,sd), C = 2×10^{-6} M, MW = 5.5×10^{4} amu; (c) (RT,1/3X,fd), C = 4×10^{-7} M, MW = 2.3×10^{5} amu; (d) (RT,1/4X,fd), C = 2×10^{-7} M, MW = 5.5×10^{5} amu; (e) (RT,1/12X,fd), C = 9×10^{-8} M, MW = 1.1×10^{6} amu.

MPCC12

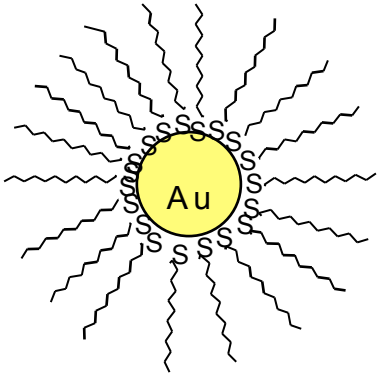

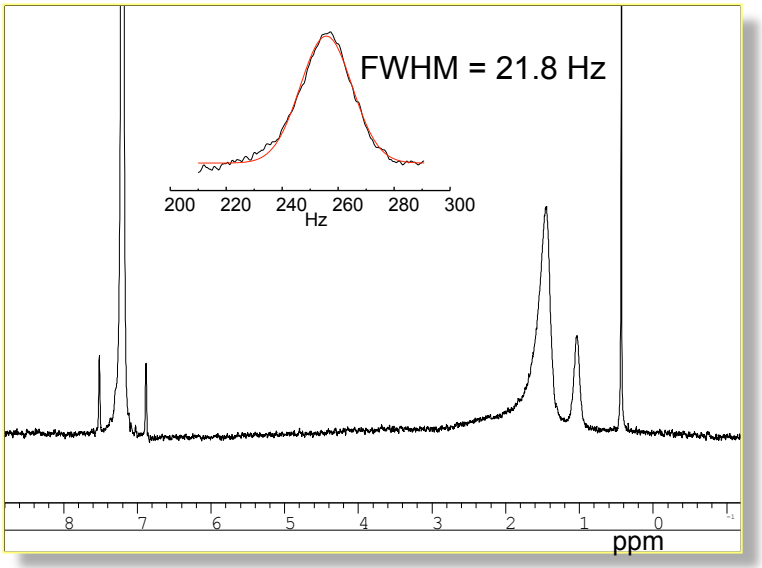

^{1}H NMR (250 MHz, C_6D_6)

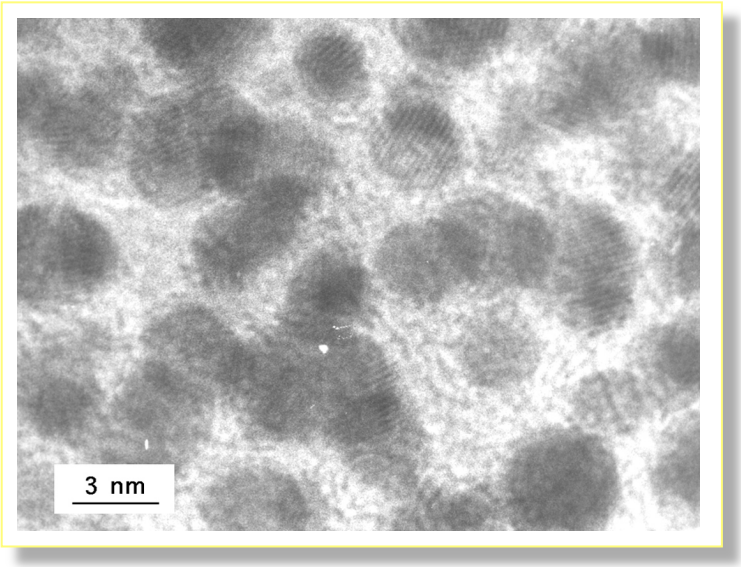

HRTEM

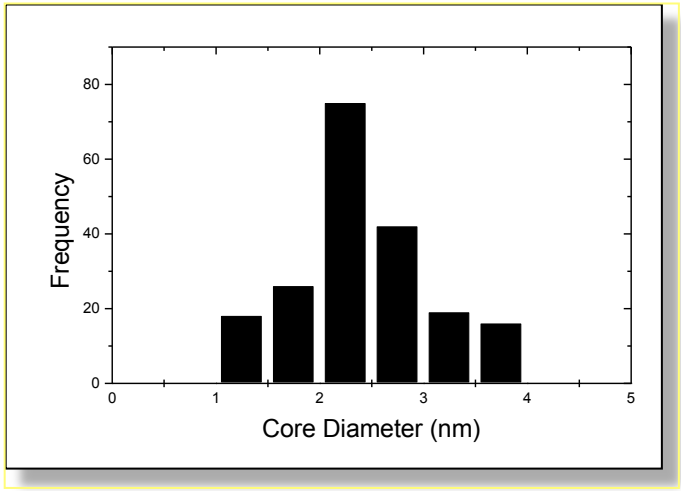

Core size histogram: core diameter 2.2 ± 0.4 nm

MPC-C12

$Au_{116}(SR)_{50}$ (MW=)

MPC-C12 - TGA Analysis

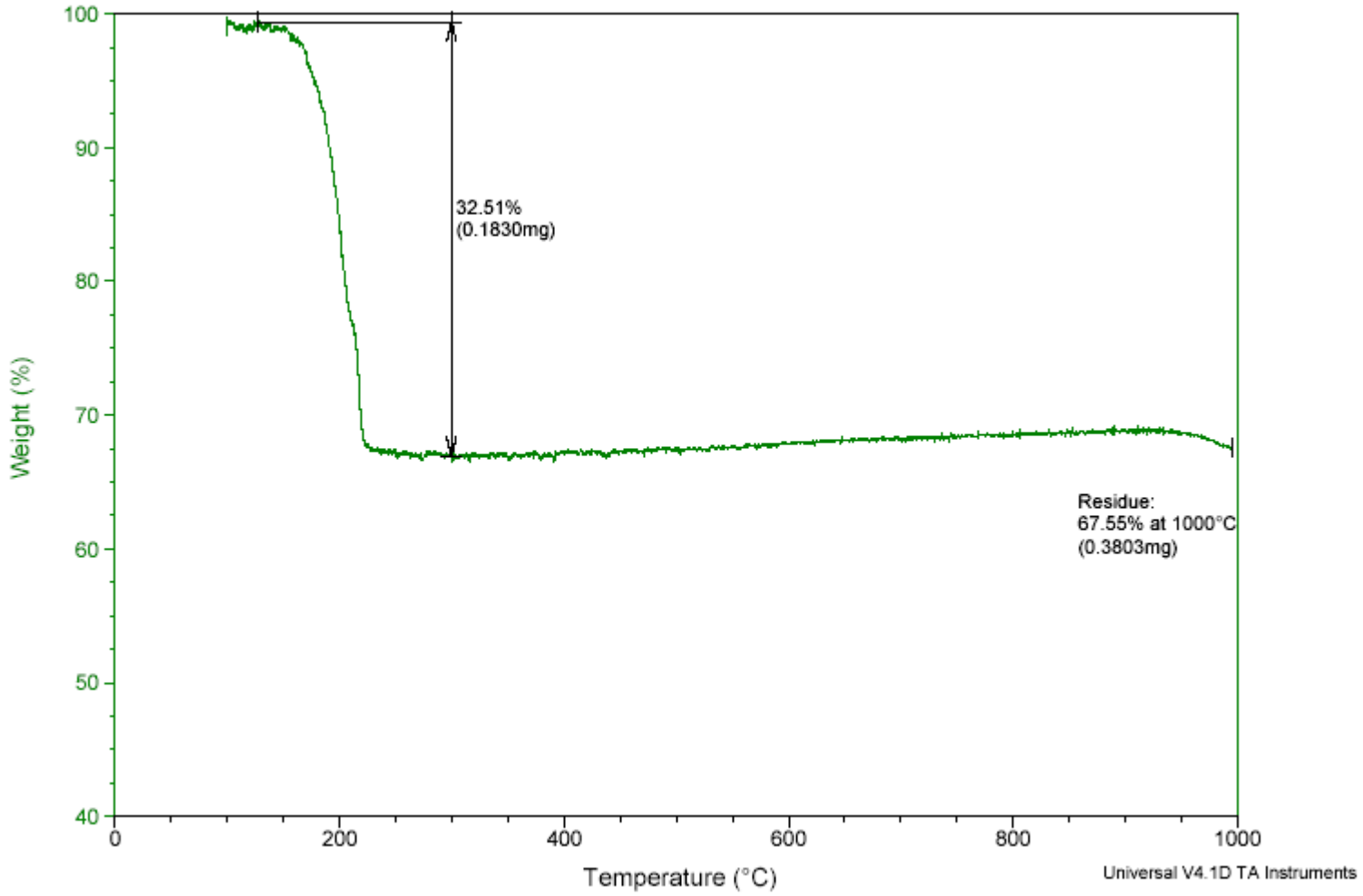

Water soluble nanoparticles

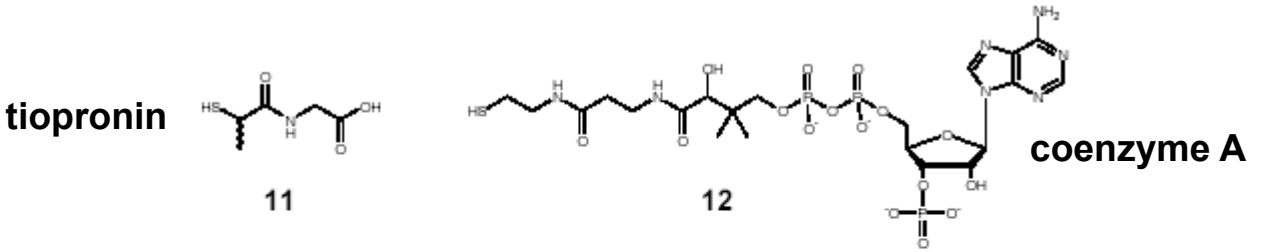

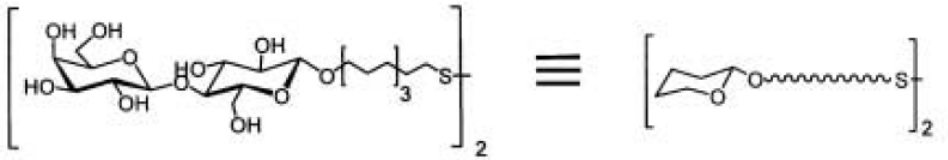

Lactose neoglycoconjugate

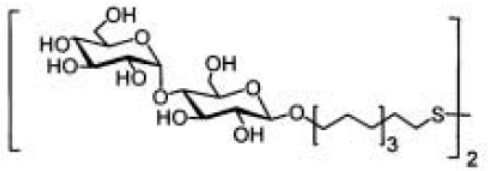

Maltose neoglycoconjugate

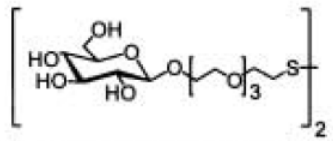

Glucose neoglycoconjugate

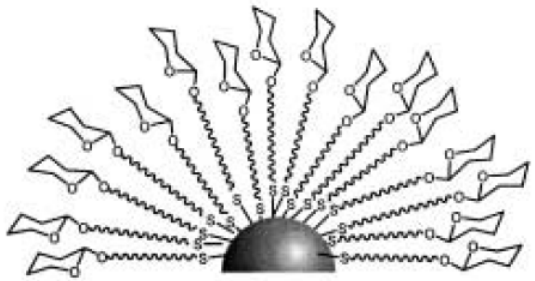

lacto-GNP
malto-GNP
gluco-GNP

Water soluble nanoparticles

$PEG_{5000}SH$

21

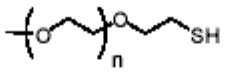

22a n = 1
22b n = 2
22c n = 3

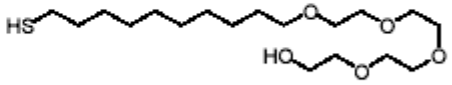

23

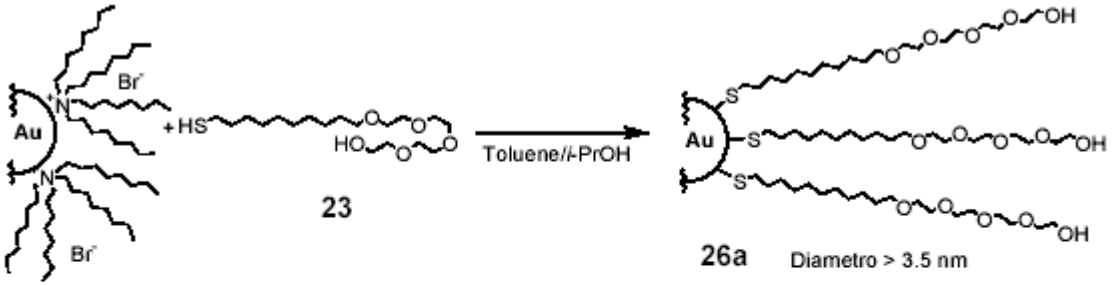

25 23 **26a** Diametro > 3.5 nm

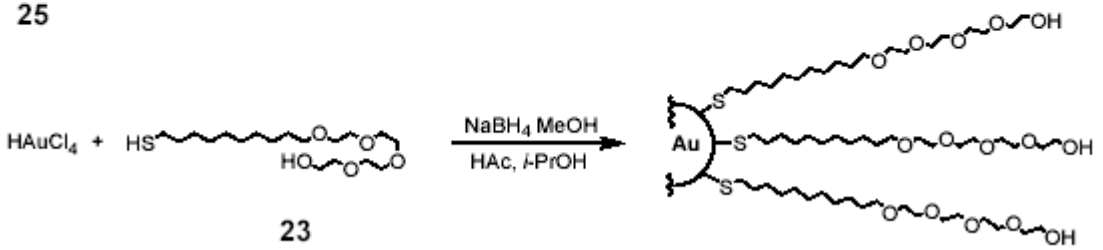

23 **26b** Diametro < 3.5 nm

Water soluble nanoparticles

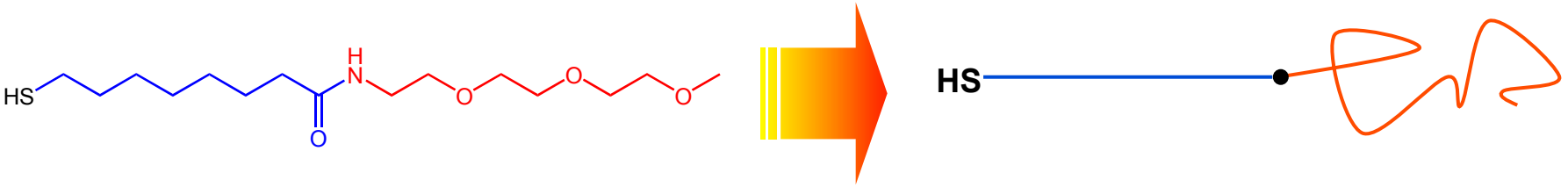

The hydrocarbon chain ensures the formation of a compact and tidy monolayer near the surface of the nanoparticle metal core

The polyether chain, even of short length, ensures MPCs solubility in water and polar solvents

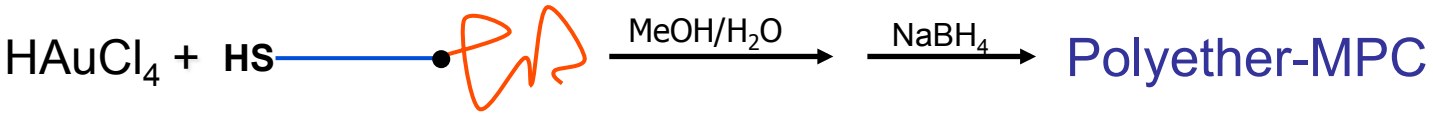

Homogeneous phase synthesis

Quantitative conversion of $HAuCl_4$

Diameter of the gold core 1.5 - 4.2 nm

Strong influence of the reduction rate

Pengo, P; Polizzi, S.; Battagliarin, M.; Pasquato, L.; Scrimin, P. *J. Mater. Chem.* **2003**, *13*, 2471-2478.

MPC-C8-TEG Characterization

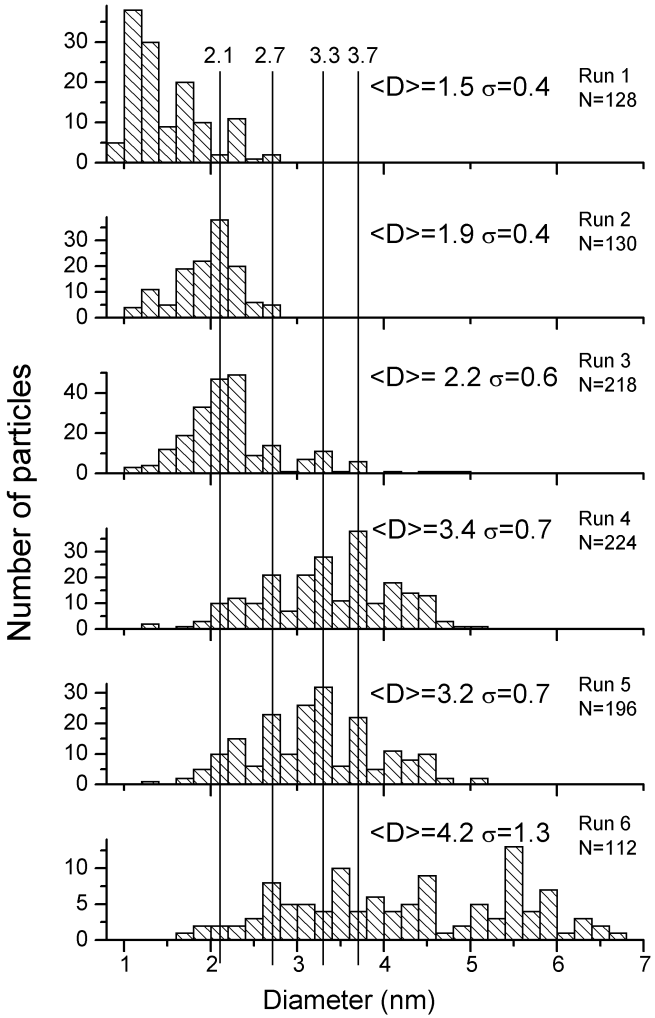

Increasing Gold / thiol ratio

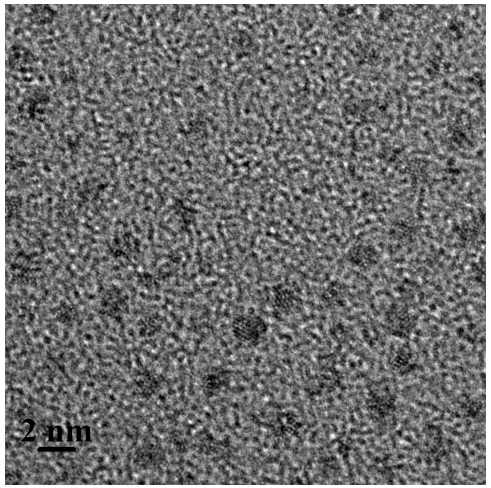

TEM image of MPCs obtained with a 1/3 gold/thiol molar ratio, $NaBH_4$ added in 10 sec.

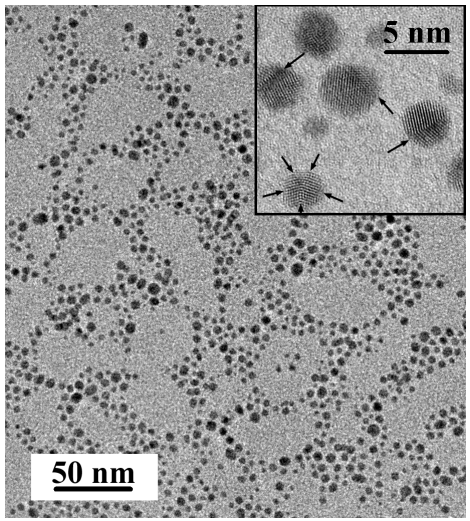

TEM image of MPCs obtained with a 3/1 gold/thiol molar ratio, adding $NaBH_4$ in 30 minutes

Thiolate Ligands for Synthesis of Water-Soluble Gold Clusters

C. J. Ackerson, P. D. Jadzinsky, R. D. Kornberg **J. AM. CHEM. SOC. 2005**, 127, 6550-6551

Table 1. Water-Soluble Thiolates and Their Ability to Passivate Gold Clusters

compound name	published synthesis	diameter (nm)[k]	soluble product	stability	synthetic method[a]	behavior in HD–PAGE gel
3-mercaptopropionic acid	ref 21	undetermined[j]	yes	days to weeks	Brust	did not enter matrix in HD or LD−PAGE[i]
4-mercaptobutyric acid	no	4.0 ± 1.2	yes	weeks	Brust	not tested
3-mercapto-1,2-propanediol	ref 14[b]	4.7 ± 1.2	yes	days	Brust	single diffuse band in HD−PAGE
cysteine	ref 12[c]	1.6 ± 0.3	yes	days	Brust[f]	entered gel matrix as single band; stalled; single band in LD−PAGE
methionine	no	2.4 ± 1.0	yes	weeks	Hutchison	did not enter matrix in HD or LD−PAGE
thiomalate	ref 13[d]	2.1 ± 1.4	yes	weeks	Brust	single tight band surrounded by large halo
2-mercaptobenzoic acid	no	2.1 ± 0.9	yes	minutes	Brust	did not enter matrix in HD or LD−PAGE
3-mercaptobenzoic acid	no	1.6 ± 0.6	yes	days	Brust	did not enter matrix; single band in LD−PAGE
4-mercaptobenzoic acid	ref 7[e]	1.8 ± 0.4	yes	months	Brust	2 tight bands
tiopronin	ref 9	1.9 ± 0.7	yes	months	Brust[f]	single diffuse pink band in HD or LD−PAGE
selenomethionine	no	1.6 ± 0.4	yes	days	Hutchison	did not enter matrix in HD or LD−PAGE
1-thio-β-D-glucose	no	2.1 ± 0.5	yes[g]	months	Brust[f]	single band in LD−PAGE
glutathione	ref 8	1.4 ± 0.4	yes	months	Brust	5 bands
ITCAE pentapeptide[h]	no	1.4 ± 0.4	yes	days	Hutchison	not tested

[a] Brust synthesis was in 1:1 water:methanol with a 3:1 thiolate:gold ratio. Typical concentrations were 10 mM gold and 30 mM thiolate. A 5-fold molar excess of $NaBH_4$ in a volume of water ~10% of the reaction volume was added to complete the cluster formation. Reactions denoted Hutchison were performed as described (ref 5). [b] A 1:1 ratio of thiolate:Au(III) and a 9-fold BH_4^- excess. [c] Cystine was used as the starting material to create cysteine MPCs. [d] Highest organothiolate:Au(III) ratio used was 5:2, with equimolar $NaBH_4$ to $HAuCl_4$, likely resulting in incomplete reduction. [e] A 1.8:1 thiolate:Au(III) ratio was used. [f] These compounds failed to form soluble products in 1:1 water:methanol, but did so under similar conditions in 6:1 methanol:acetic acid. [g] This compound formed product that remained in suspension following low-speed centrifugation, indicating cluster formation, but failed to redissolve after methanol precipitation; this product was not repeatably precipitable in methanol, but could be purified from starting materials by gel filtration and, otherwise, behaved as a stable water-soluble MPC. [h] The pentapeptide had the sequence Ile-Thr-Cys-Ala-Glu. [i] LD−PAGE was a standard 12% SDS−PAGE gel. [j] Particles form aggregates within which individual particle diameters cannot be measured. [k] See Supporting Information for images, histograms, and further analysis.

Nanoparticles - functionalization

- **synthesis using a mixture of thiols**

  thiols should survive under the reaction conditions

- **Ligand exchange**

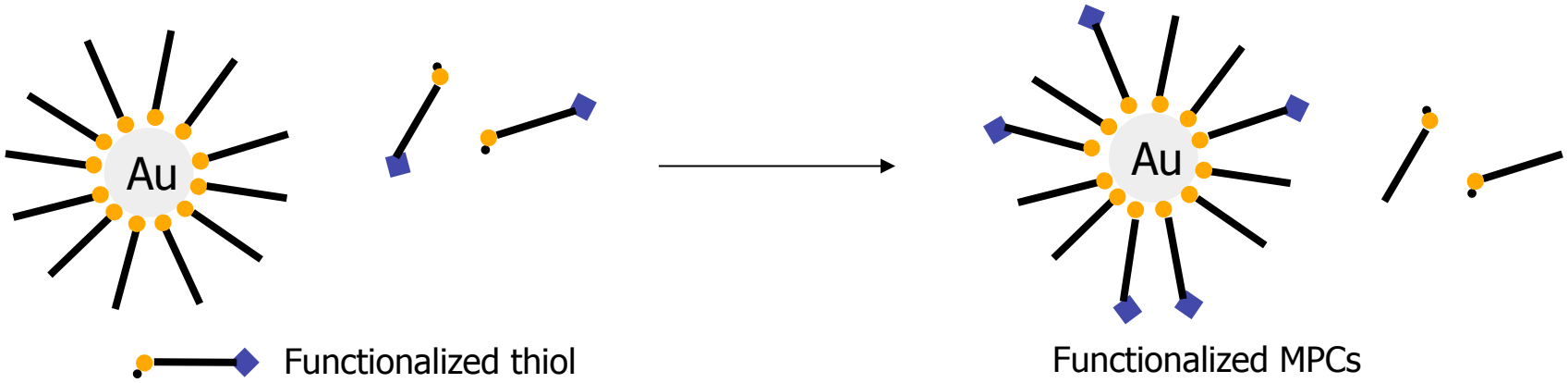

Hostetler, M. J.; Green, S. J.; Murray, R. W. *J. Am. Chem. Soc.,* **1996**, *118*, 4212 - 4213.

Nanoparticles - functionalization

Synthesis of the monolayer with a blend of thiols

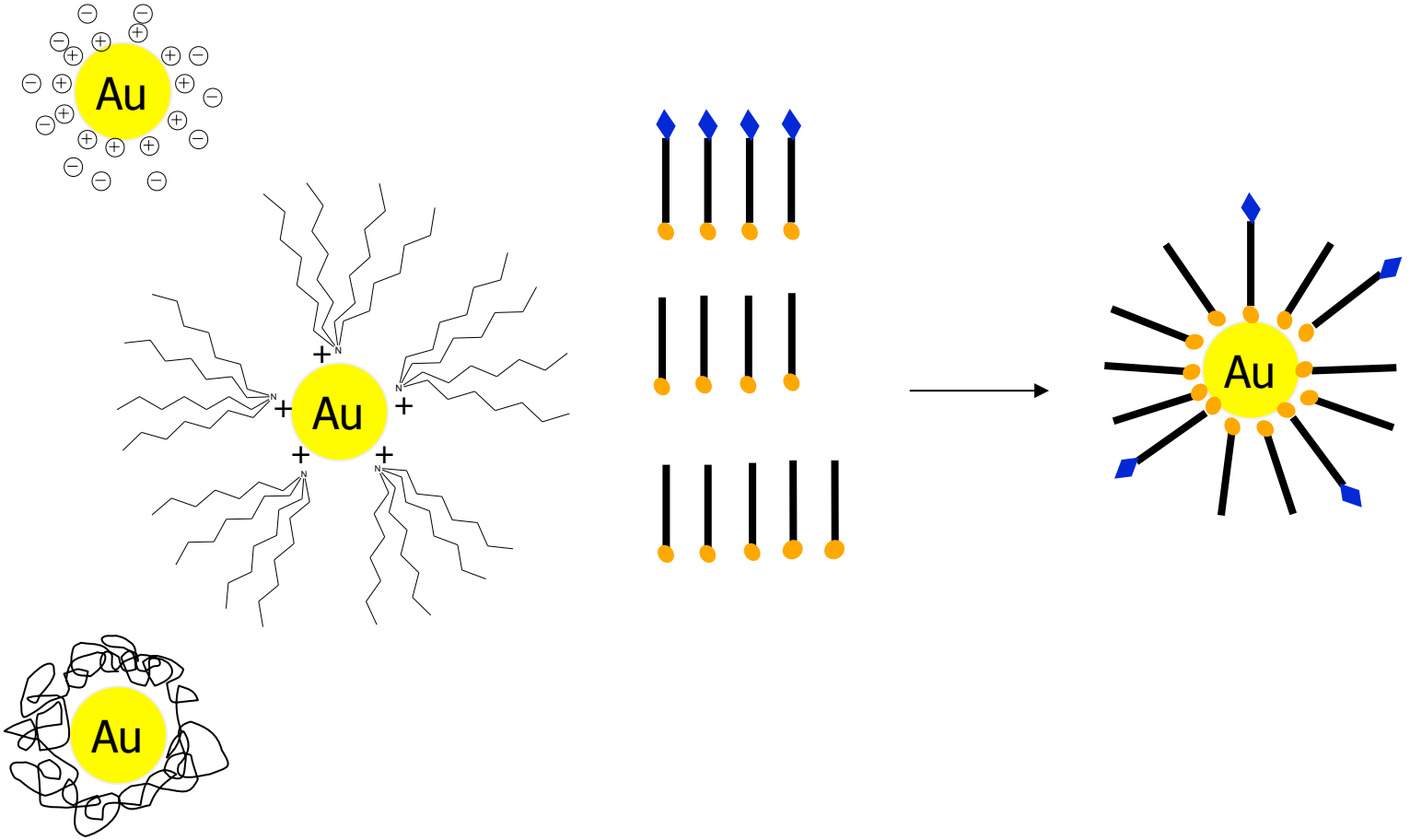

Nanoparticles - functionalization

Covalent Modification

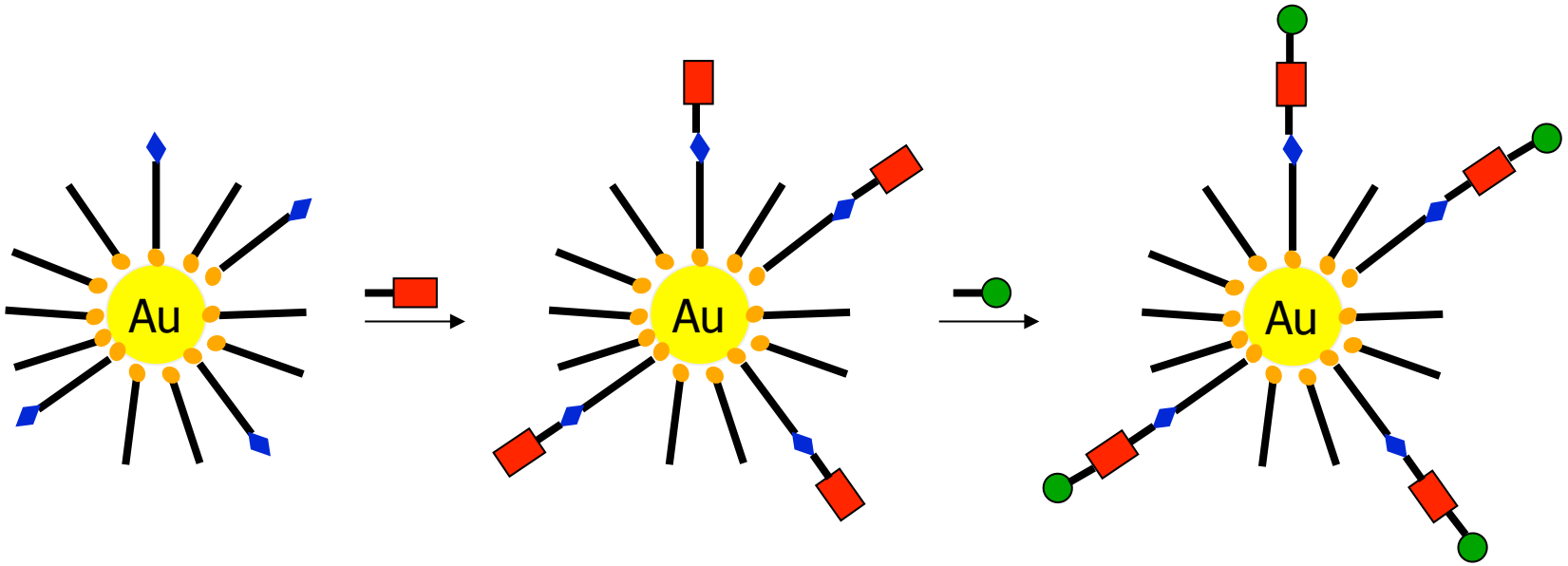

Templeton, A. C.; Hostetler, M. J.; *Warmoth, E. K.; Chen, S.; Hartshorn, C. M.; Krishnamurthy, V. M.; Forbes, M. D. E.; Murray, R. W. J. Am. Chem. Soc.* ***1998****, 120*, 4845-4849.

Mixed Self-Assembled Monolayers

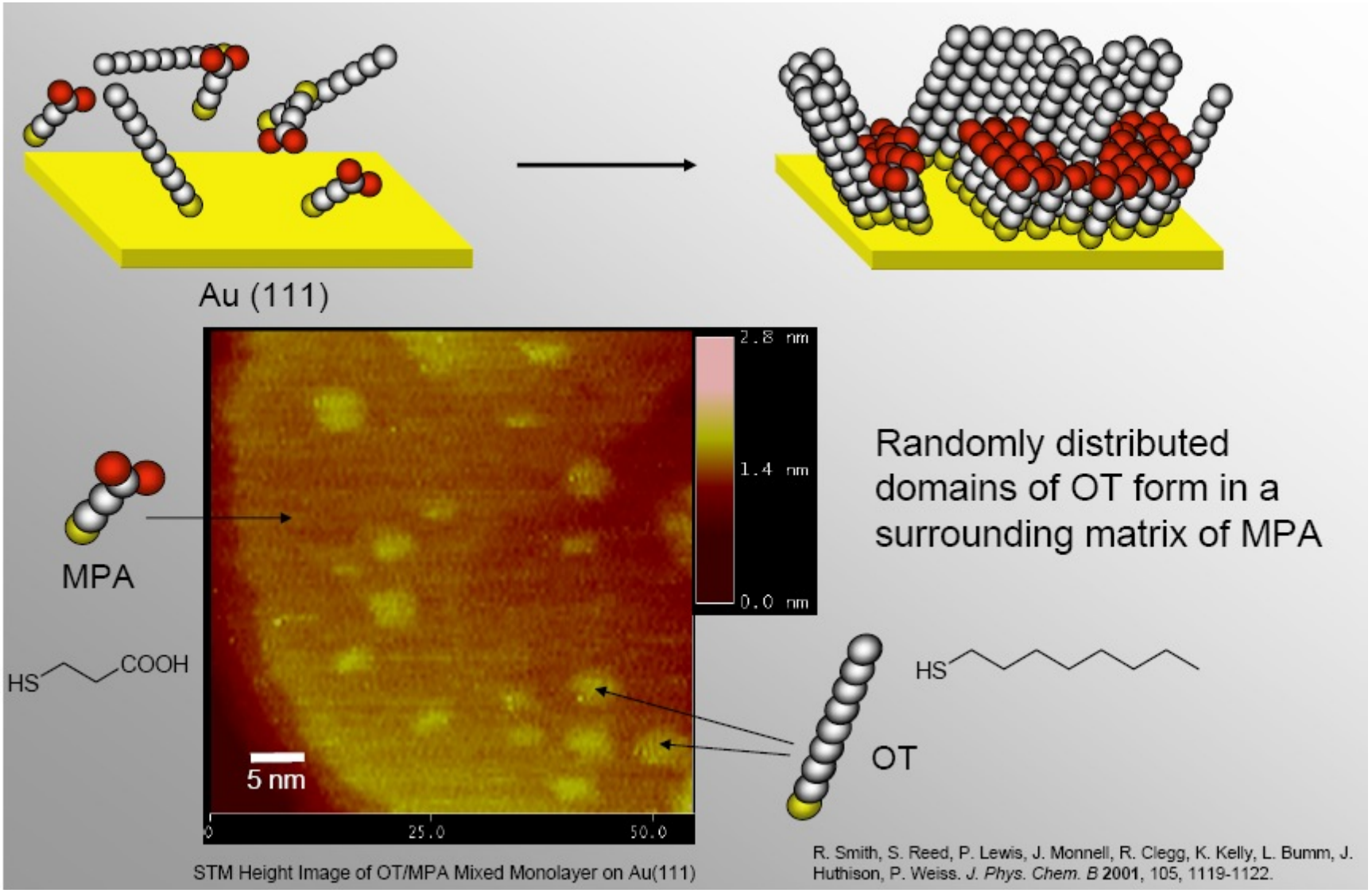

STM Height Image of OT/MPA Mixed Monolayer on Au(111)

R. Smith, S. Reed, P. Lewis, J. Monnell, R. Clegg, K. Kelly, L. Bumm, J. Huthison, P. Weiss. *J. Phys. Chem. B* **2001**, 105, 1119-1122.

Ordered Domains on NPs

Quantitative Analysis of Scanning Tunneling Microscopy Images of Mixed-Ligand-Functionalized Nanoparticles

Fabio Biscarini,*[,†] Quy Khac Ong,[‡] Cristiano Albonetti,[§] Fabiola Liscio,[∥] Maria Longobardi,[⊥] Kunal S. Mali,[#] Artur Ciesielski,[○] Javier Reguera,[‡] Christoph Renner,[⊥] Steven De Feyter,[#] Paolo Samorì,[○] and Francesco Stellacci[‡]

Langmuir 2013, 29, 13723−13734

topographical power spectral density (PSD)

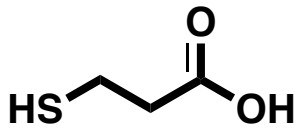

MPA

Octanethiol

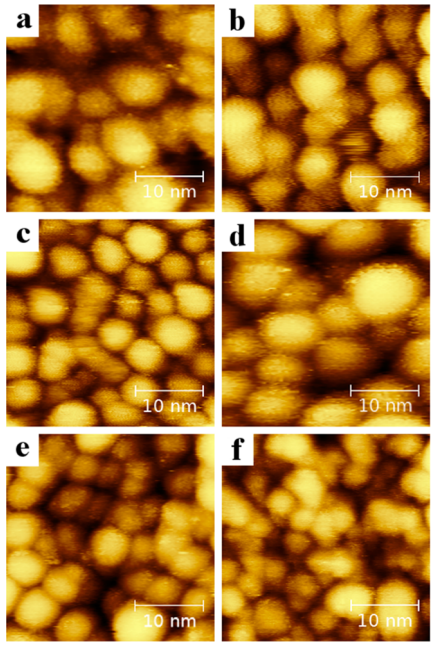

Jackson, A. M et al *Nat. Mat.,* **2004**, *3*, 330; Jackson, A. M. et al *J. Am. Chem. Soc.*, **2006**, *128*, 11135;

Determination of monolayer-protected gold nanoparticle ligand–shell morphology using NMR

Xiang Liu[1], Miao Yu[1], Hyewon Kim[2], Marta Mameli[1] & Francesco Stellacci[1]

Nature Commun. 2012

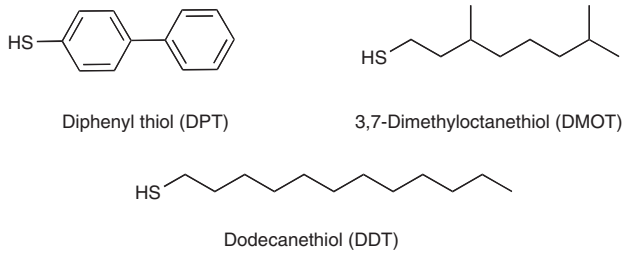

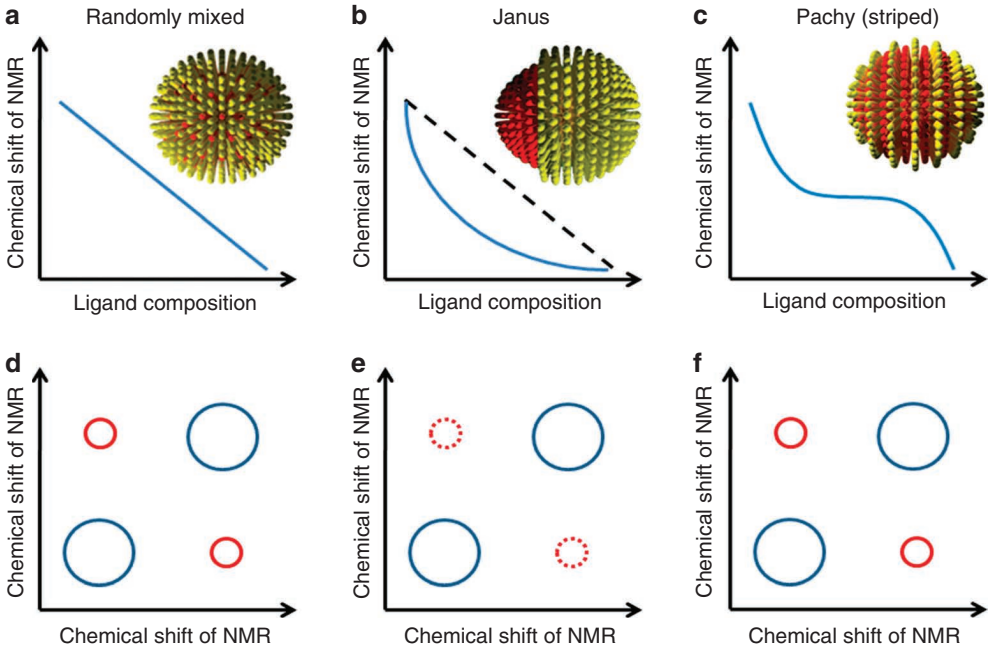

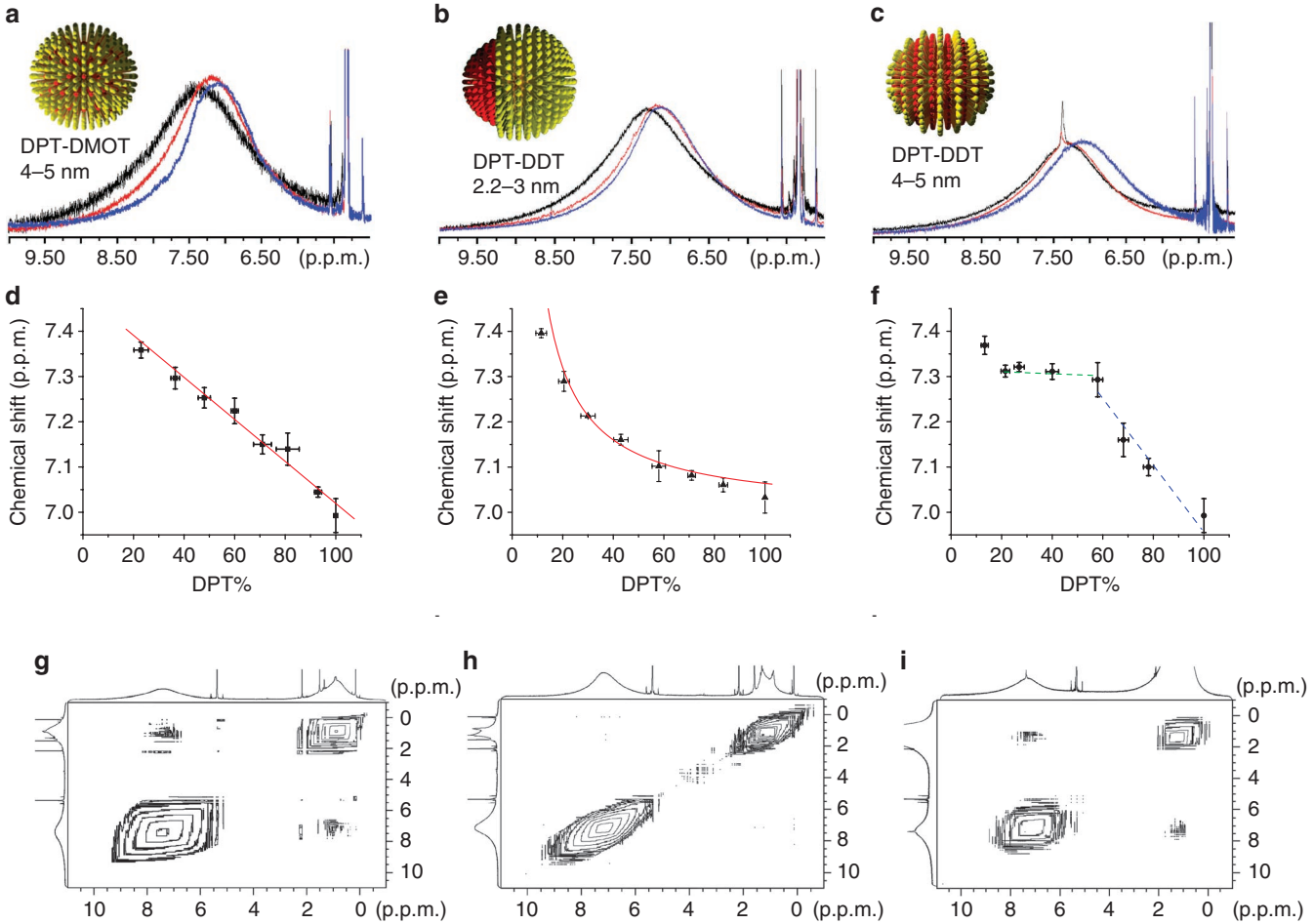
a
DPT-DMOT
4–5 nm
9.50 8.50 7.50 6.50 (p.p.m.)
b
DPT-DDT
2.2–3 nm
9.50 8.50 7.50 6.50 (p.p.m.)
c
DPT-DDT
4–5 nm
9.50 8.50 7.50 6.50 (p.p.m.)
d
Chemical shift (p.p.m.)
7.4 7.3 7.2 7.1 7.0
0 20 40 60 80 100
DPT%
e
Chemical shift (p.p.m.)
7.4 7.3 7.2 7.1 7.0
0 20 40 60 80 100
DPT%
f
Chemical shift (p.p.m.)
7.4 7.3 7.2 7.1 7.0
0 20 40 60 80 100
DPT%
g
(p.p.m.)
0 2 4 6 8 10
10 8 6 4 2 0 (p.p.m.)
h
(p.p.m.)
0 2 4 6 8 10
10 8 6 4 2 0 (p.p.m.)
i
(p.p.m.)
0 2 4 6 8 10
10 8 6 4 2 0 (p.p.m.)

Scanning tunneling microscopy and small angle neutron scattering study of mixed monolayer protected gold nanoparticles in organic solvents†

Mauro Moglianetti,‡[a] Quy Khac Ong,‡[a] Javier Reguera,‡[a] Kellen M. Harkness,[a] Marta Mameli,[a] Aurel Radulescu,[b] Joachim Kohlbrecher,[c] Corinne Jud,[d] Dmitri I. Svergun*[e] and Francesco Stellacci*[a]

Chem. Sci., 2014, **5**, 1232

Table 1 Contrasts of the phases in the hybrid particles (in units 10^{-6} $Å^{-2}$) (a) and discrepancy of the fits (b)

(a) Contrasts	C6 : d-C12	d-C6 : C12
Phase 1 : gold	1.4	1.4
Phase 2 : C12	2.5	−3.4
Phase 3 : C6	−3.4	1.9
(b) Discrepancy values[a]	**C6 : d-C12**	**d-C6 : C12**
Striped particle	1.2	1.1
Janus particle	15.2	7.7
Randomly mixed particles	1.8	4.2

[a] Chi squared.

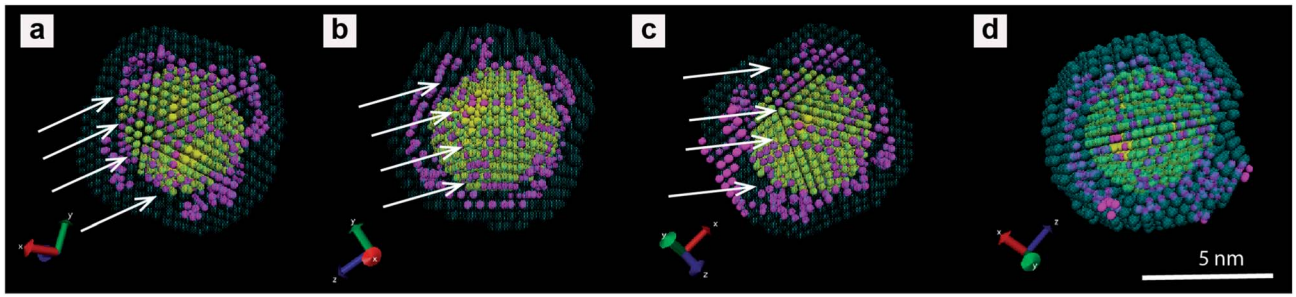

Fig. 5 Four different projections of a typical multiphase 3D low-resolution model of the C6 : C12 particles obtained from the fitting of the SANS data. Yellow beads indicate the gold nanoparticle core regions, the magenta beads represent the C6 moiety, and the cyan beads the C12 moiety. The beads in the model act as low-resolution place holders to depict the space occupied by the gold, C6 and C12 moieties. The image (d) on the right has the cyan beads in a lower transparency mode to highlight the C12 moieties. The C6 regions form elongated domains within the bulk of the C12 phase in excellent agreement with the model of striped nanoparticles. Scale bar, 5 nm. The arrows indicate elongated C6 domains that roughly align along a preferential direction. These features would provide aligned domain boundaries in the STM images (the arrows are spaced by about 1 nm).

Characterization of Ligand Shell for Mixed-Ligand Coated Gold Nanoparticles

Quy Ong,[†] Zhi Luo,[†] and Francesco Stellacci*

DOI: 10.1021/acs.accounts.7b00165
Acc. Chem. Res. 2017, 50, 1911−1919

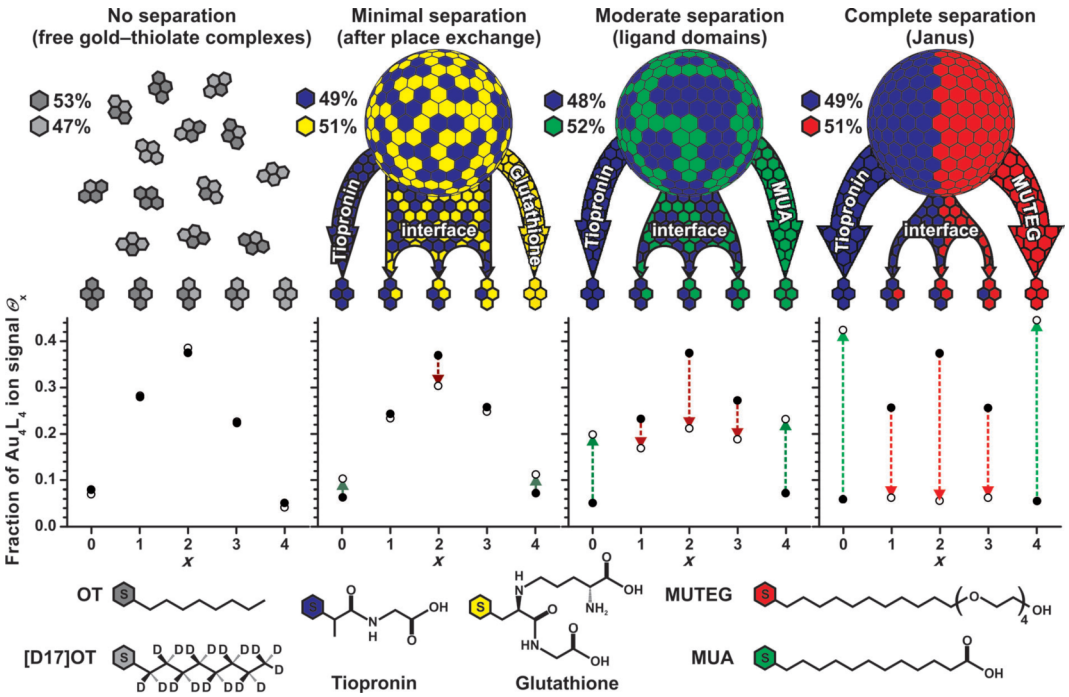

Figure 5. MALDI-MS investigation of molecular phase separation in mixed ligand coated NPs. Among the fragments of Au-thiol complexes caused by the MALDI process, only the Au_4L_4 ion species are analyzed since they are the most abundant fragments. For a binary ligand coated gold NP, 5 combinations of Au_4L_4 will be found and they are labeled from 0 to 4 in the *x*-axis of the plots. In other words, if the ligand shell contains a binary mixture of thiols A and B, the 5 species of the Au_4L_4 complexes analyzed are $Au_4A_{4-x}B_x$ (x = 0, 1, 2, 3, 4). Their corresponding abundances obtained experimentally from 4 different types of mixed ligand coated gold NPs are illustrated by open circles. The binomial distribution, which corresponds to random morphology, is presented by filled black dots. The deviations from the binomial distribution, represented by an arrow for each species, indicate the presence of molecular phase separation in the ligand shell that ranges from completely mixed, to patchy domains, and to the Janus structure. The ligand shell compositions of the 4 investigated particles are octanethiol (OT)/deuterated OT, tiopronin/glutathione, 11-mercaptoundecanoic (MUA)/glutathione, tiopronin/mercaptoundecyltetraethylene glycol (MUTEG), respectively. Reproduced with permission from ref 35. Copyright 2011 Wiley-VCH.

Entropy-Mediated Patterning of Surfactant-Coated Nanoparticles and Surfaces

Chetana Singh,[1] Pradip K. Ghorai,[1] Mark A. Horsch,[1] Alicia M. Jackson,[2] Ronald G. Larson,[1]
Francesco Stellacci,[2] and Sharon C. Glotzer[1,3,*]

PRL 99, 226106 (2007)

AuNP 7.0 nm in diameter

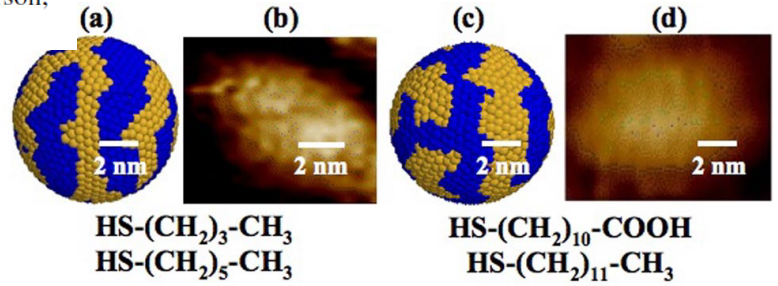

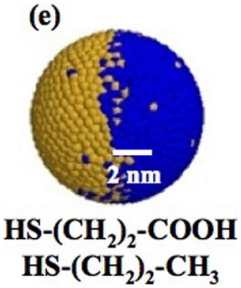

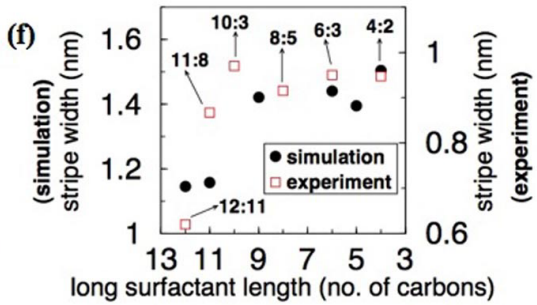

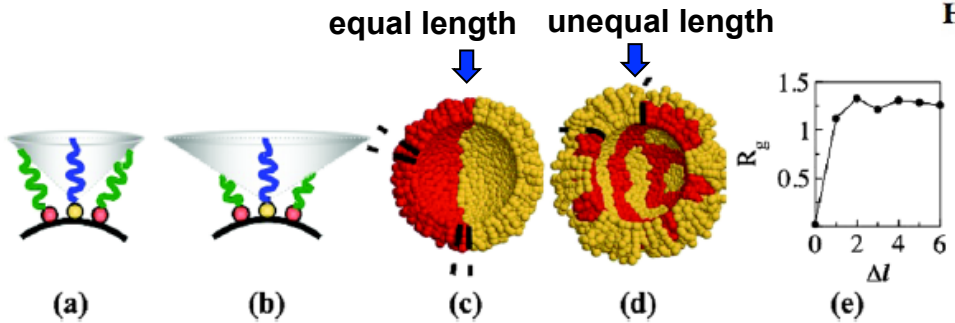

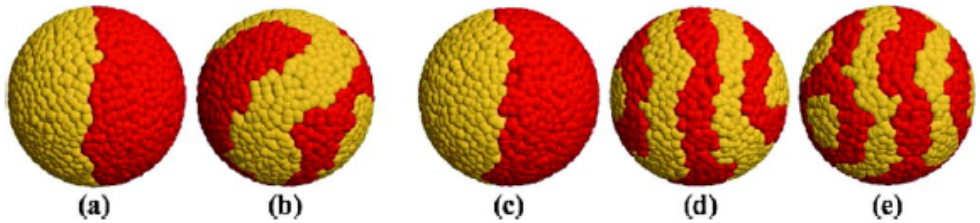

(a) Length ratio 4:4, equal bulkiness. (b) Length ratio 6:6 with one surfactant (yellow heads) having a bulkier tail group. (c)–(e) Length ratios 4:6, 4:7 and 4:13, respectively, with equal bulkiness.

morphologies of mixed-monolayers

Entropy-Mediated Patterning of Surfactant-Coated Nanoparticles and Surfaces

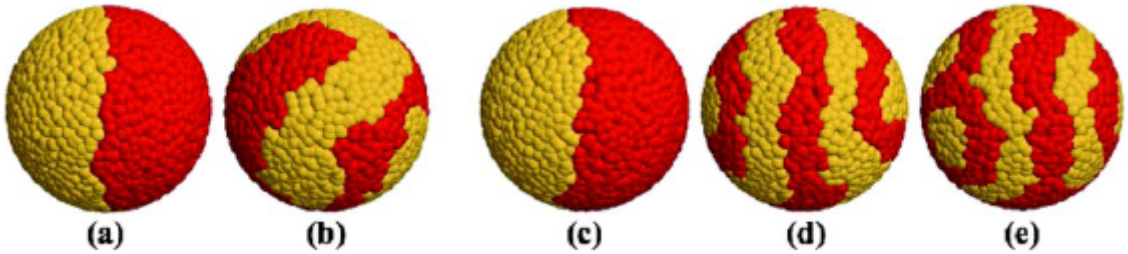

same length

same length different tail group bulkiness

4:6

4:7

4:13

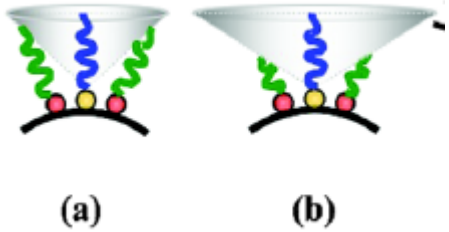

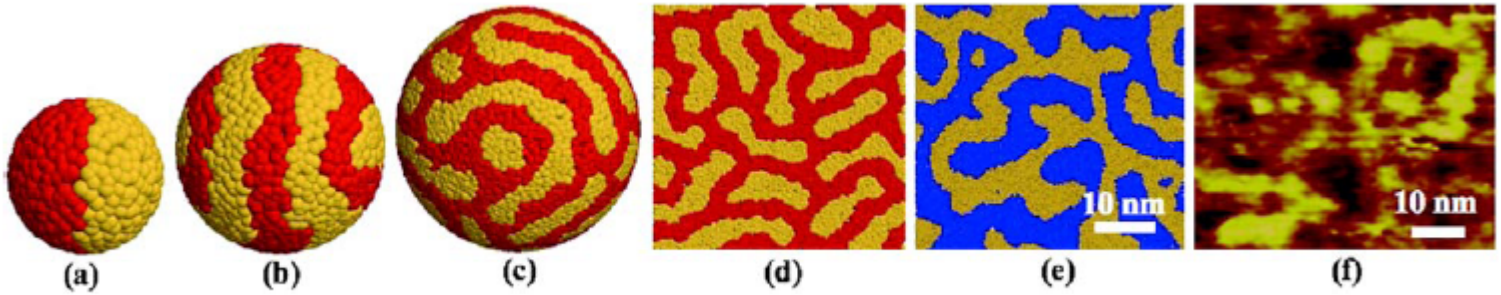

surfaces with varying degrees of curvature, different length C4:C6, same end group.

mixed-monolayer properties

tuning the surface chemistry

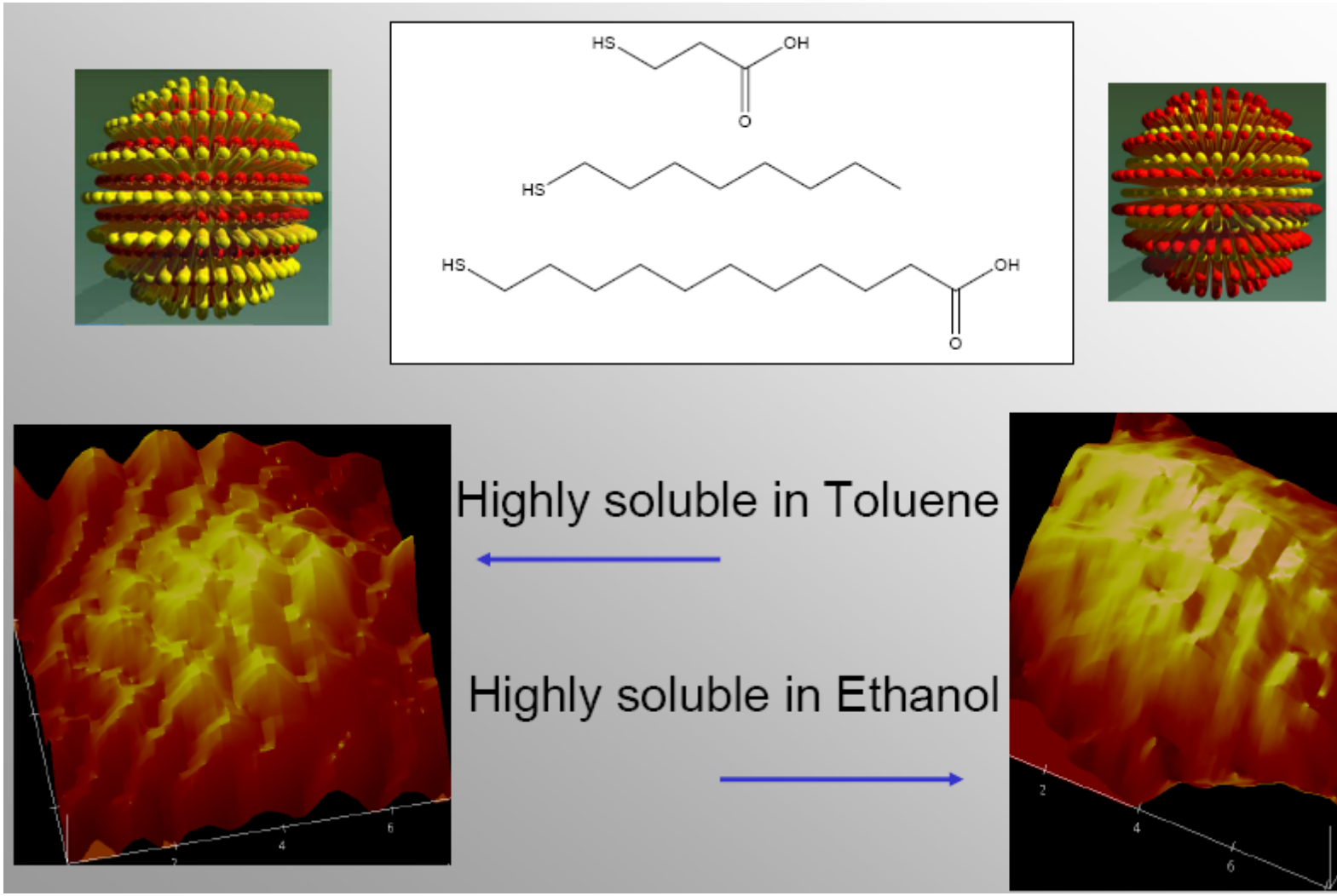

Centrone, A. et al *PNAS*, **2008**, *105*, 9886.

mixed-monolayer properties

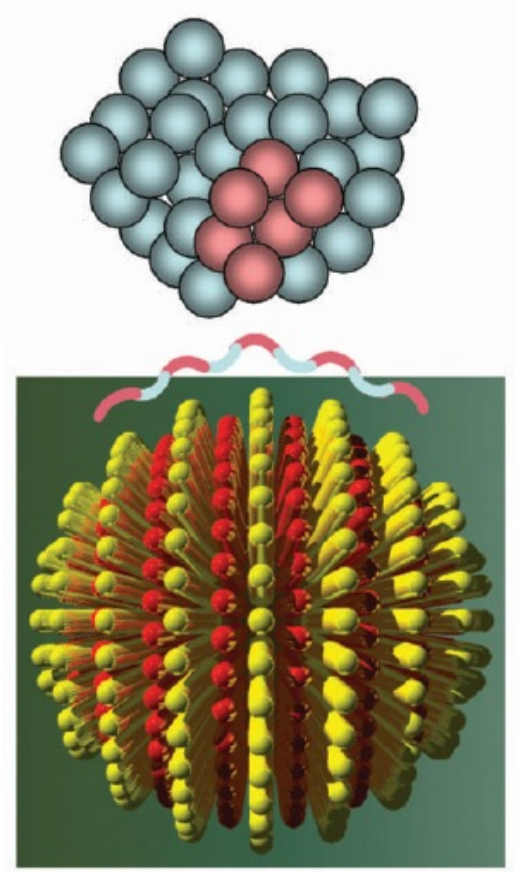

Figure 5 Schematic drawing of a generic protein (top) and a rippled nanoparticle (bottom). The pink and blue contour line on top of the nanoparticle shows the hydrophobic and the hydrophilic regions of the particle,respectively.The same colour scheme is used to show the outside shell of the chosen protein.It is evident (as the drawing is approximately to scale) how,despite the enormous conformational freedom that the proteins have,there will always be regions of attraction and regions of repulsion when interacting with nanostructured nanoparticles.

A. M. Jackson, J. W. Myerson, F. Stellacci, *Nat. Mater.* **2004**, *3*, 330-336.

protein nonspecific absorption

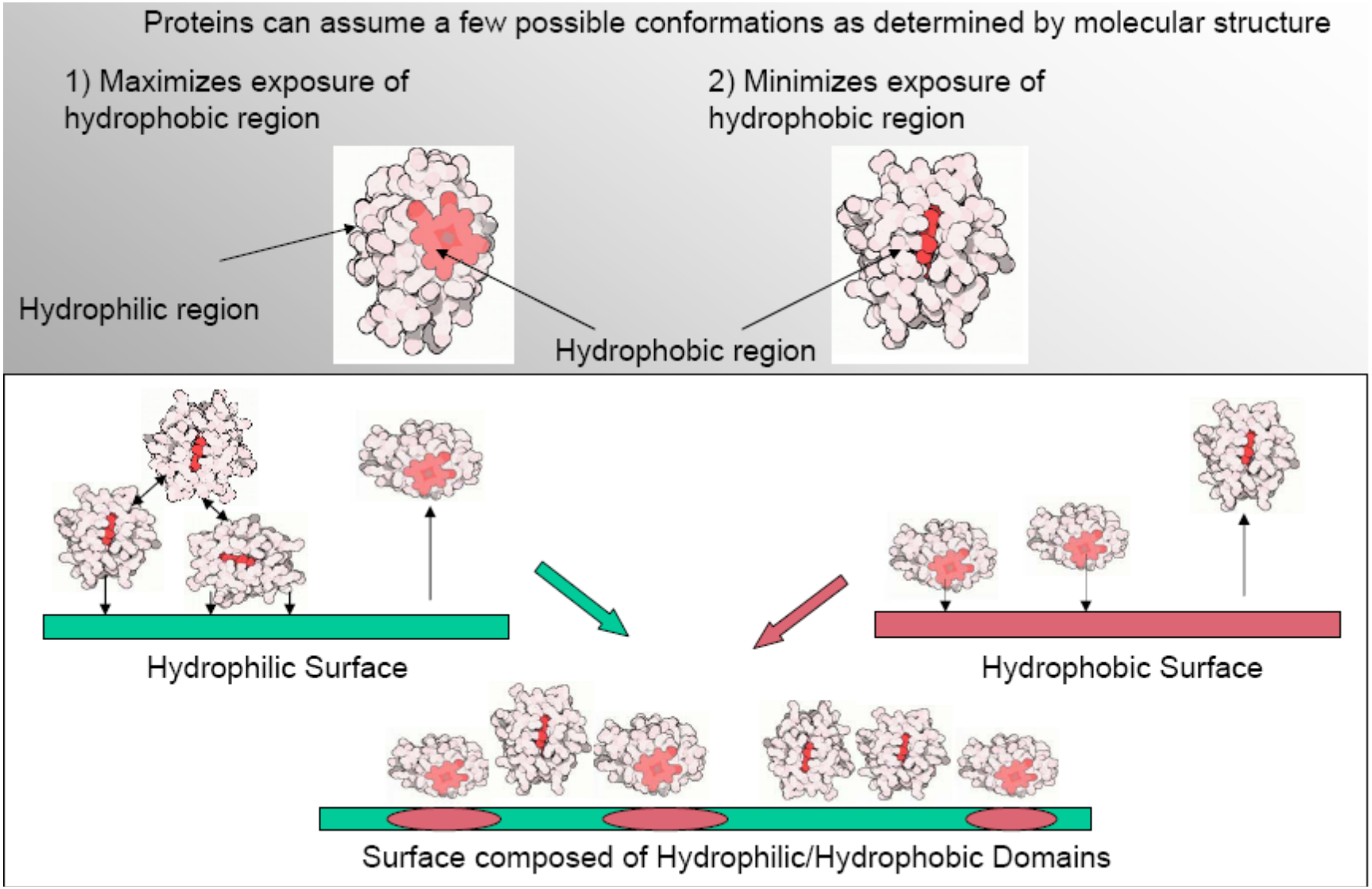

The Nano Lotus Leaf Effect

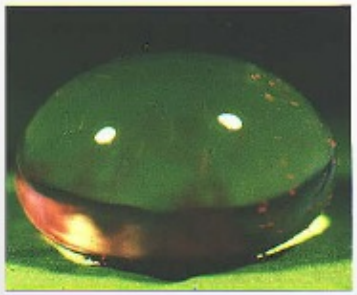

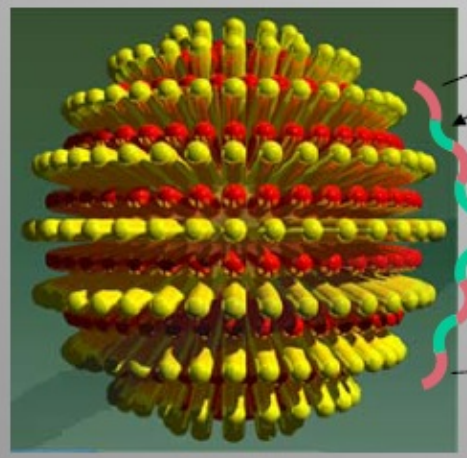

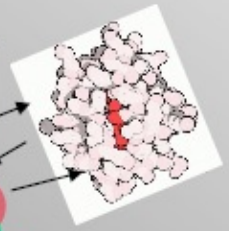

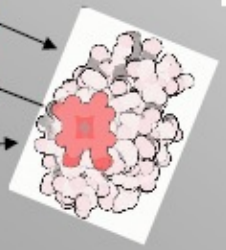

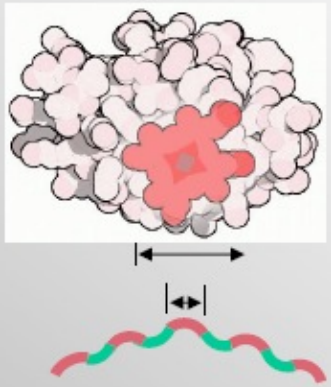

Size of hydrophobic/hydrophilic regions of protein are greater than size scale of ligand domains on the nanoparticles.

Proteins are conformationally frustrated and cannot adsorb to nanoparticle surface.

organization of mixed - monolayers

3D SAMs composed of thiols with immiscible chains

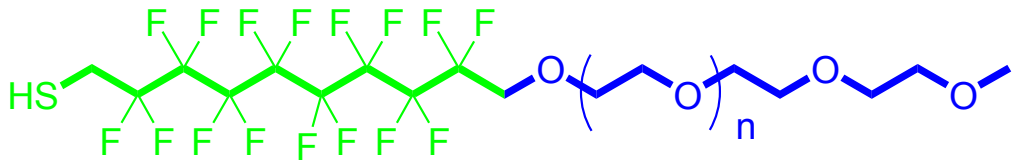

n = 8,9

HS-F8-PEG

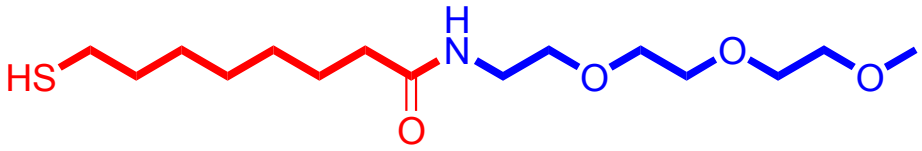

HS-C8-TEG

ESR Spectroscopy as a tool to investigate the monolayer properties

phase segregation of hydrogenated/fluorinated units

block terpolymer

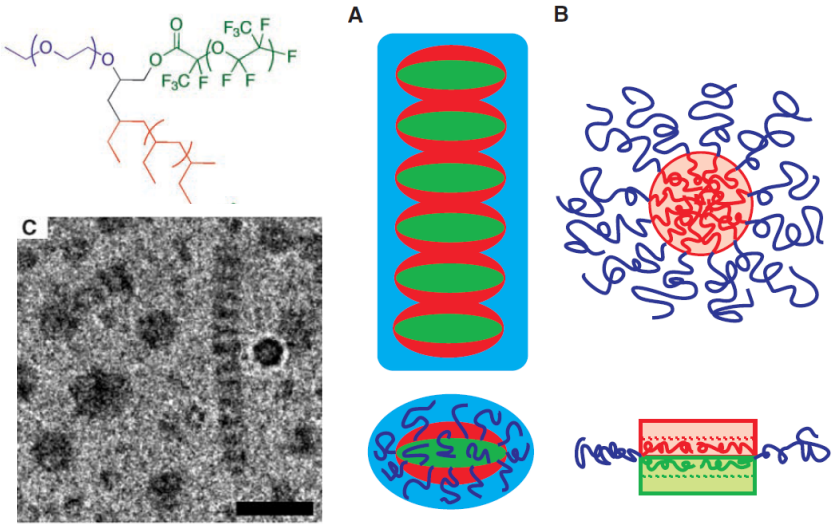

*T. P. Lodge et al. Science **2004**, 306, 98*

monolayers

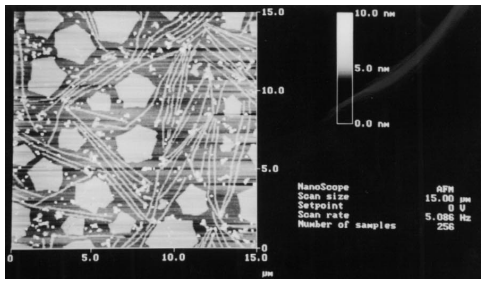

*AFM images of a mixed monolayer of 1:1 $C_{18}H_{37}SO_3Na$–$C_8F_{17}COOH$ deposited on a freshly cleaved mica surface at a compression rate of 35 cm^2 min^{-1}. Coll. Surf. A, **1999**, 157, 63–71.*

Liposomes

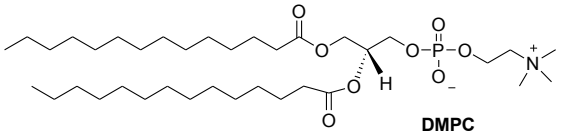

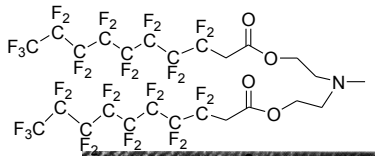

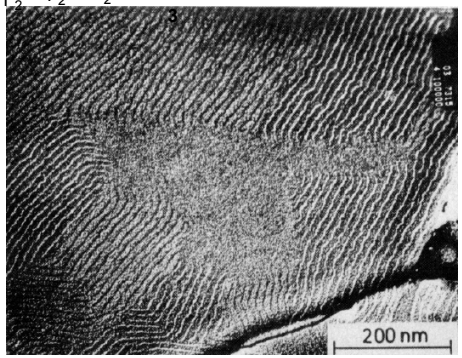

Freeze fracture electron micrograph of a phase-separated
*liposomal membrane (95 mol % **DMPC** and 5 mol % fluorinated lipid **3**. The ripple structure shows the parts of membrane composed of DMPC, surrounding a domain*
*of the fluorinated lipid (smooth surface). R. Elbert, T. Folda, and H. Ringsdorf J. Am. Chem. Soc. **1984**, 106, 7687-1692*

metal nanoparticles protected by fluorinated ligands

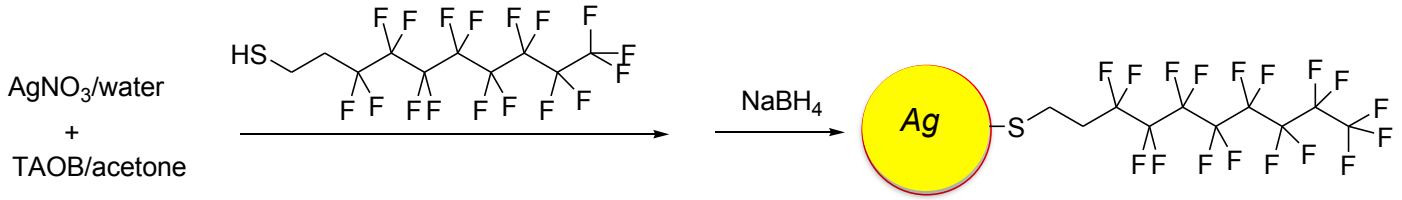

*K. P. Johnston, B. A. Korgel et al. JACS **2000**, 122, 4245.*

dispersion in acetone and liquid and sc. CO_2

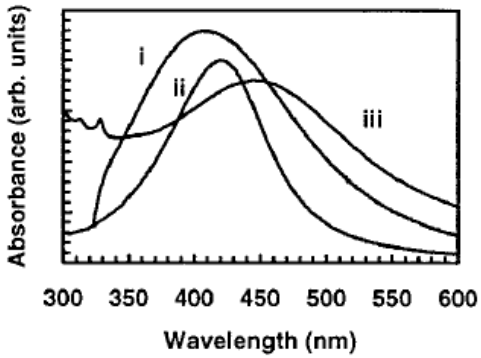

UV-visible absorbance spectra of AgNPs (i) coated with fluorinated ligands dispersed in acetone; (ii) coated with hydrocarbon ligands dispersed in hexane; (iii) coated with fluorinated ligands dispersed in sc-CO_2.

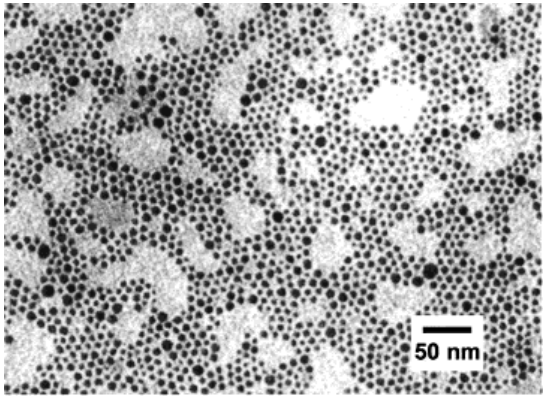

TEM image of silver nanocrystals coated with fluorinated ligands.

average size 5.5 nm

gold nanoparticles protected by fluorinated ligands

- use of commercially available F-thiols

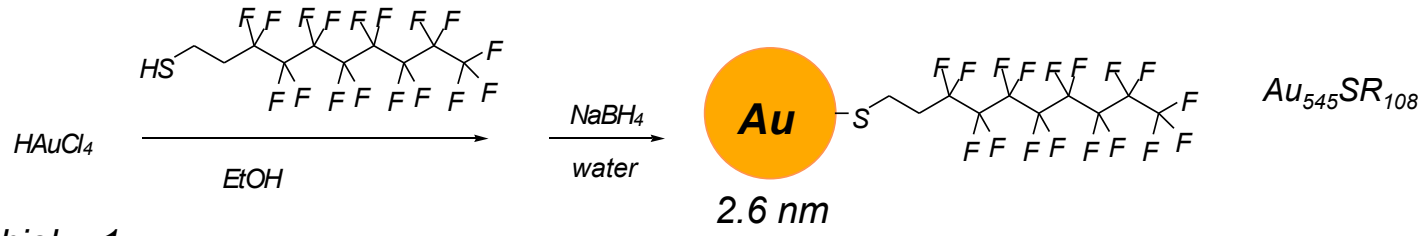

Au / thiol = 1

T. Yonezawa, et al. Langmuir, **2001**, 17, 2291-2293.

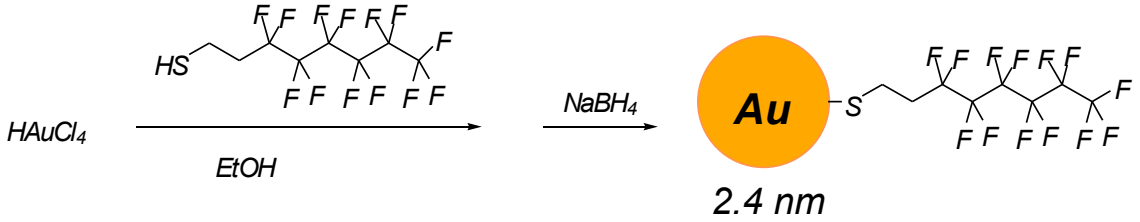

insoluble in common organic solvents
ethanol, acetone, chloroform, DMSO

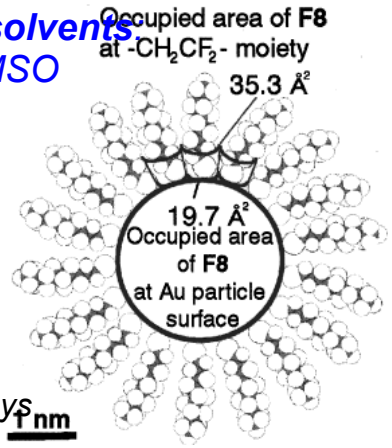

a dispersion in HCFC-225 dropcasted on a carbon-coated copper grid displays ordered hexagonal assembly

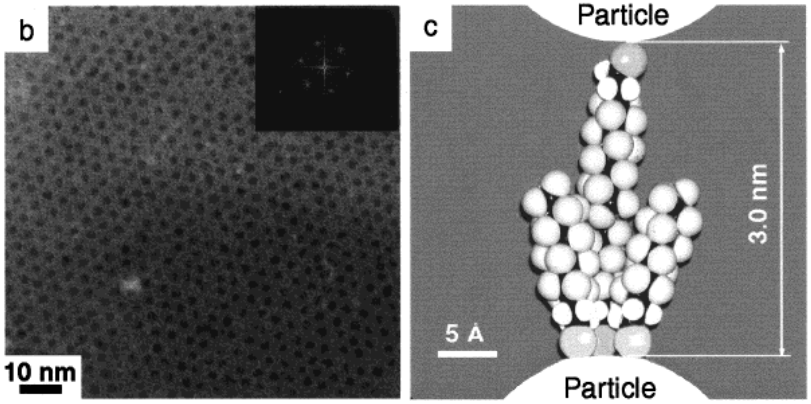

gold nanoparticles protected by fluorinated ligands

- synthesis by ligand exchange

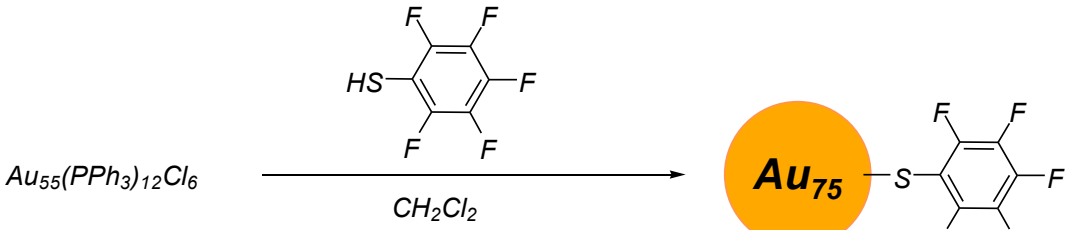

~ 1.4 nm

soluble in CH_2Cl_2, THF, DMF

- synthesis by Brust reaction

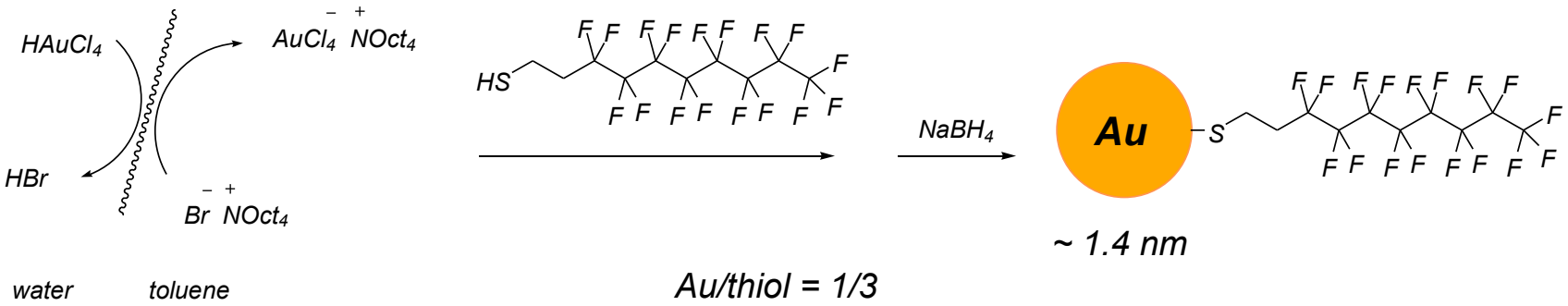

~ 1.4 nm

Au/thiol = 1/3

AuNPs soluble in non polar fluorinated solvents only

A. Dass, R. Guo, J. B. Tracy, R. Balasubramanian, A. D. Douglas, R. W. Murray Langmuir, **2008**, 24, 310-315.

- Au/thiol = 3/1 averge core diameter 2.5 nm; J. Im, A. Chandekar, J. E. Whitten Langmuir, **2009**, 25, 4288-4292.

gold nanoparticles protected by fluorinated ligands

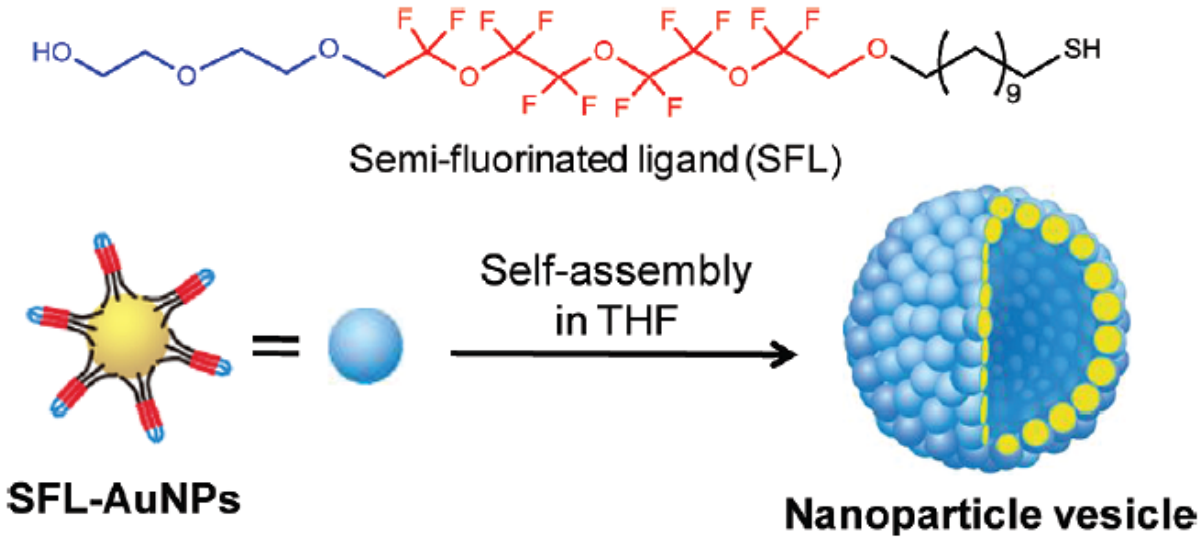

5, 10, 20 nm

the solvophobic feature of the fluorinated bundles is the driving force for NP assembly

K. Niikura et al. J. Am. Chem. Soc. ***2012****, 134, 7632.*

synthesis of water-soluble fluorinated Au NPs

Synthesis

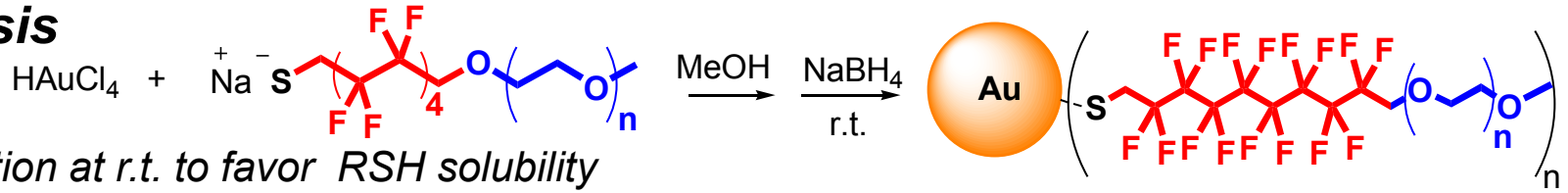

- ✧ *reaction at r.t. to favor RSH solubility*
- ■ *for n= 3, 4 and 6 NPs precipitate in MeOH, they are scarcely soluble in DCM and chloroform*

n = 3
n = 4
n = 6
n = 12,13 **NP-F8-PEG**

RSH/Au	***NP core average diameter (nm)***
0.7	*2.9*
2	*2.7*
2.5	*1.6*

average composition: $Au_{670}(SF8PEG)_{107}$

- ■ *NPs are soluble in water, methanol, DCM and chloroform*

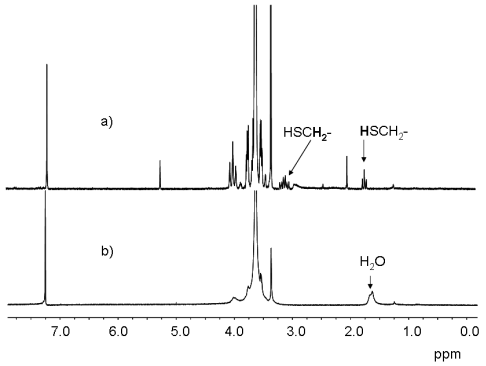

(a) ^{1}H NMR of HS-F8-PEG and (b) ^{1}H NMR of MPC-F8-PEG prepared with a thiol/Au ratio of 2:1.

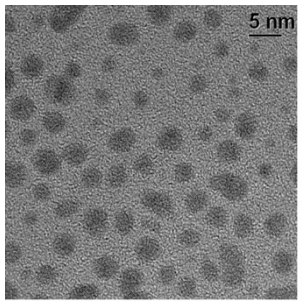

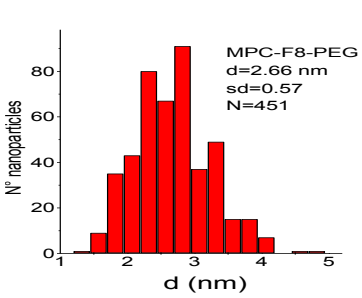

TEM image and histogram of MPC-F8-PEG.

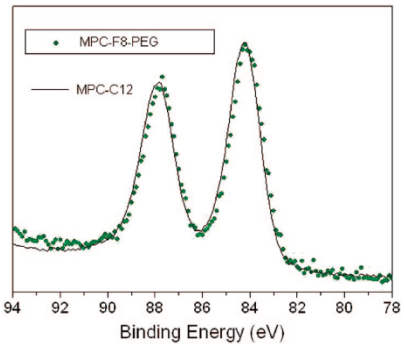

XPS Au 4f core level spectra of MPC-F8-PEG and MPC-C12.

C. Gentilini, F. Evangelista, P. Rudolf, P. Franchi, M. Lucarini, L. Pasquato J. Am. Chem. Soc. ***2008****, 130, 15678-15682.*

synthesis of Au NPs capped by a mixture of H- and F- thiolates

■ *Homogeneous phase synthesis (methanol/water) using mixtures of thiolates with **immiscible chains***

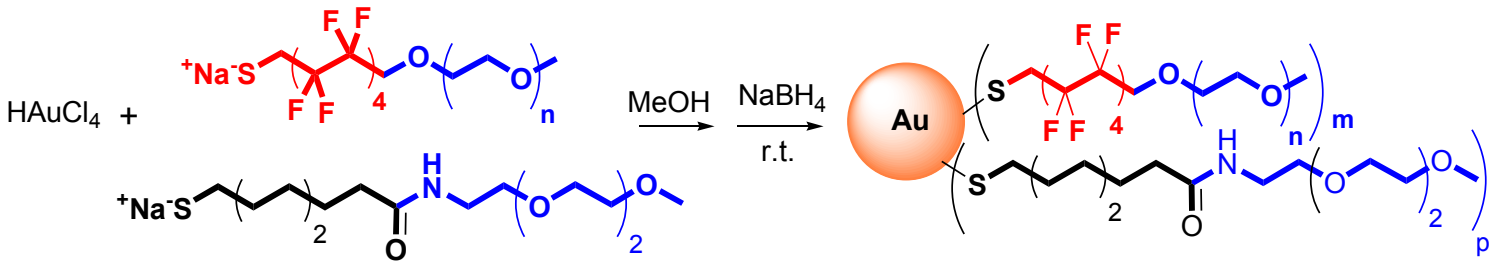

n = 10,11

NP-C8-TEG/F8-PEG

■ *synthesis of mixed-monolayer by exchange reaction*

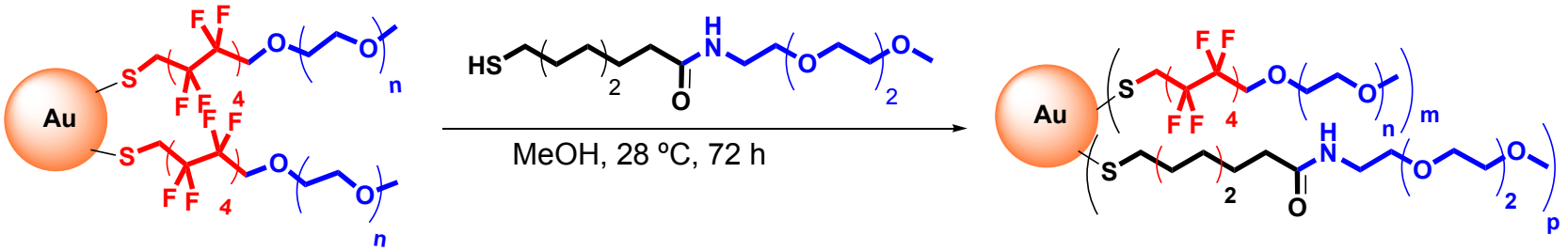

NP-F8-PEG

NP-C8-TEG/F8-PEG

C. Gentilini, P. Franchi, E. Mileo, S. Polizzi, M. Lucarini, L. Pasquato Angew. Chem. Int. Ed. ***2009****, 48, 3060.*

gold nanoparticles protected by amphiphilic fluorinated ligands

ESR studies

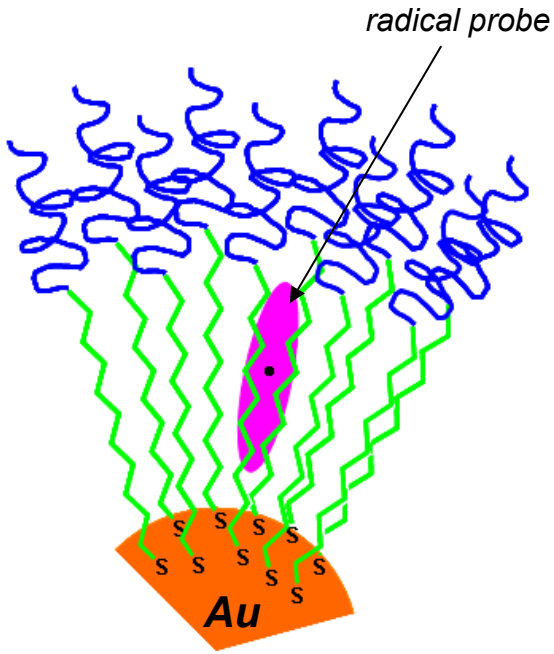

perfluorinated alkyl chain

poly(oxoethylene) chain

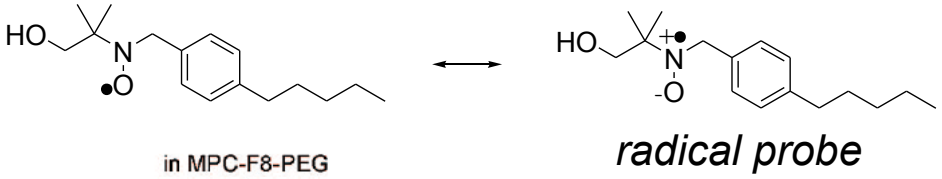

radical probe

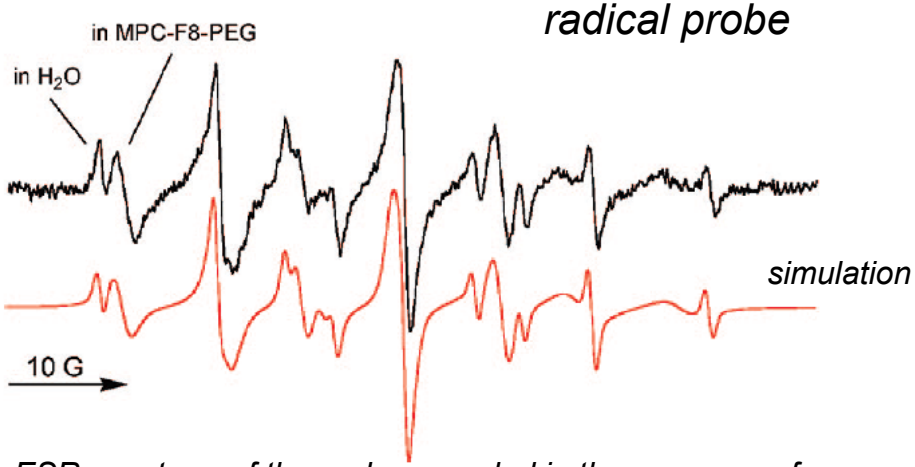

ESR spectrum of the probe recorded in the presence of NP-F8-PEG 0.56 mM (in black) and the corresponding computer simulation (in red).

ESR parameters of the radical probe (1 G = 0.1 mT) and partition equilibrium (K_{eq}) constants at 298 K.

	***a*(N)/G**	***a*($2H_\beta$)/G**	***g*-factor**	K_{eq} / M^{-1}
water[a]	16.25	10.14	2.0056	—
NP-F8-PEG	15.46	8.68	2.0057	176
NP-C8-TEG	15.67	8.97	2.0057	87[c]

[a] *Contains 10% (v/v) of methanol.*

C. Gentilini, F. Evangelista, P. Rudolf, P. Franchi, M. Lucarini, L. Pasquato J. Am. Chem. Soc. ***2008****, 130, 15678-15682.*

gold nanoparticles protected by H-/F- mixed-monolayers

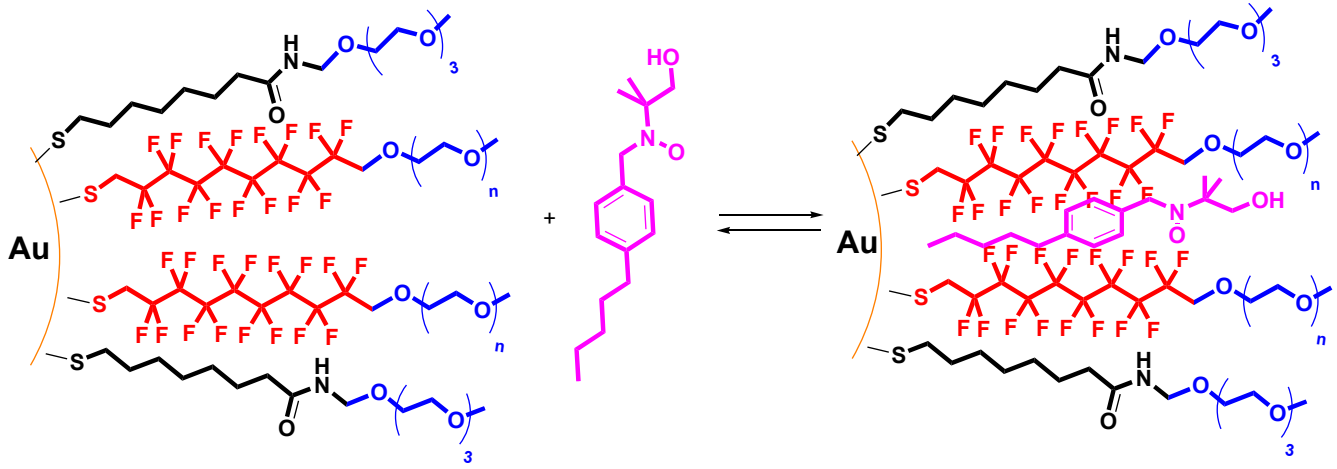

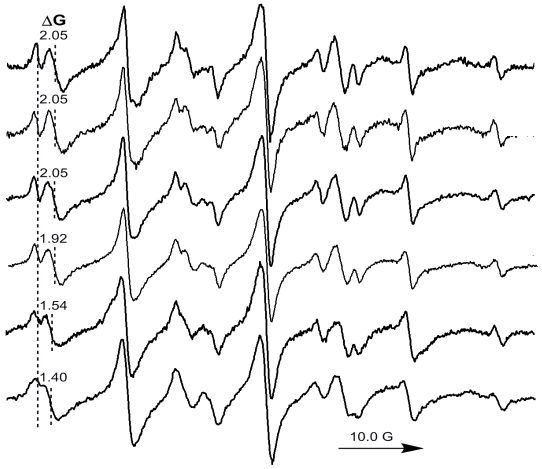

NP-F8-PEG

R_{SAM} *1*

R_{SAM} *2.5*

R_{SAM} *4*

R_{SAM} *20*

NP-C8-TEG

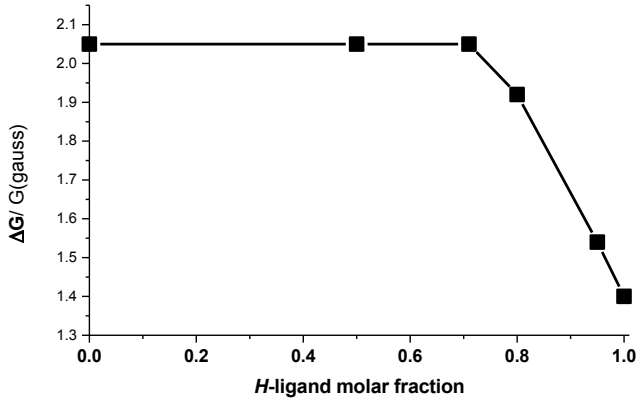

C. Gentilini, P. Franchi, E. Mileo, S. Polizzi, M. Lucarini, L. Pasquato Angew. Chem. Int. Ed. ***2009****, 48, 3060.*

gold nanoparticles protected by H-/F- mixed-monolayers

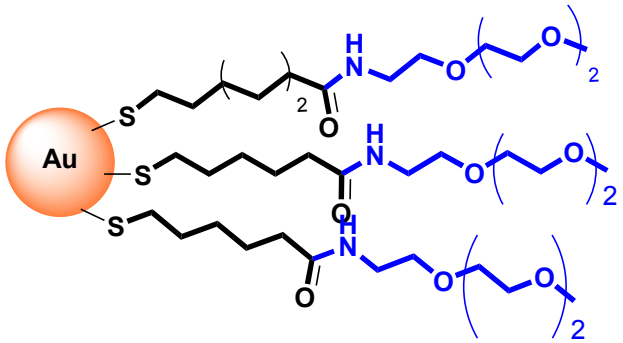

NP-C8-TEG

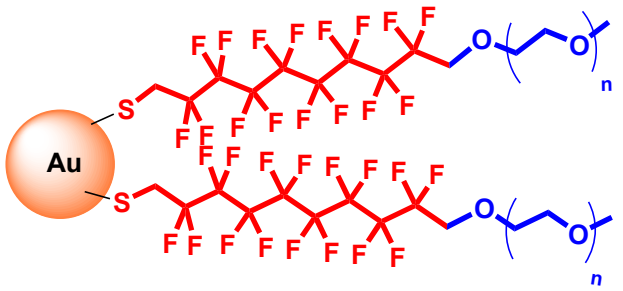

NP-F8-PEG

ESR Parameters in the Presence of Homoligand NP Mixtures

χ	$[3]_{monolayer}/[3]_{water}$ [b]	$\Delta G/G$ [c]
0	9.9 (9.8)	2.05 (2.05)
0.5	8.1 (7.8)	1.90 (1.82)
0.71	7.4 (7.1)	1.84 (1.69)
0.80	6.7 (6.5)	1.68 (1.60)
0.95	6.0 (6.1)	1.50 (1.45)
1	6.0 (6.0)	1.45 (1.40)

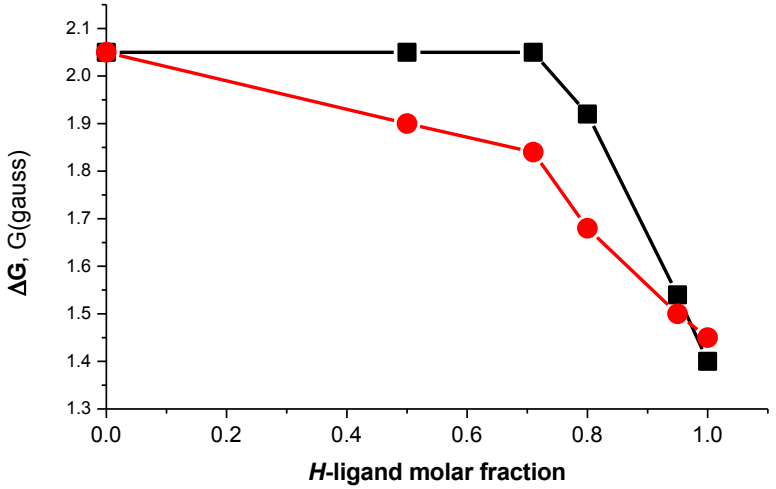

P. Posocco, et al., ACS Nano ***2012****, 6, 7243-7253.*

gold nanoparticles protected by H-/F- mixed-monolayers

Mesoscopic simulations details

in collaboration with Sabrina Pricl Paola Posocco and Maurizio Fermeglia

- ✓ *Self-assembled organization was predicted at the nanoscale using corse grained (CG) simulations in presence of solvent*
- ✓ *CG calculations allow to reach time and length scales larger than classical atomistic predictions and closer to those involved in the experimental phenomena*
- ✓ *An ad hoc multiscale molecular modeling procedure was developed. It employs the information obtained from atomistic molecular dynamics simulation to parametrize mesoscale dissipative particle dynamics (DPD) models, thus incorporating all chemical details even at the CG level*

*L. Pasquato et al., ACS Nano **2012**, 6, 7243-7253.*

gold nanoparticles protected by H-/F- mixed-monolayers

- ***multiscale molecular simulation: validation of the procedure***

Au NP with a core size of 4.5 nm coated by a mixture of 2:1 of MUS and OT ligands (F. Stellacci et al. Chem. Commun. 2008, 196.)

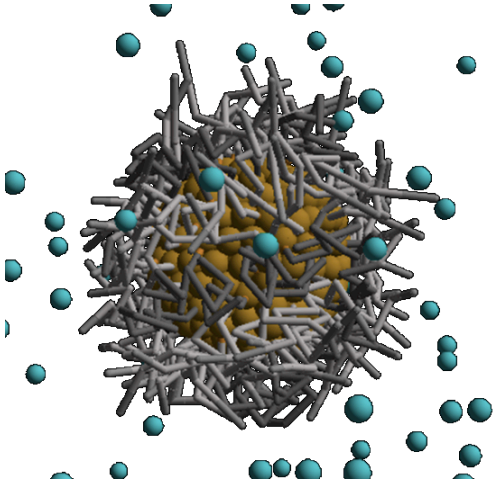

MUS

OT

water

gold core

Rippled morphology predicted using a multiscale approach.

L. Pasquato, et. al. ACS Nano ***2012****, 6, 7243-7253.*

gold nanoparticles protected by H-/F- mixed-monolayers

- ***multiscale molecular simulation***

Ligand organization on the surface of gold NPs at different molar fraction of the two ligands

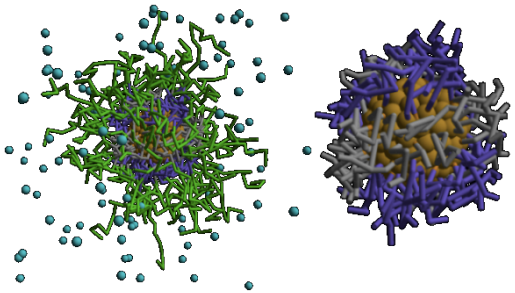

χ_H = 0.50, ∅ 2.2 nm

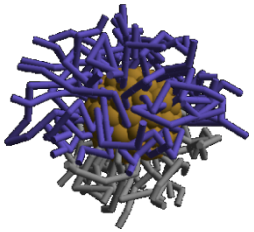

χ_H = 0.50, ∅ 1.6 nm

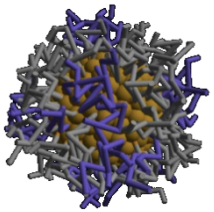

χ_H = 0.71, ∅ 2.5 nm

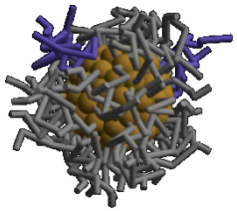

χ_H = 0.80, ∅ 1.9 nm

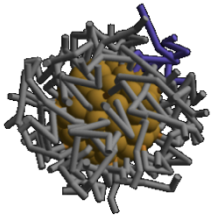

χ_H = 0.95, ∅ 1.9 nm

L. Pasquato, et al. ACS Nano ***2012****, 6, 7243-7253.*

drug loading by mixed-SAMs

Equilibrium constants in the presence of heteroligand mixed-monolayers as determined from ESR measurements

***H*-ligand molar fraction**	K_F[a]/M^{-1}
0	176
0.50	200
0.71	350
0.80	762
0.95	600
1.0	-

atomistic and mesoscale calculations

		Shell thickness (nm)
Homoligand NPs	F8PEG	2.82
	C8TEG	1.40
Heteroligand NPs	F8PEG	2.60
	C8TEG	1.59

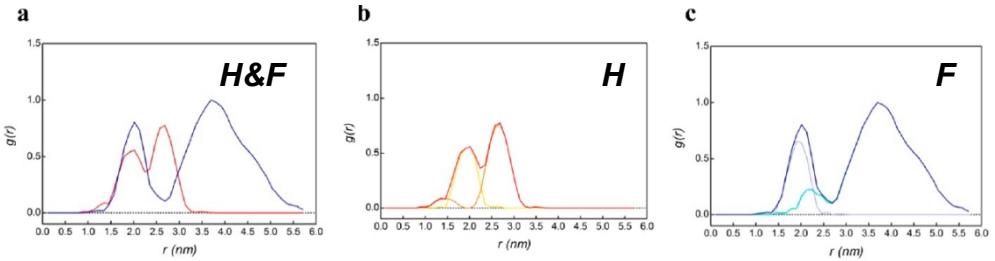

Radial distribution functions (RDFs) for the SAM components of MPC-C8-TEG/F8-PEG, 1:1.

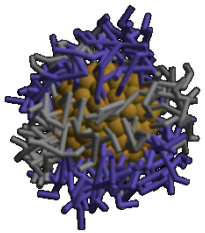

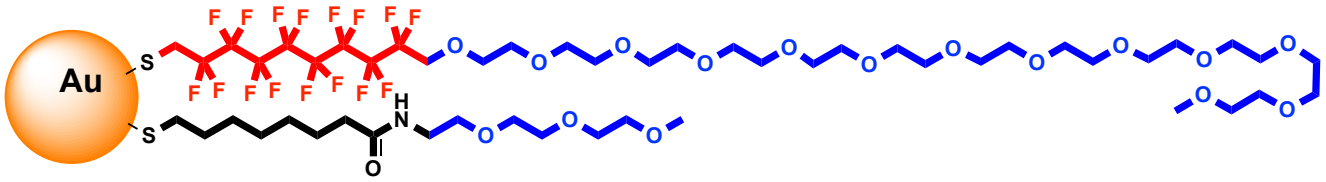

L. Pasquato et al., ACS Nano ***2012****, 6, 7243-7253.*

Surface properties of proteins

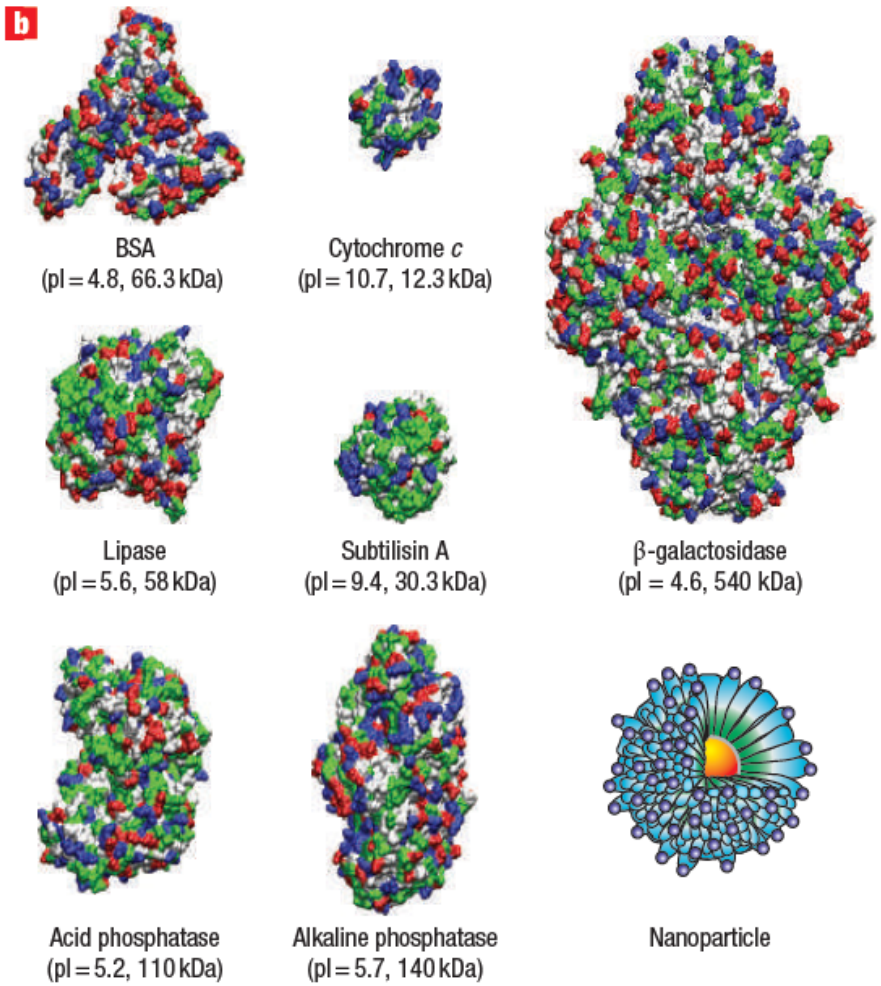

Colour scheme for the proteins: nonpolar residues (grey), basic residues (blue), acidic residues (red) and polar residues (green).

C.-C. You et al. Nature Nanotech. 2007

the mechanism of membrane penetration and toxicity depends on surface structure

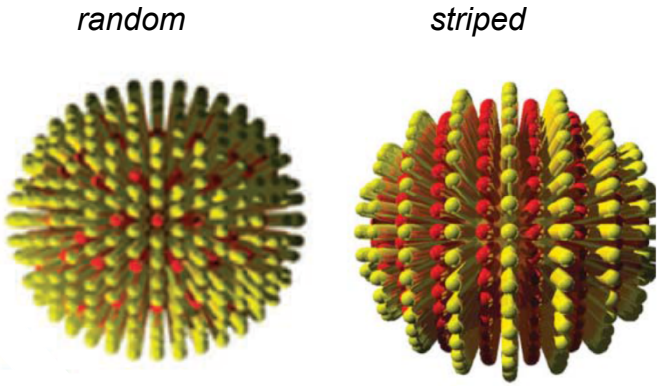

A. Verma et al. Nature Mater. 2008
S. Sabella et al. Nanoscale 2014

Effect of the NP surface morphology on cellular uptake and toxicity

Surface-structure-regulated cell-membrane penetration by monolayer-protected nanoparticles

AYUSH VERMA[1], OKTAY UZUN[1], YUHUA HU[2], YING HU[1], HEE-SUN HAN[3], NICKI WATSON[4], SUELIN CHEN[1], DARRELL J. IRVINE[1,5]* AND FRANCESCO STELLACCI[1]*

Nature Mater. 2008

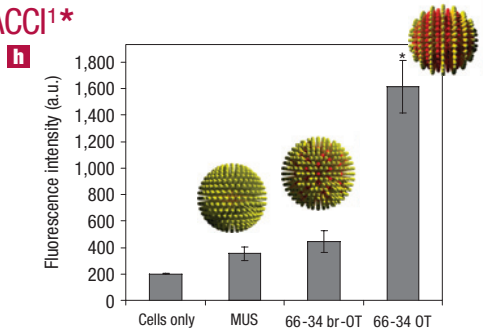

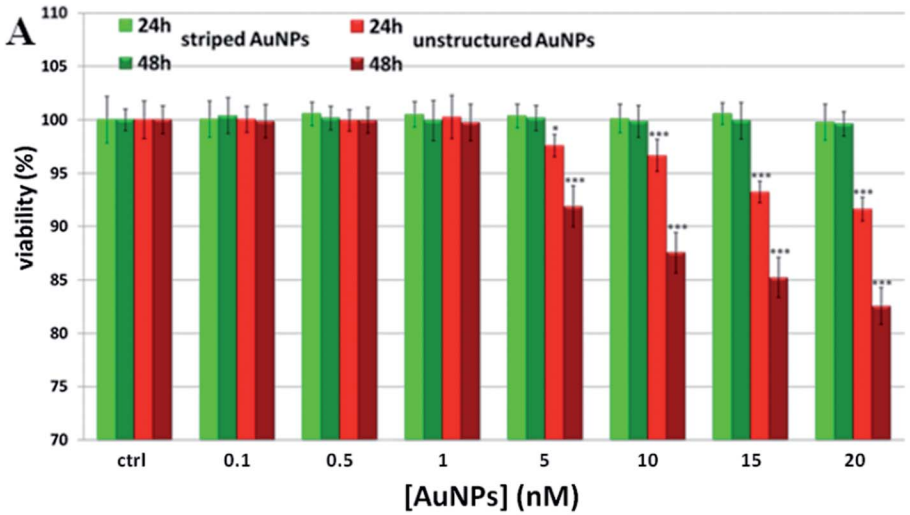

S. Sabella et al. Nanoscale, 2014, 6, 7052

Interaction of Nanoparticles with cells

system 1

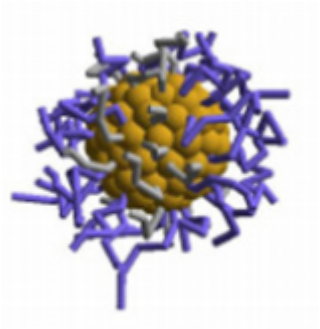

striped-NPs
core diam. 1.9 nm
NP diam. ~ 7.1 nm
$Au_{260}(C8TEG)_{20}(F8PEG)_{36}$

system 2

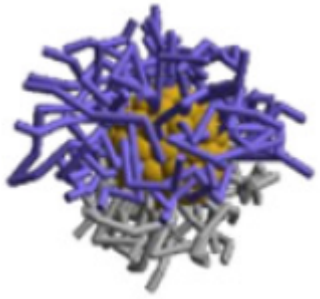

Janus-NPs
core diam. 1.6 nm
NP diam. ~ 6.8 nm
$Au_{140}(C8TEG)_{24}(F8PEG)_{32}$

credits to: Alessandro Tossi
Sabrina Pacor
Milena Guida

- *three types of cells:*

U937 – leukemia cells
MEC-1 – lymphoma cells
A549 – lung adenocarcinoma

- *tests for mitocondrial activity: DiOC6/PI and JC-1*
- *MTT: cell proliferation test to evaluate toxicity*

- *Biacore experiments to have evidence of the interaction with liposomial membrane*

Citotoxicity: MTT test

credits to: Alessandro Tossi
Sabrina Pacor
Milena Guida

MEC-1 cells, complete medium, 24h

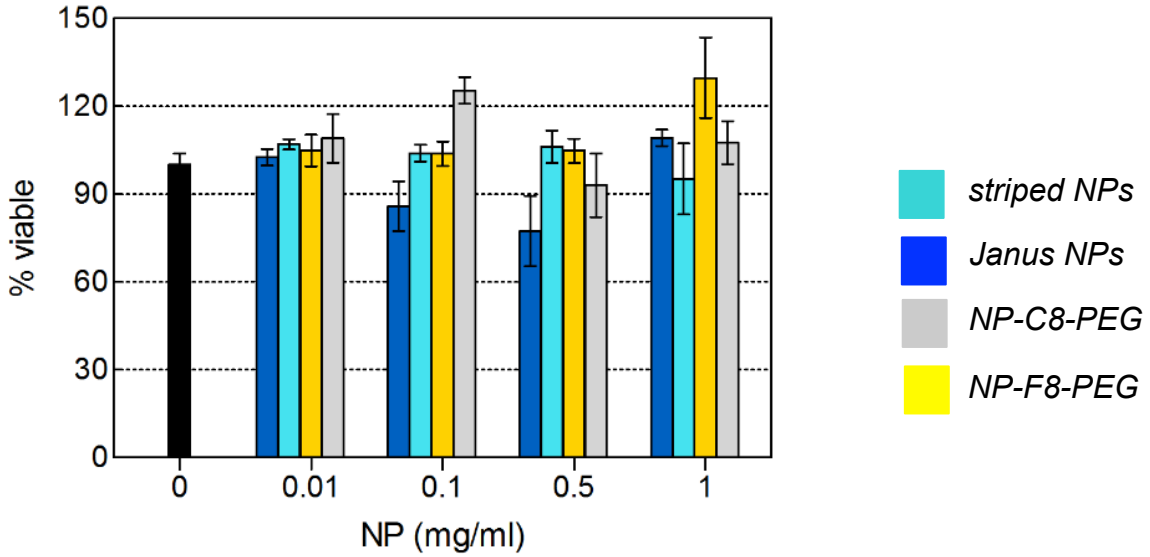

Cytotoxicity of NPs treated cells. MEC-1 cells viability, evaluated by MTT assay, after 24h treatment with the NPs at concentrations indicated on x-axes; data are expressed as mean ± SEM of the measured O.D. of experiments repeated at least three times and performed at least in triplicate.

L. Pasquato, P. Posocco, Small 2019.

Mitochondrial activity

evaluation of apoptotic damage to mitochondrial functionality

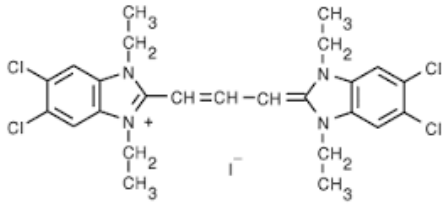

JC-1 mitochondrial potential sensor

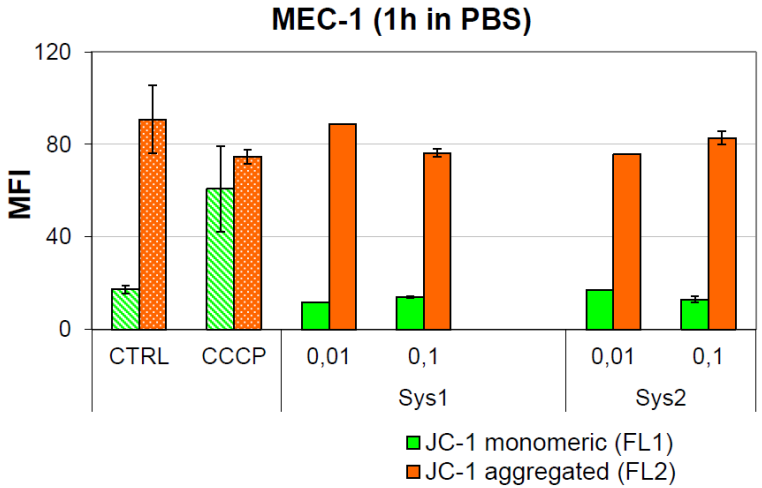

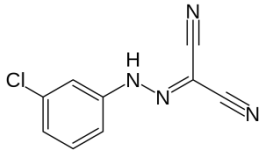

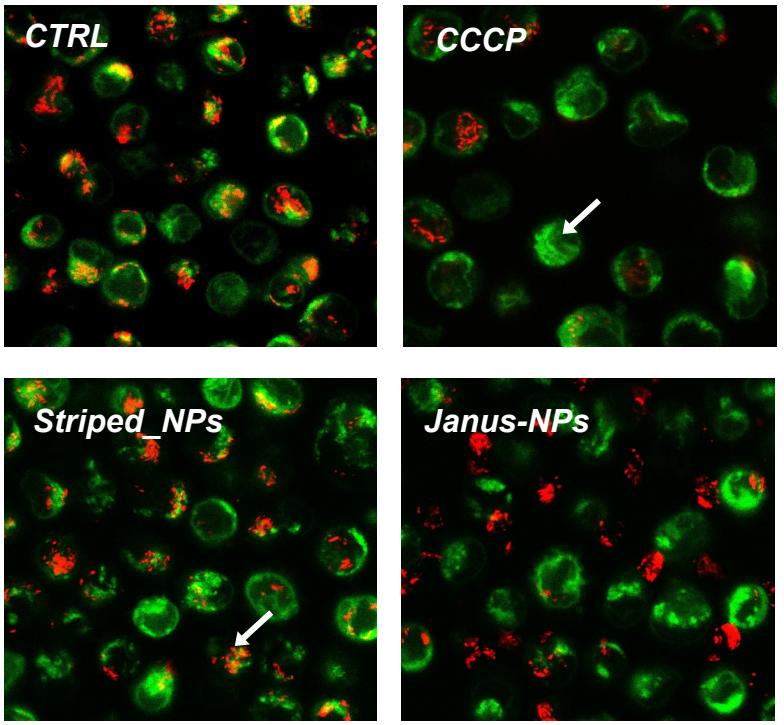

Flow cytometry: *Striped- and Janus- GNP did not decrease the orange fluorescence of treated cells with respect to untreated controls.*

Confocal microscopy: *only the positive control CCCP caused disaggregation, conc. 0.1 mg/ml.*

GNPs do not cause mitochondrial damage

L. Pasquato, P. Posocco, Small 2019.

cell internalization of NPs

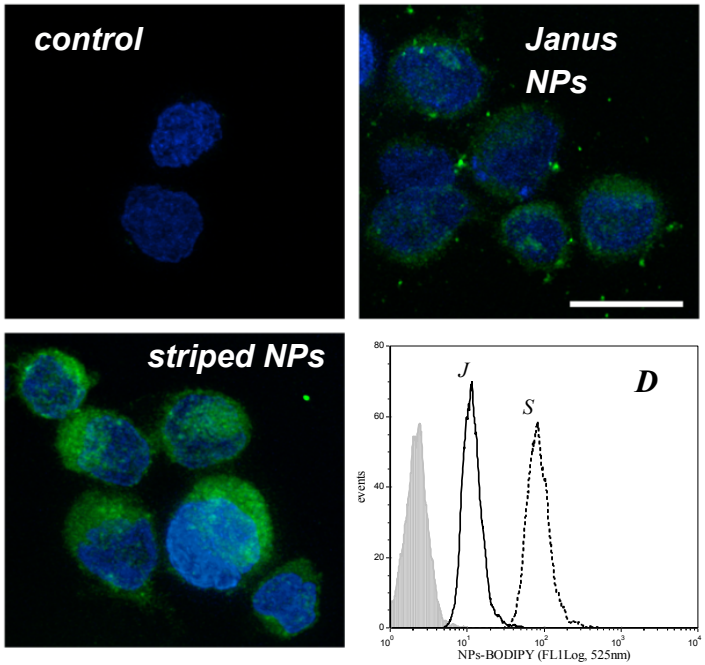

Janus and striped NPs cross the plasma membrane and reach the cytoplasm

internalization is favoured by the stripe-like morphology of the monolayer.

*MEC-1 cells treated with **BODIPY-tagged NPs**. **A**) Confocal images of control cells, **B**) cells treated with 1 mg/ml Janus NP and **C**) cells treated with 0,1 mg/ml striped, for 60 min prior to counterstaining nuclei with Hoecst dye. Panel **D** represents the flow cytometric overlay of green fluorescence emitted from untreated (grey peak) and BODIPY-NP treated cells, 1mg/ml Janus (J) and 0,1 mg/ml striped (S).*

L. Pasquato, P. Posocco, Small 2019.

SPR Experiments – binding NPs-model membranes

The sensor surface is dextran coated, chip L1
Liposomes of DOPC

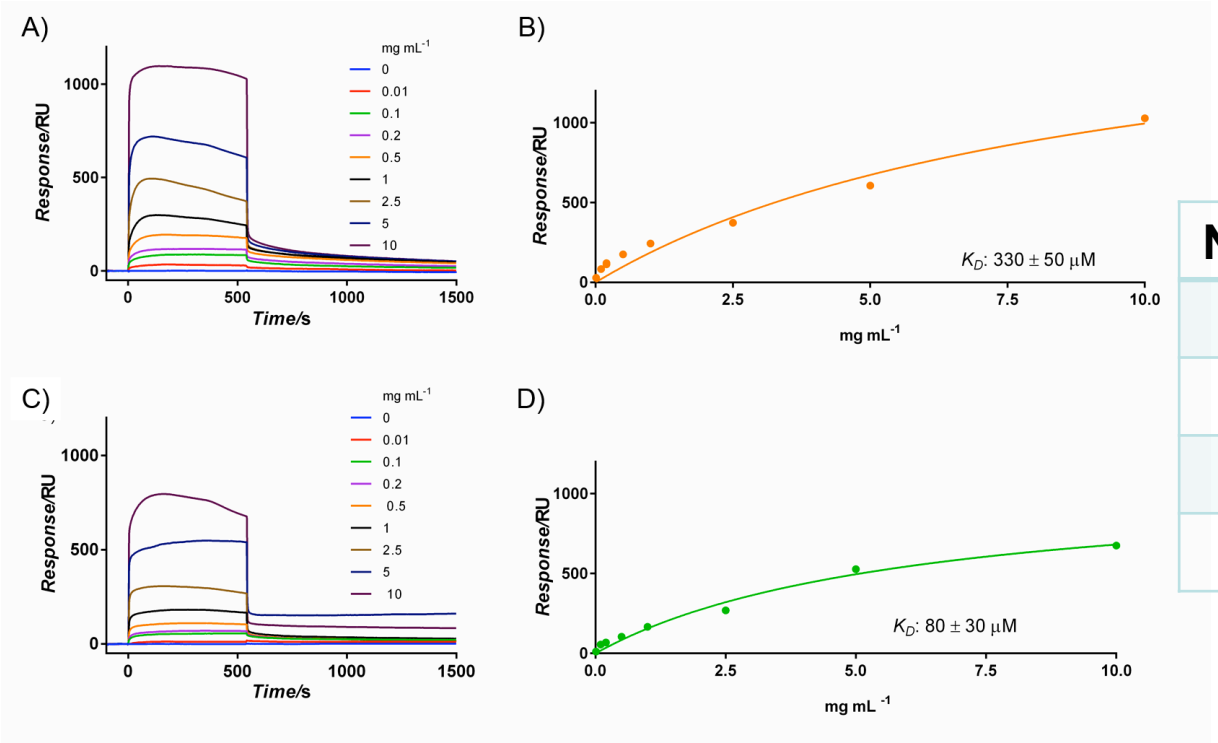

Nanoparticles	K_{diss}, μM
NP-striped	80 ± 28
NP-Janus	330 ± 50
NP-F8-PEG	60 ± 50
NP-C8-PEG	118 ± 50

L. Pasquato, P. Posocco, Small 2019.

Computational studies of NP-membrane interaction by MARTINI mapping

credits to: Paola Posocco
Domenico Marson

Nanoparticle/ composition	ΔG_{adh} [kcal/ mol]	$N_{contacts}$	% contacts non-PEG component	% contacts PEG component
NP-Striped	-38.9 ± 1.0	25 ± 1	37	63
NP-Janus	-28.6 ± 1.5	21 ± 2	41	59
NP-F8-PEG	-51.0± 1.2	32 ± 2	27	73
NP-C8-PEG	-44.1 ± 0.8	31 ± 2	28	72

Detachment of NP from the membrane by «umbrella sampling»

L. Pasquato, P. Posocco, Small 2019.

Role of fluorintated ligands in the interaction with biological structures

Perfluoroalkylchain conjugation as a new tactic for enhancing cell permeability of peptide nucleic acids (PNAs) via reducing the nanoparticle size

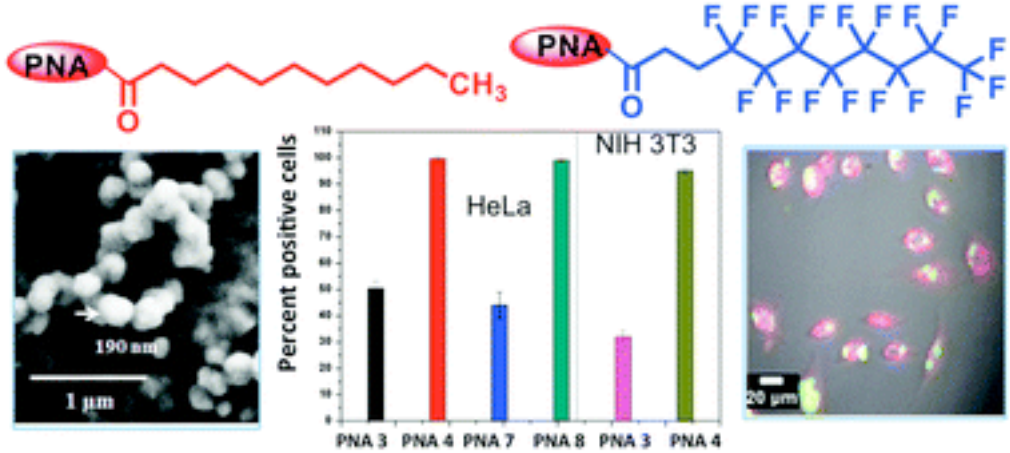

S. Ellipilli et al. Chem. Commun. 2016

Role of fluorintated ligands in the interaction with biological structures

Influence of fluorinated and hydrogenated nanoparticles on the structure and fibrillogenesis of amyloid beta-peptide

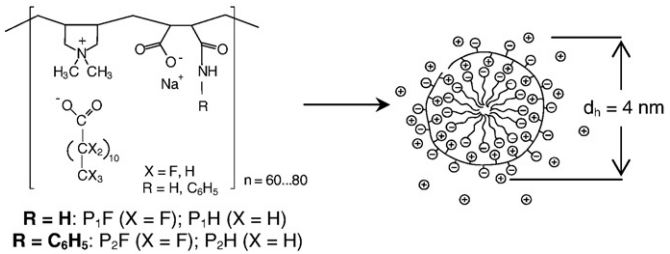

Fig. 2. Complexes of polyampholytes and the sodium salt of dodecanoic acid (X=H) and perfluorododecanoic acid (X=F) [23].

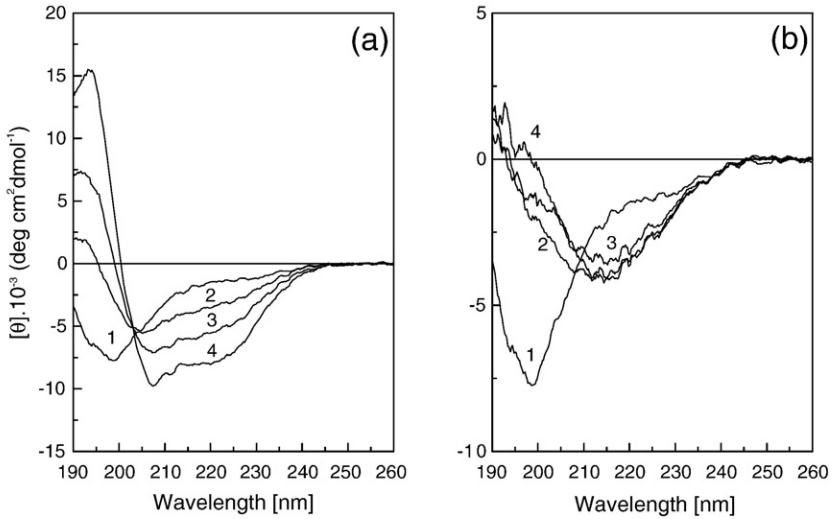

CD data of Aβ40 (50 μM) in the presence of different concentrations of fluorinated (a) and hydrogenated (b) P1 complexes: 0 g L^{-1} (curve 1), 2 g L^{-1} (curve 2), 4 g L^{-1} (curve 3) and 8 g L^{-1} (curve 4).

S. Rocha et al. Biophys. Chem. 2008

Fluorinated and charged nanoparticles

A

Ligands for the preparation of mixed monolayer nanoparticles

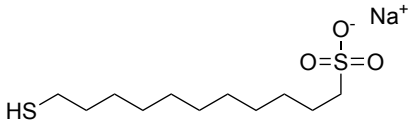

HMUS

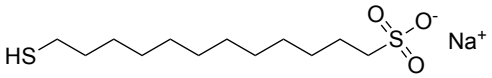

HMDDS

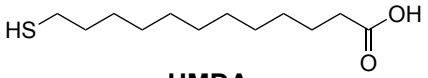

HMDA

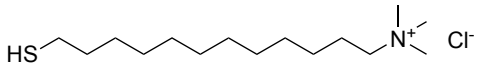

HTMDA

HF8

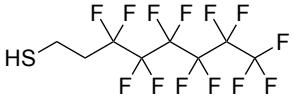

HF6

B

Ligands for the preparation of homoligand nanoparticles

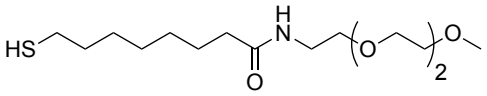

HC8TEG

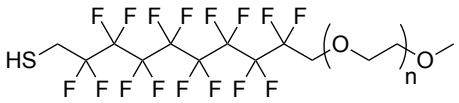

n = 12-13

HF8PEG

C

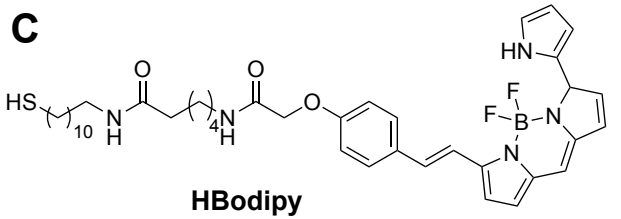

HBodipy

drug loading - influence of the monolayer properties

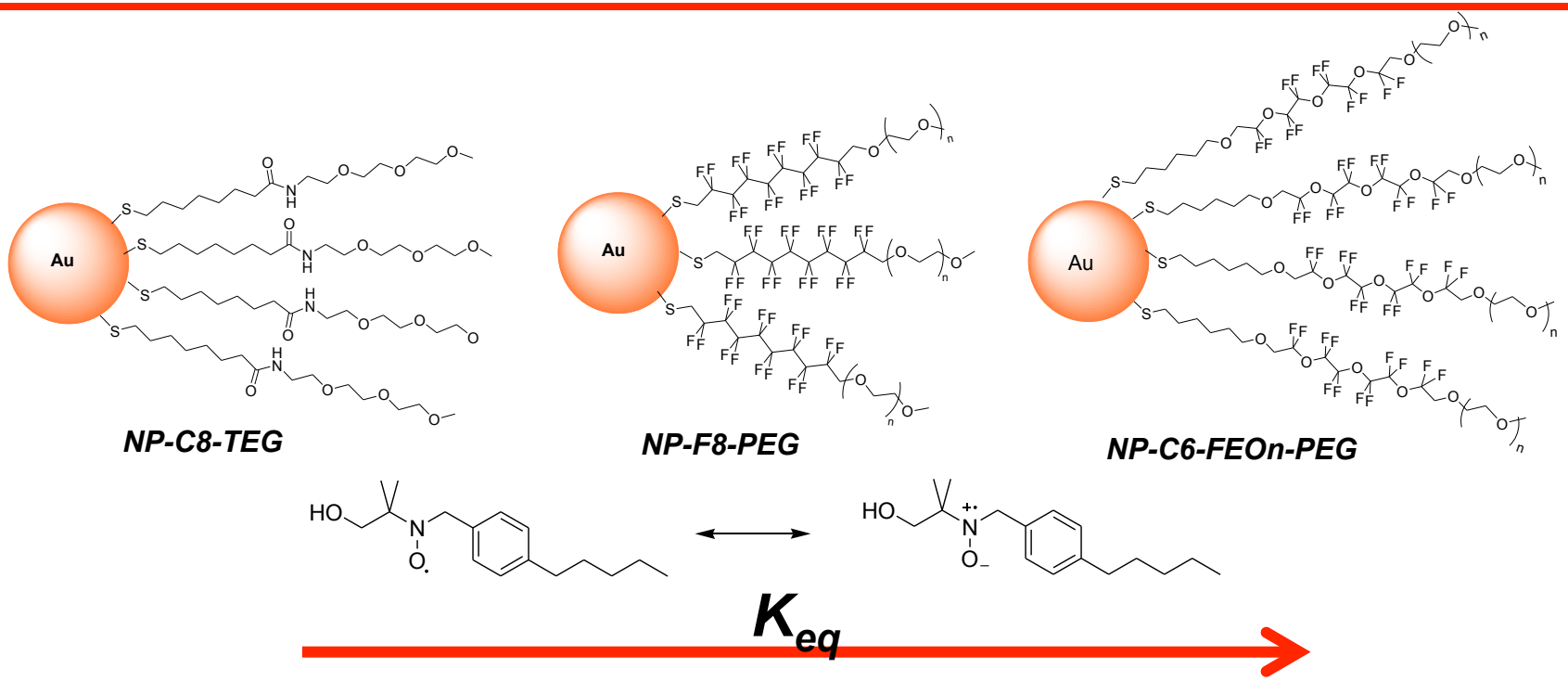

	a(N)/G	$a(2H_\beta)$/G	g-factor	d core	K_{eq}/M^{-1}
Water	16.25	10.14	2.0056	-	-
NP-C8-TEG	15.67	8.97	2.0057	1.6 nm	104
NP-F8-PEG	15.46	8.68	2.0057	2.7 nm	176
NP-C6-FEOn-PEG	**15.45**	**8.65**	**2.0057**	**1.4 nm**	**593**

L. Pasquato et al. J. Mater. Chem. 2015, 3, 432-439.

drug loading - H- vs. F-monolayer

- *desolvation energy*
- *hydrophobic interactions*
- *halogen bonds*

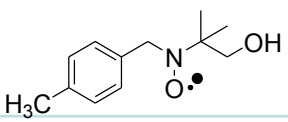

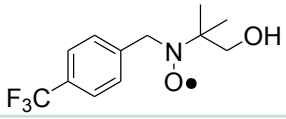

	K_{eq} / M^{-1}		K_{eq} / M^{-1}		$K_{eq}(F)/K_{eq}(H)$
NP-C8-TEG	2.2	2.6	4	7.2	1.8
NP-F8-PEG	5.7	2.8	29	3.4	5.1
NP-FEO$_n$-PEG	16		100		6.2

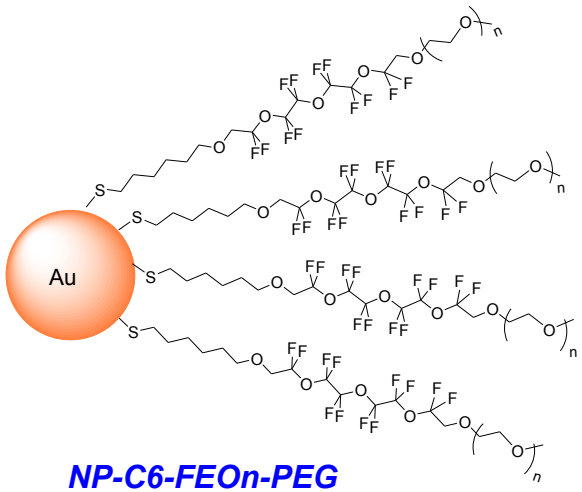

NP-C6-FEOn-PEG

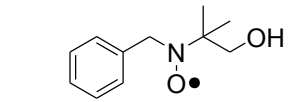

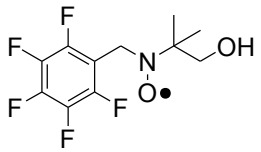

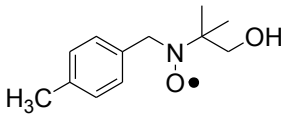

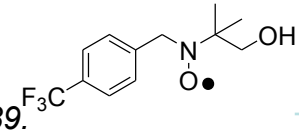

K_{eq} / M^{-1}	$K_{eq}(F)/K_{eq}(H)$
6.2	12.9
80	
16	6.25
100	

L. Pasquato et al. J. Mater. Chem. 2015, 3, 432-439.

release of the drug

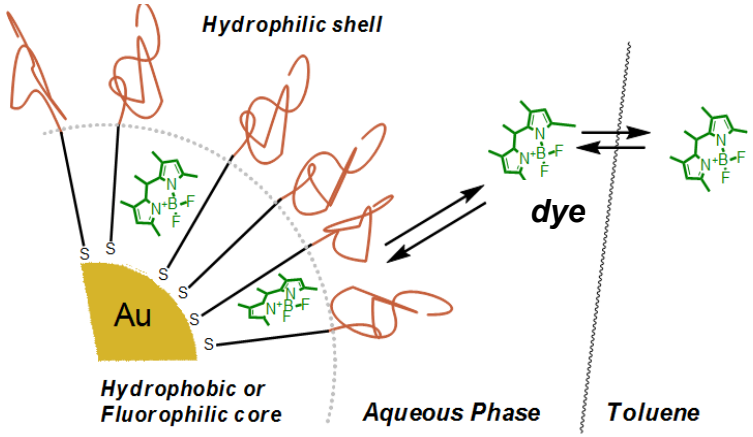

NP	k_1, s^{-1}	k_2, s^{-1}	[NPs], μM	[dye], μM
None	0.03	-	-	0.168
NP C8PEG	0.02	2×10^{-4}	0.426	0.168
NP F8PEG	5×10^{-3}	-	0.632	0.168
NP C6OFPEG 3 nm	0.02	5×10^{-4}	0.229	0.153
NP C6OFPEG 1.4 nm	0.03	4×10^{-4}	1.15	0.168

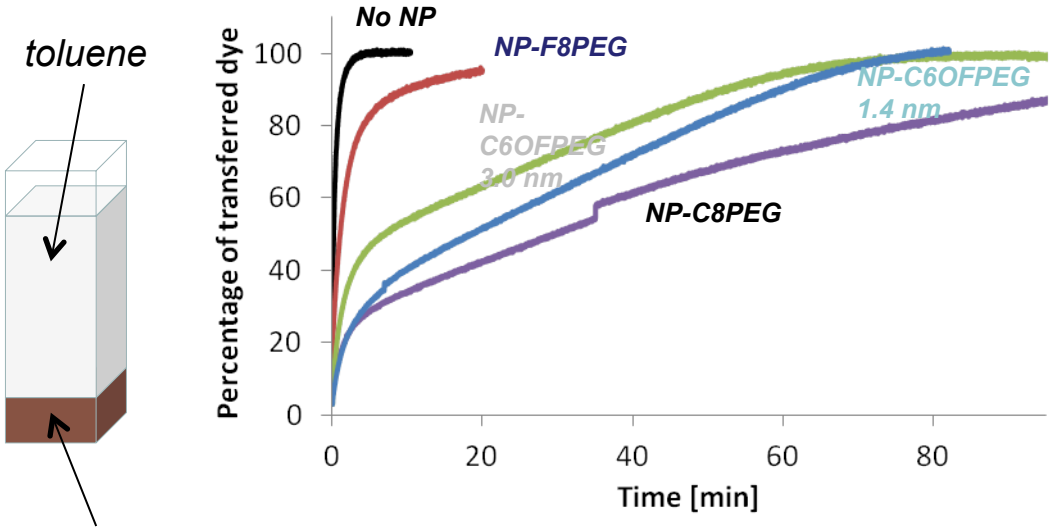

Bodipy solution (μM) in the presence of NPs (μM)

Effect of the NPs monolayers on the phase transfer rate *of the hydrophobic fluorescent bodipy dye from an aqueous solution containing NPs to a toluene layer.*

L. Pasquato et al. J. Mater. Chem. 2015, 3, 432-439.

GNPs for ^{19}F MRI

design, synthesis and use of gold NPs protectected by fluorinated ligands as nanomaterial for imaging and therapy

modular system

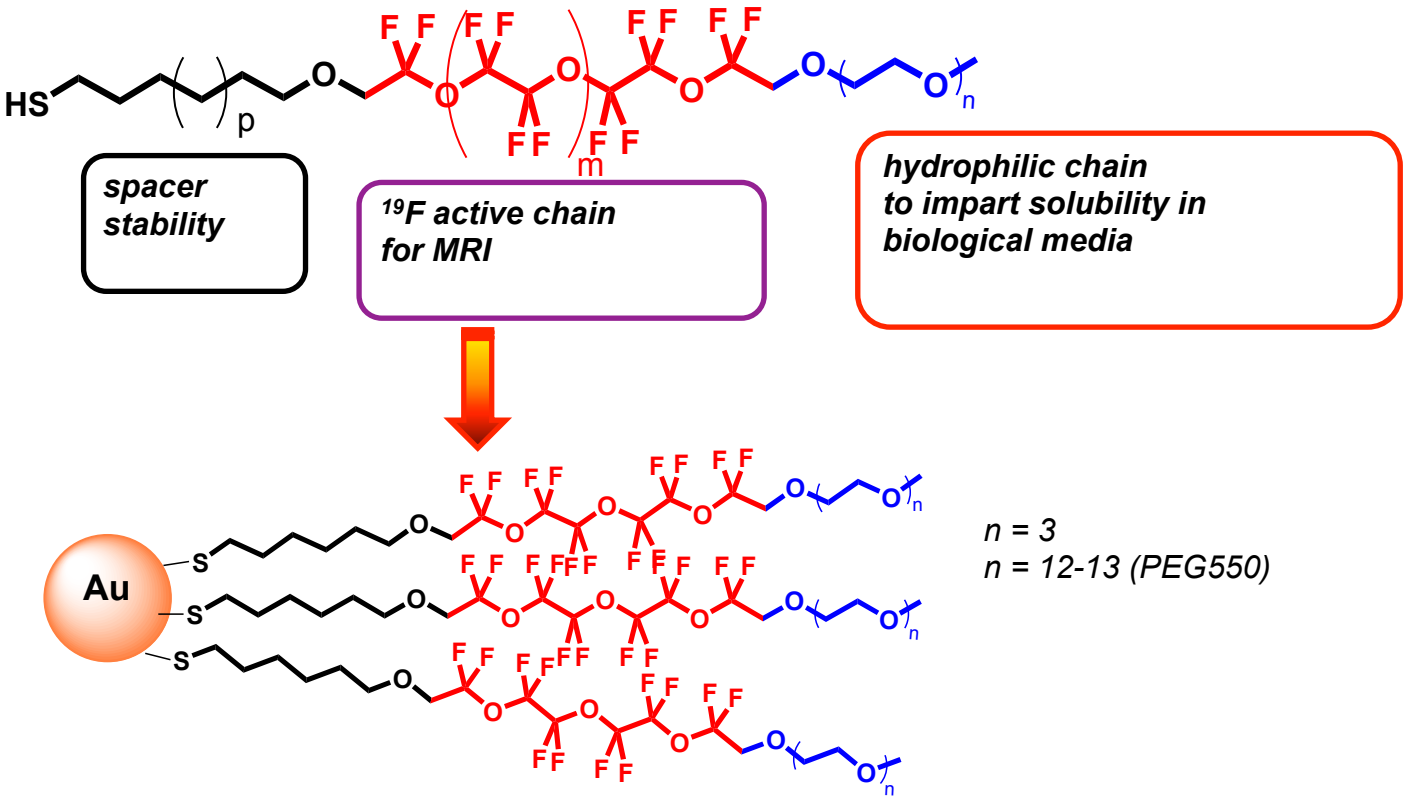

L. Pasquato et al. Chem. Commun. ***2013****, 49, 8794.*

GNPs for ^{19}F MRI

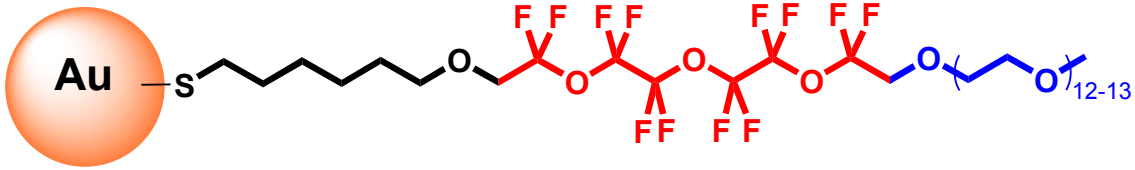

^{1}H NMR

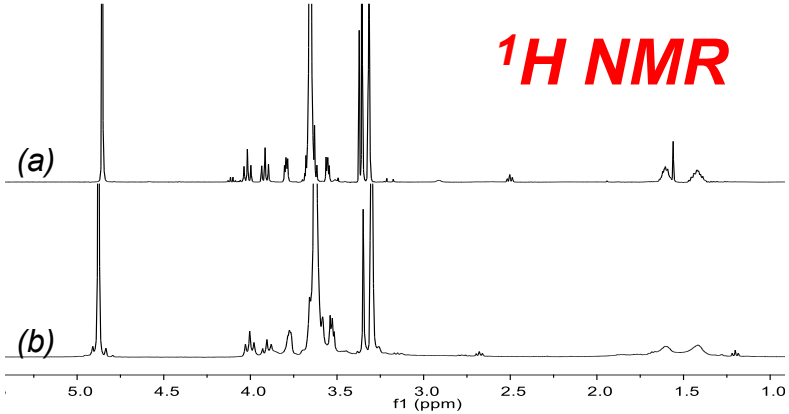

^{1}H NMR (500 MHz, CD_3OD) of thiol (a) and MPC C6-OF-PEG (b).

^{19}F NMR

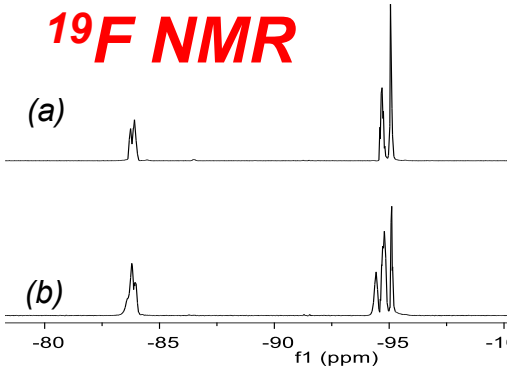

^{19}F NMR (500 MHz, CD_3OD) of protected thiol (a) and MPC C6-OF-PEG (b).

UV-Vis

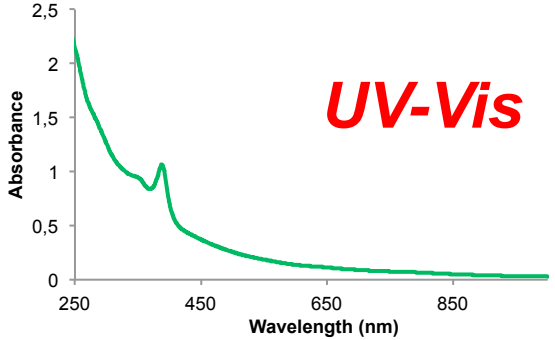

UV-Vis spectrum in methanol.

TGA

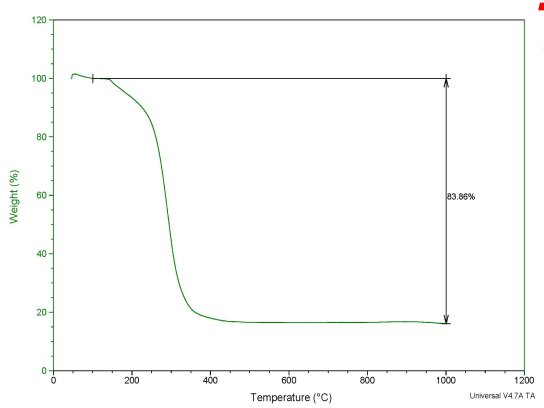

GNPs for ^{19}F MRI

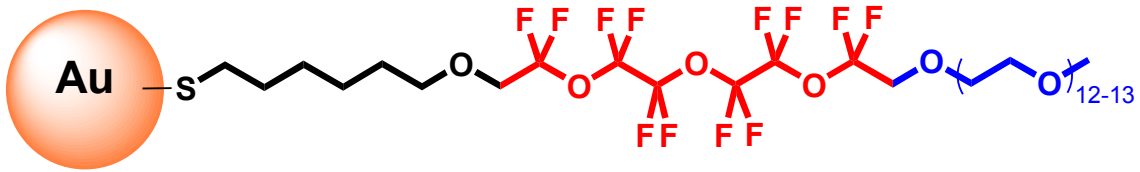

TEM

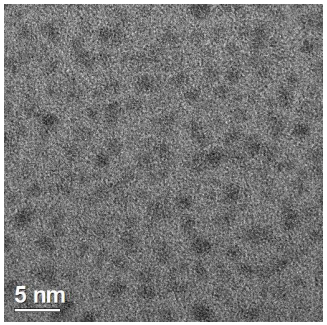

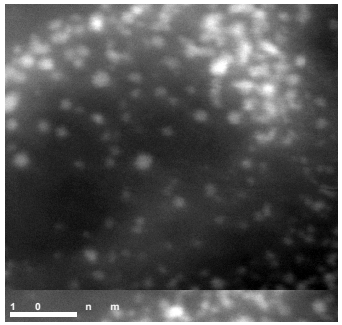

STEM-HAADF

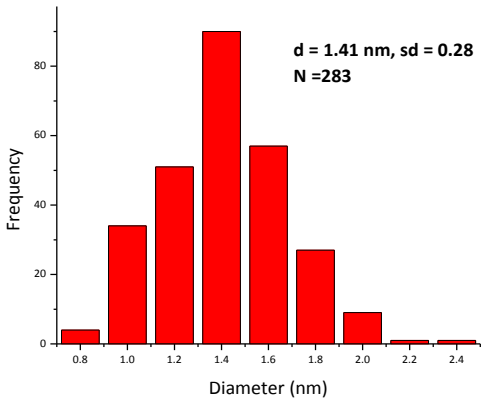

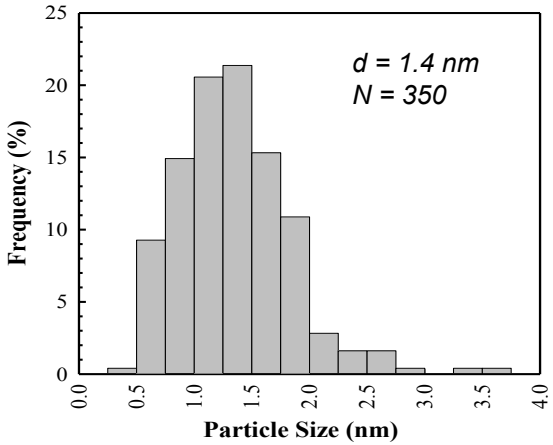

Juan J. Delgado, Univ. de Cádiz, Spain

GNPs for ^{19}F MRI

NMR/MRI

Relaxation times (^{19}F-NMR)

T1 (spin-lattice relaxation time)
Inversion Recovery

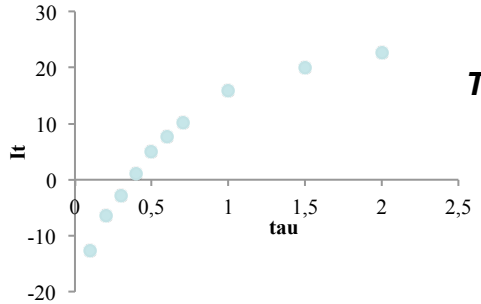

T1 = 588 ms

T2 (spin-spin relaxation time)
CPMG sequence
(Carr-Purcell Meiboom-Gill)

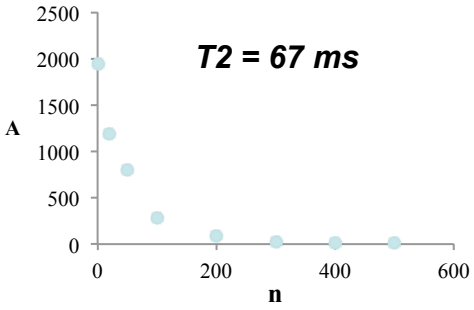

T2 = 67 ms

^{19}F-MR images

18.75 mg/mL of NPs (6.06x10^{19} ^{19}F/mL)

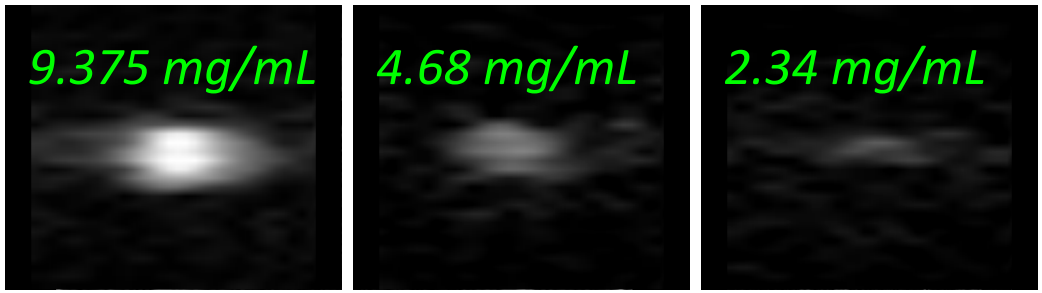

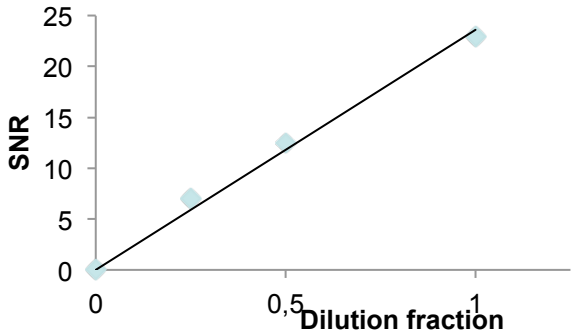

L. Pasquato et al. Chem. Commun. ***2013****, 49, 8794.*

NP-C6-FEO-PEG, cellular uptake

4 h incubation with HeLa cells at 37 °C, and 30 min RBC

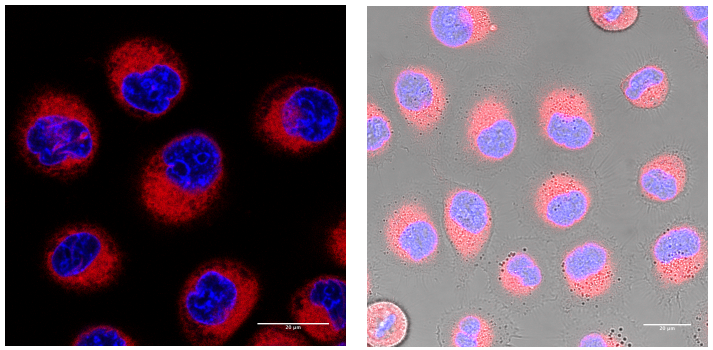

Confocal laser microscopy images of HeLa cells (nucleus stained in blue, Hoechst dye) loaded with F-MPCs ***4b*** *(red fluorescent signal) for 4 h at 37 °C.*

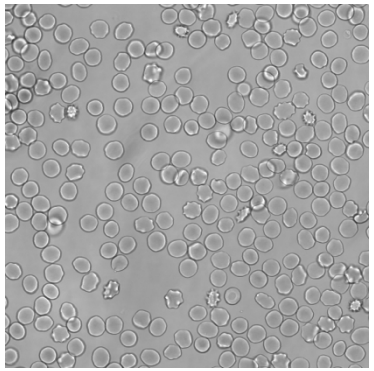

RBCs do not uptake NPs only free dye is able to penetrate their cell membrane or remain attached to the membrane.

No unbound Bodipy *was detected by RBC test.*

4 h incubation with HeLa cells at 4 °C *(endocytic/ pinocytic mechanisms are arrested)*

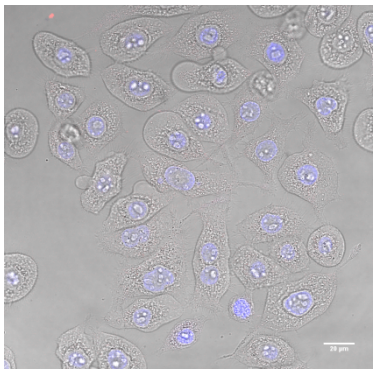

No visible red signal, *only very little is possible visualized with the enhanced signal.*

F. Sousa, IEO, Milan

NP-C6-FEO-PEG, cellular viability

UL – dead cells not labeled with NPs
UR - dead cells labeled with NPs
LL – viable cells not labeled with NPs
LR- viable cells labeled with NPs

FACS for PI of HeLa incubated 4 hrs with MPC C6-FEO-PEG

PI

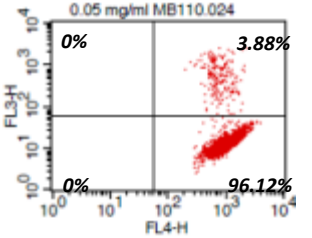

Quad	% Gated	% Total	X Mean	Y Mean
UL	0.00	0.00	***	***
UR	3.88	3.76	837.01	664.12
LL	0.00	0.00	***	***
LR	96.12	93.20	1039.46	13.15

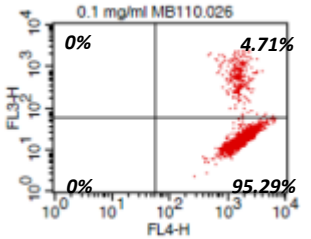

Quad	% Gated	% Total	X Mean	Y Mean
UL	0.00	0.00	***	***
UR	4.71	4.58	1637.27	750.07
LL	0.00	0.00	***	***
LR	95.29	92.67	1811.77	17.82

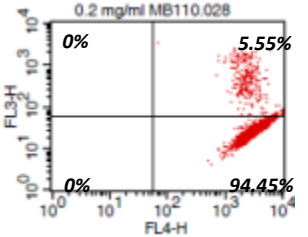

Quad	% Gated	% Total	X Mean	Y Mean
UL	0.00	0.00	***	***
UR	5.55	5.41	3212.32	615.86
LL	0.00	0.00	***	***
LR	94.45	91.97	3016.69	24.87

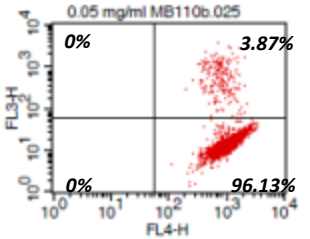

Quad	% Gated	% Total	X Mean	Y Mean
UL	0.00	0.00	***	***
UR	3.87	3.76	856.39	714.69
LL	0.00	0.00	***	***
LR	96.13	93.37	1053.28	13.30

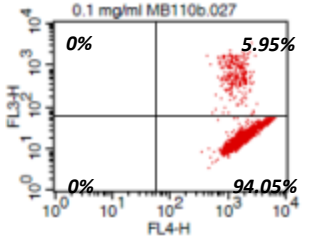

Quad	% Gated	% Total	X Mean	Y Mean
UL	0.00	0.00	***	***
UR	5.95	5.78	1466.03	756.91
LL	0.00	0.00	***	***
LR	94.05	91.43	1859.41	18.15

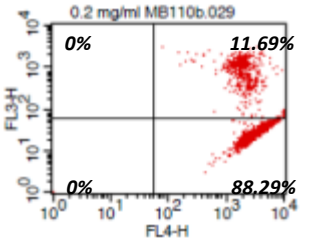

Quad	% Gated	% Total	X Mean	Y Mean
UL	0.00	0.00	***	***
UR	11.69	11.19	2331.72	932.99
LL	0.02	0.02	1.63	2.59
LR	88.29	84.56	3067.29	25.01

*The percentage of viable cells is above **95%** after taken up NPs. The percentage of dead cells labeled with NPs are very similar to all concentrations tested.*

second generation GNPs for ^{19}F MRI

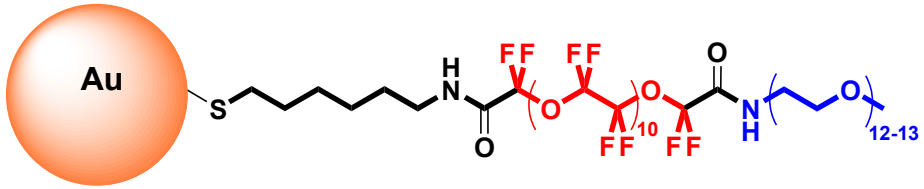

excellent solubility in water

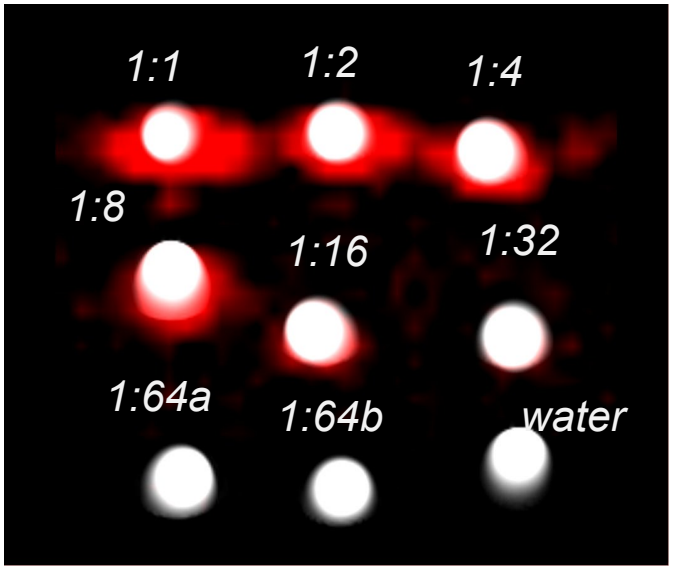

^{1}H (white) and ^{19}F MRI (red).

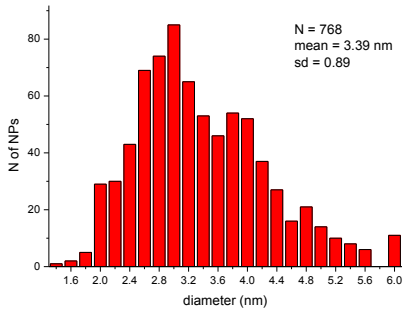

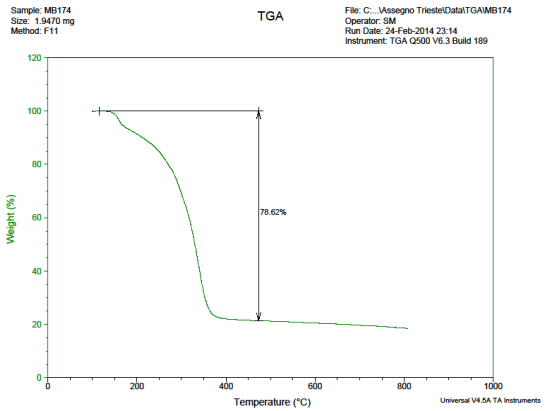

in solution of 1 mg/ml T1 = 490 ms

T2 = 15.34 ms

T2 = 0.41*

second generation GNPs for ^{19}F MRI

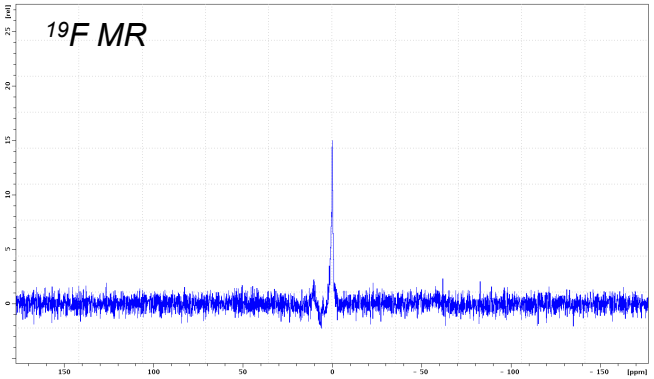

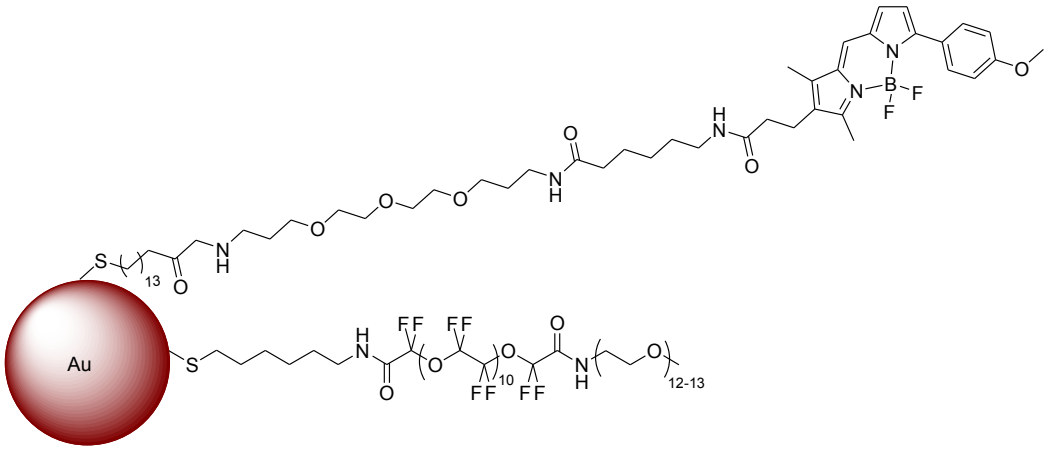

7 Tesla

^{19}F MRI

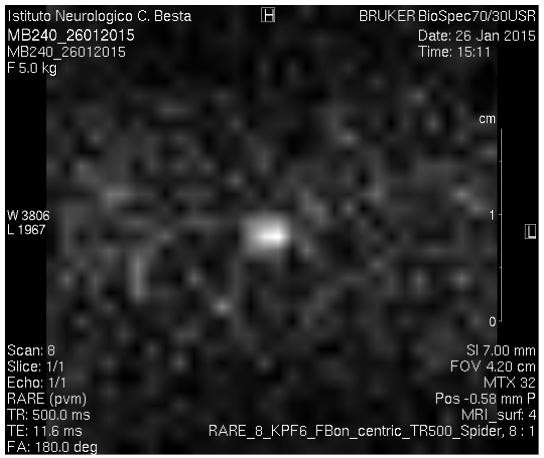

$T1 = 455.67 \pm 11.44$ ms

$T2 = 29.75 \pm 2.52$ ms

$T2^* = 1.45 \pm 0.22$ ms

1 μL of solution 8.4 mg/mL, 1 h acquisition time

ANISOTROPIC METAL NANOPARTICLES

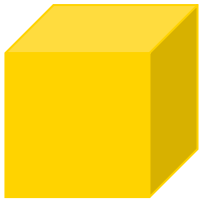

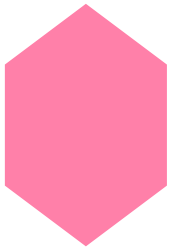

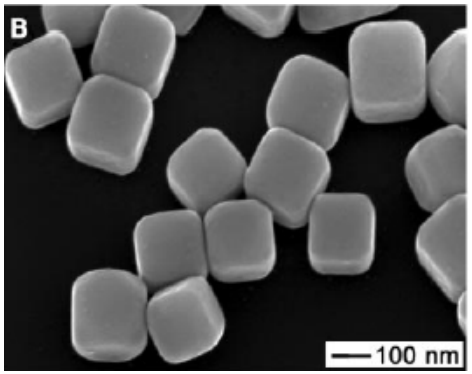

SEM image of Silver Nanocubes[1]

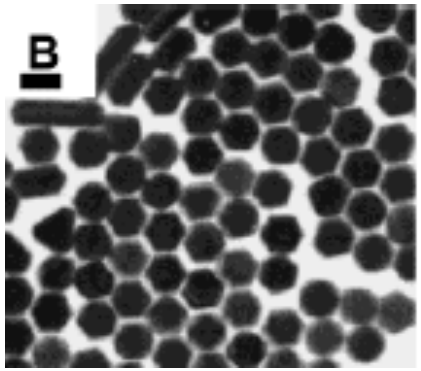

TEM images of Au nanoparticles. Scale 100 nm[2]

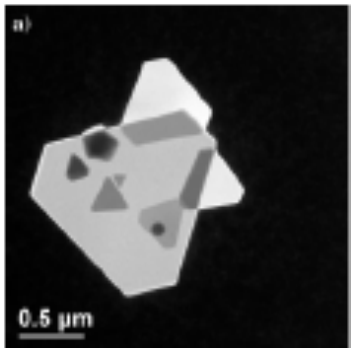

HAADF image of Au nanoparticles: synthesized @ 100°C[3]

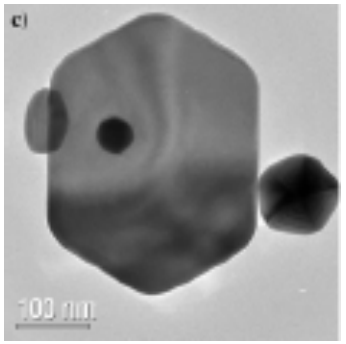

TEM image of particles sinthesized @ 190°C[3]

gold nanorods

Seed-mediated Growth in Solution

1. Chemical reduction of a metal salt with strong reducing agent ($NaBH_4$),
2. Use of a capping agent to prevent particle growth (citrate),
3. Addition of the seeds to a solution that contains more metal salt, a weak reducing agent (AA) and a rodlike micellar template (cetyltrimethylammonium bromide, CTAB).

Aspect ratio is controlled by the ratio of metal seed to metal salt.

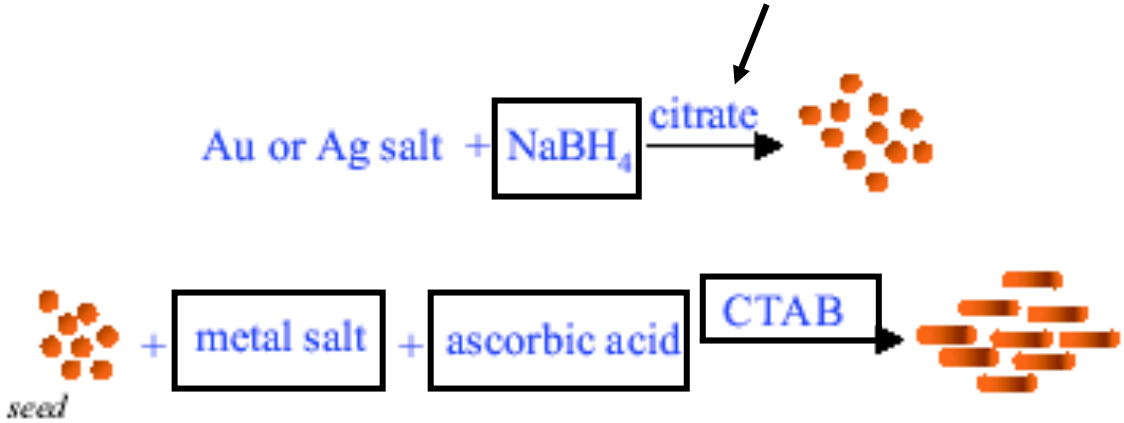

C.J.Murphy, N.R.Jana, *Adv.Mater.* 2002, 14 (80-82)

gold nanorods

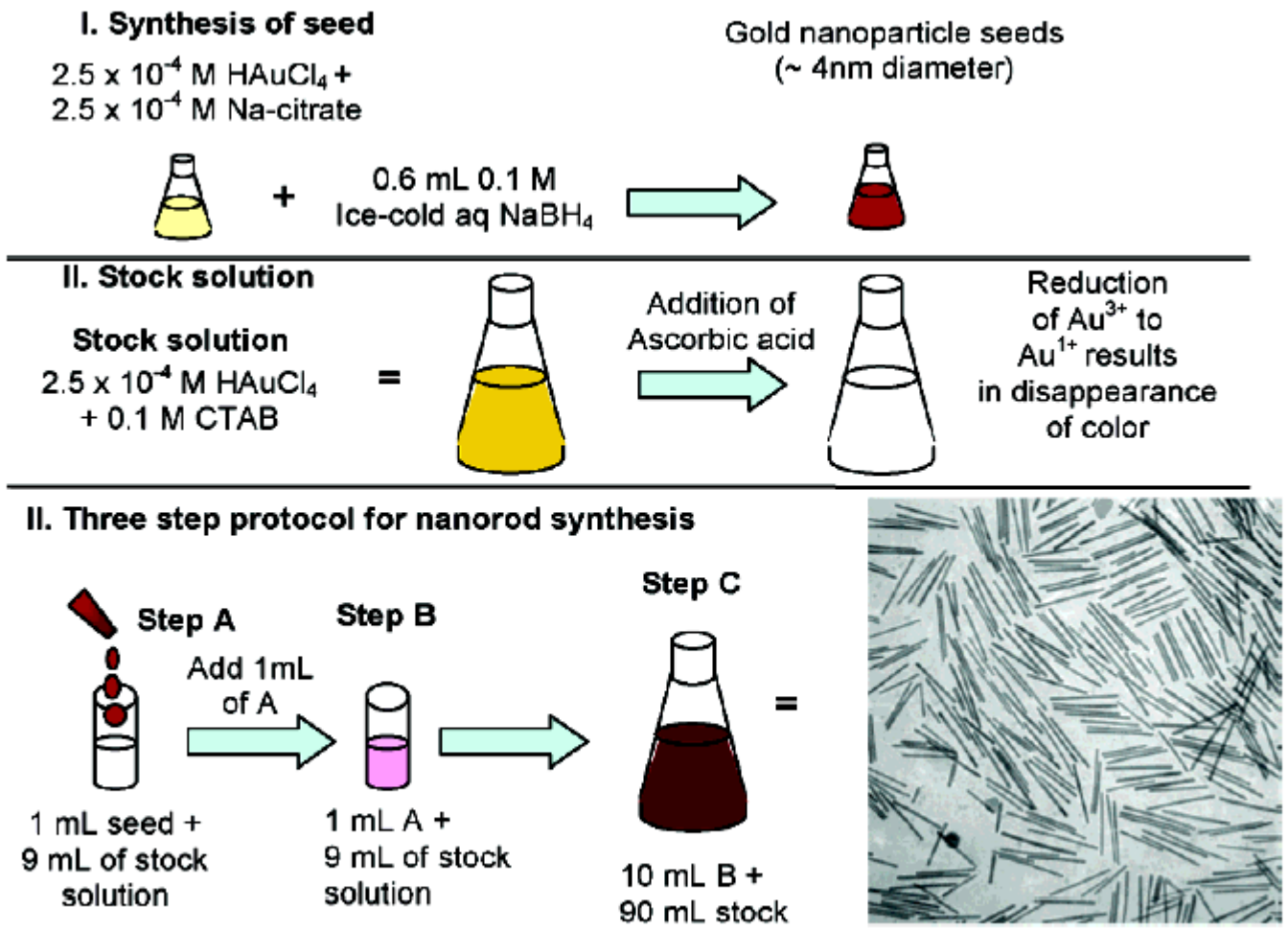

Figure 2. Seed-mediated growth approach to making gold and silver nanorods of controlled aspect ratio. The specific conditions shown here, for 20 mL volume of seed solution, lead to high-aspect ratio gold nanorods. (bottom right) Transmission electron micrograph of gold nanorods that are an average of 500 nm long.

Nikoobahkt and El-Sayed, *Chem. Mater.* **2003**, *15*, 1957;
Sau and Murphy, *Langmuir* **2004**, *20*, 6414.

gold nanorods

Influence of the reaction parameters

✓ Effect of the Seed Concentration

An **increase** in the **$[Au]_{seed}$ decreased** the **rod length** for a given concentration of Au^{3+}.

✓ Effect of AA concentration

The **rod length decreases** with an **increase in [AA]** keeping all other conditions the same.

✓ Effect of $AgNO_3$

When **silver nitrate** is **not used** nanorods are obtained in **low yield** and quite **long**.

✓ Effect of $[Au^{3+}]$

The **less** quantity of **Au^{3+} ions** per seed particle available the **short** are the nanorods.

✓ Effect of [CTAB]

Lower CTAB concentrations can lead to **non-rod-shaped** particles.

gold nanorods

Variation in the absorption of visible light

Short aspect ratio Au nanorods are especially interesting because of their optical properties: they exhibit tranverse and longitudinal plasmon bands.

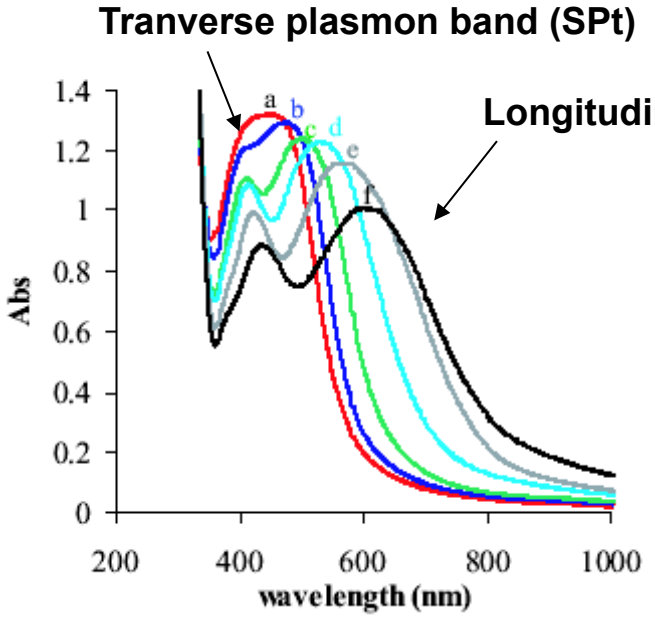

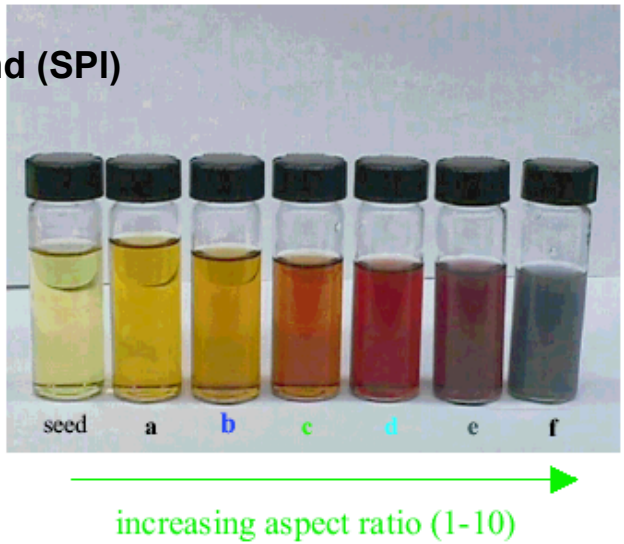

Aspect ratio: the length of the major axis divided by the width of the minor axis.

The larger the aspect ratio, the more red-shifted the longitudinal plasmon band.

gold nanorods

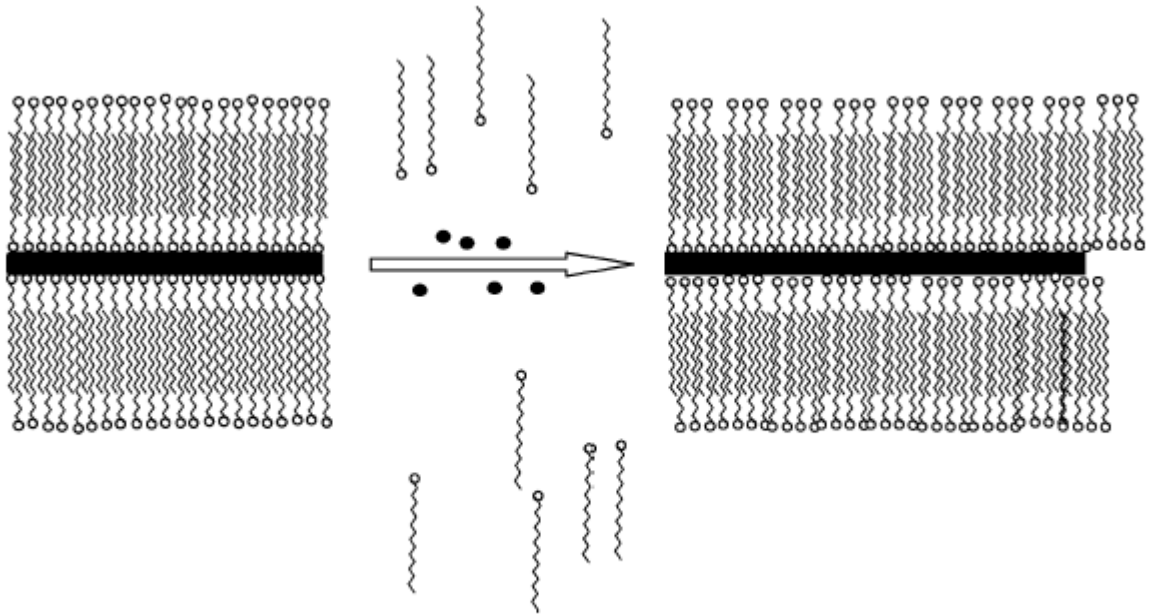

Figure 7. Cartoon illustrating "zipping": the formation of the bilayer of CnTAB (squiggles) on the nanorod (black rectangle) surface may assist nanorod formation as more gold ion (black dots) is introduced. Reproduced from ref 104 with permission.

gold nanorods

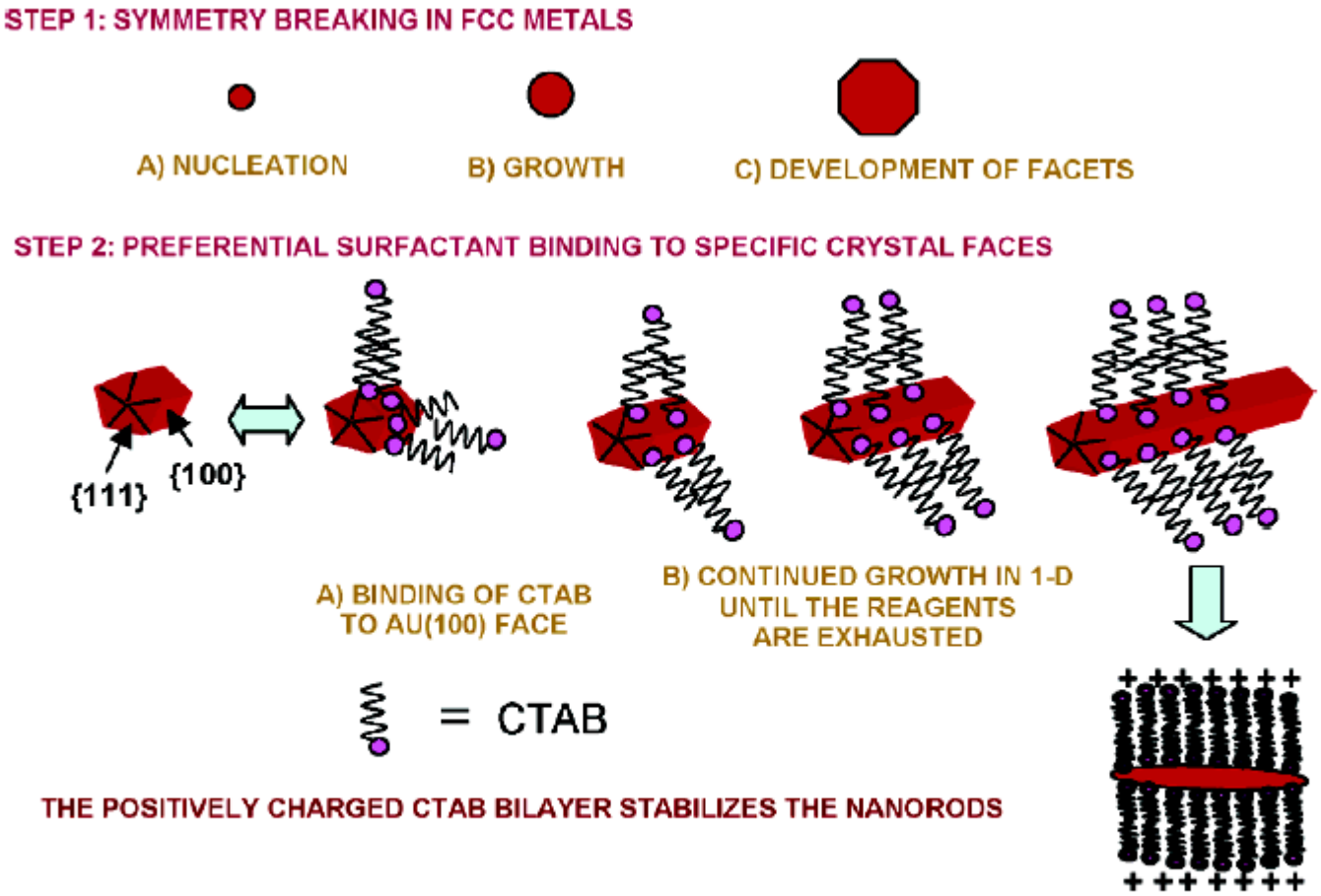

Figure 8. Proposed mechanism of surfactant-directed metal nanorod growth. The single crystalline seed particles have facets that are differentially blocked by surfactant (or an initial halide layer that then electrostatically attracts the cationic surfactant). Subsequent addition of metal ions and weak reducing agent lead to metallic growth at the exposed particle faces. In this example, the pentatetrahedral twin formation leads to Au {111} faces that are on the ends of the nanorods, leaving less stable faces of gold as the side faces, which are bound by the surfactant bilayer.

gold nanorods - functionalization

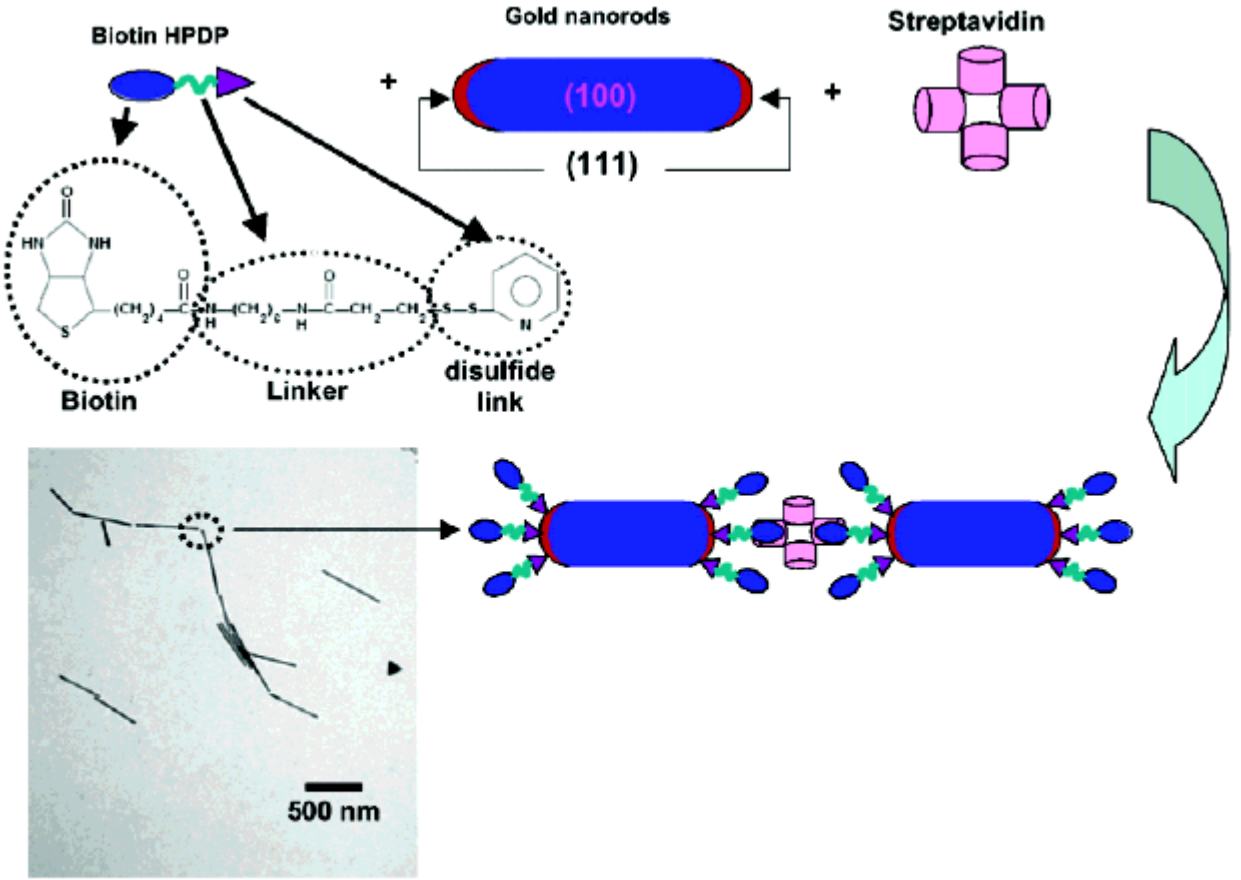

Figure 9. Cartoon of biotin-streptavidin assembly of gold nanorods; a biotin disulfide is added to biotinylate the rods, and subsequent addition of streptavidin causes noncovalent assembly. Inset: transmission electron micrograph of gold nanorod-streptavidin assemblies. The original data are from ref 86.

ANISOTROPIC METAL NANOPARTICLES

Branched structures: Tripods & Tetrapods

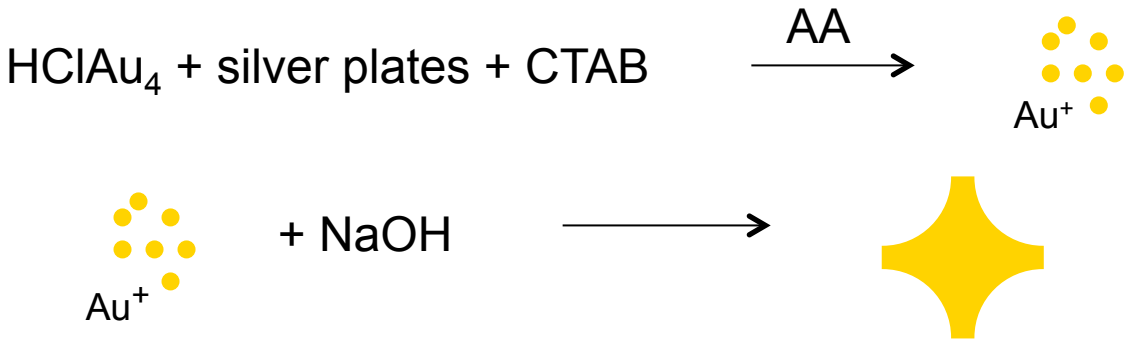

The forced reduction of gold by ascorbic acid through the addition of NaOH is the key step for particle branching.

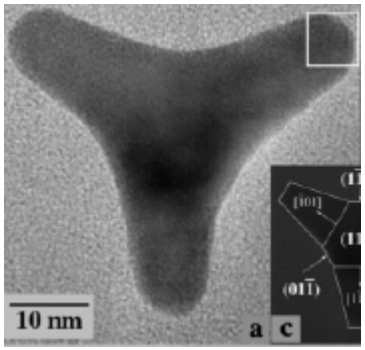

TEM image of a regular tripod nanocrystal

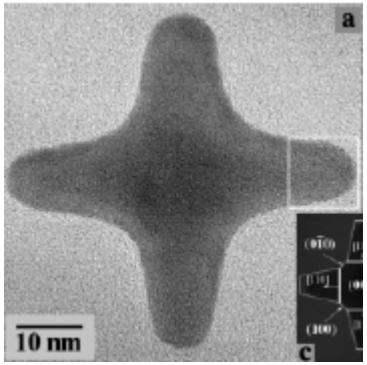

TEM image of a tetrapod nanocrystal

J.Am.Chem.Soc. 2003, 125, 16186-16187

ANISOTROPIC METAL NANOPARTICLES

From Ag nanocubes to Au nanoboxes

When Silver nanocubes are treated with a gold salt, an oxidation-reduction reaction ensues. In this reaction, the silver nanocubes serve as a sacrificial hard template to make hollow crystalline gold nanoboxes.

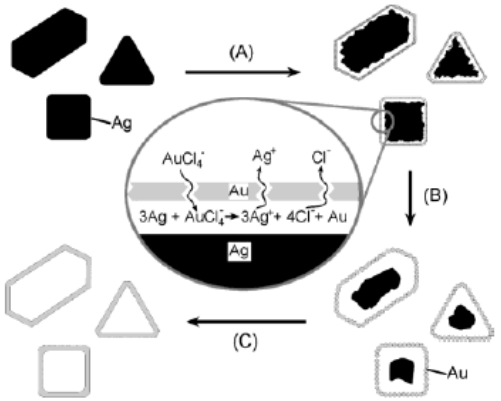

$$3\,Ag(s) + HAuCl_4(aq) \longrightarrow Au(s) + 3AgCl(aq) + HCl(aq)$$

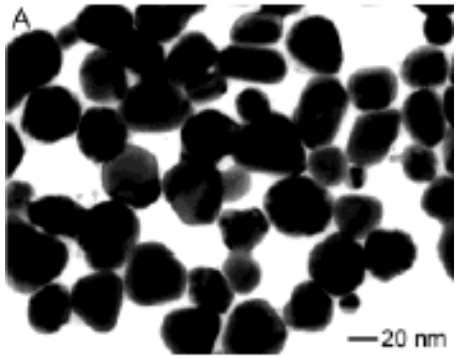

TEM image of silver nanoparticles synthesized using the polyol process.

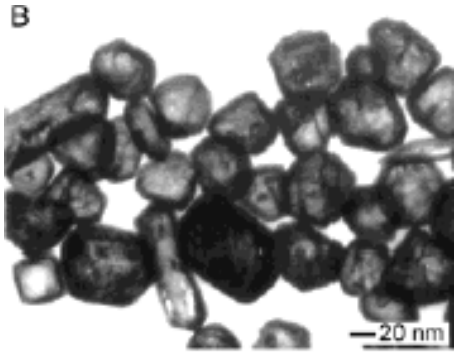

TEM image of gold nanoshells.

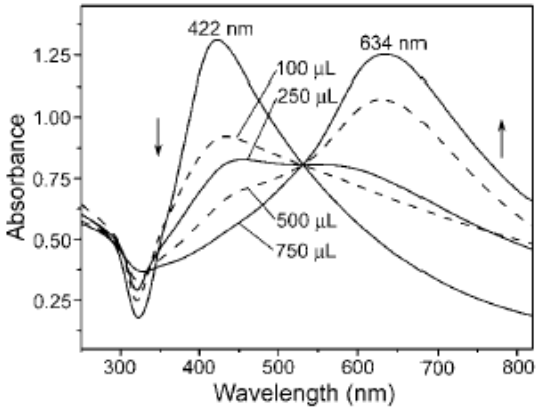

UV-vis absorption spectra of an aqueous dispersion of Ag nanoparticles.

Y. Sun, B.T. Mayers and Y. Xia, *Nano Letters,* 2, 481- 485

Au nanoboxes

By controlling the molar ratio between Ag and $HAuCl_4$, the gold nanocages could be tuned to display surface plasmon resonance peaks around 800 nm, a wavelength commonly used in optical coherence tomography (OCT) imaging.

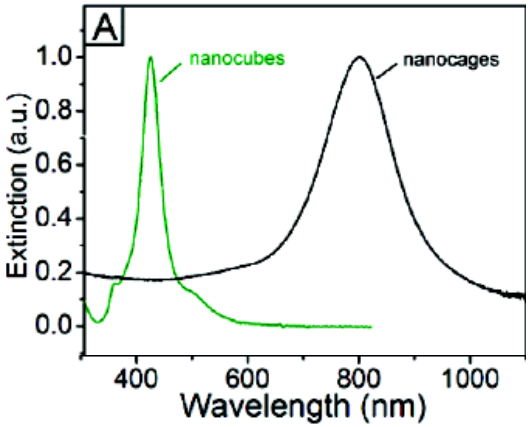

UV exctinction spectra recorded from solutions of Ag nanocubes and Au nanocages.

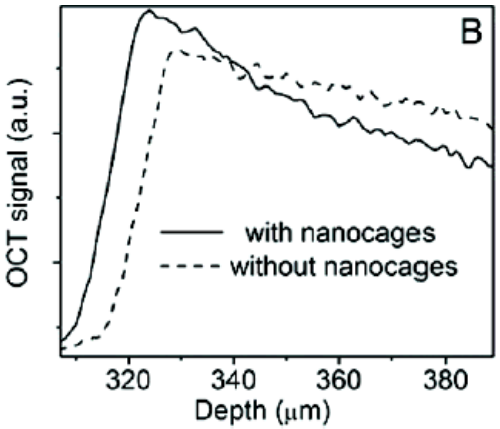

Plot of the OCT signals on a long scale as a function of depth.

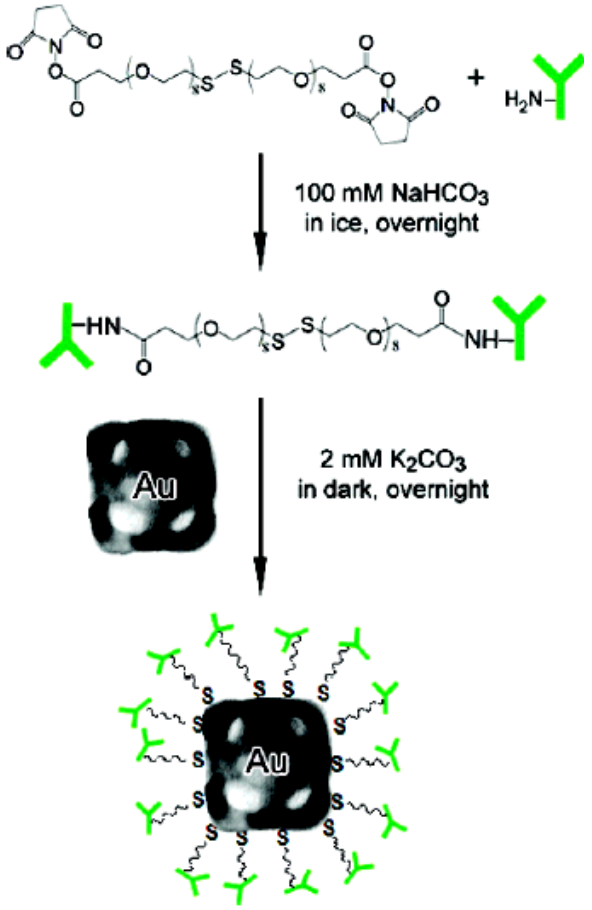

Gold nanocages functionalized with tumor-specific antibodies.

J.Chen, Y.Xia et al, *Nano Letters*, 2005, 5, 473-477.

Nanoparticles - Applications

- *NP for gene and drug delivery*
- *DNA sensing*
- *proteins sensing*
- *recognition and multivalency*
- *imaging*
- *enzyme mimiking*
- *new materials*

Nanoparticle-based Sensors

hydrogen bonds drive self-assembly

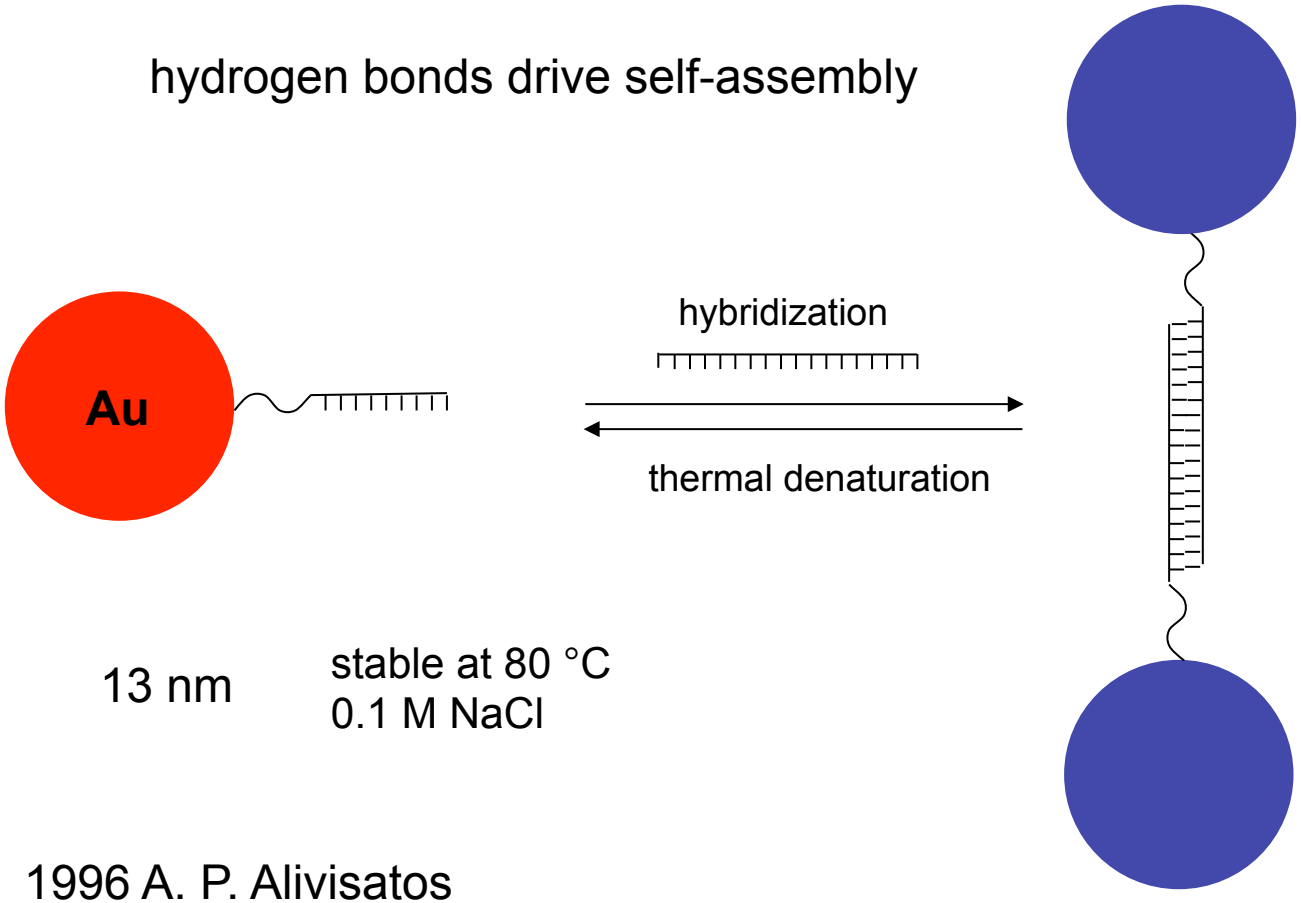

13 nm

stable at 80 °C
0.1 M NaCl

1996 A. P. Alivisatos
C. A. Mirkin

Mirkin, C. A.; Letsinger, R. L.; Mucic, R. C.; Storhoff, J. J. *Nature*, **1996**, *382*, 607-609.
Alivisatos, A. P.; Johnsson, K. P.; Peng, X.; Wilson, T. E.; Loweth, C. J.; Bruchez, M. P. Jr.; Schultz, P. G. *Nature*, **1996**, *382*, 609-611.

Nanoparticle-based Sensors

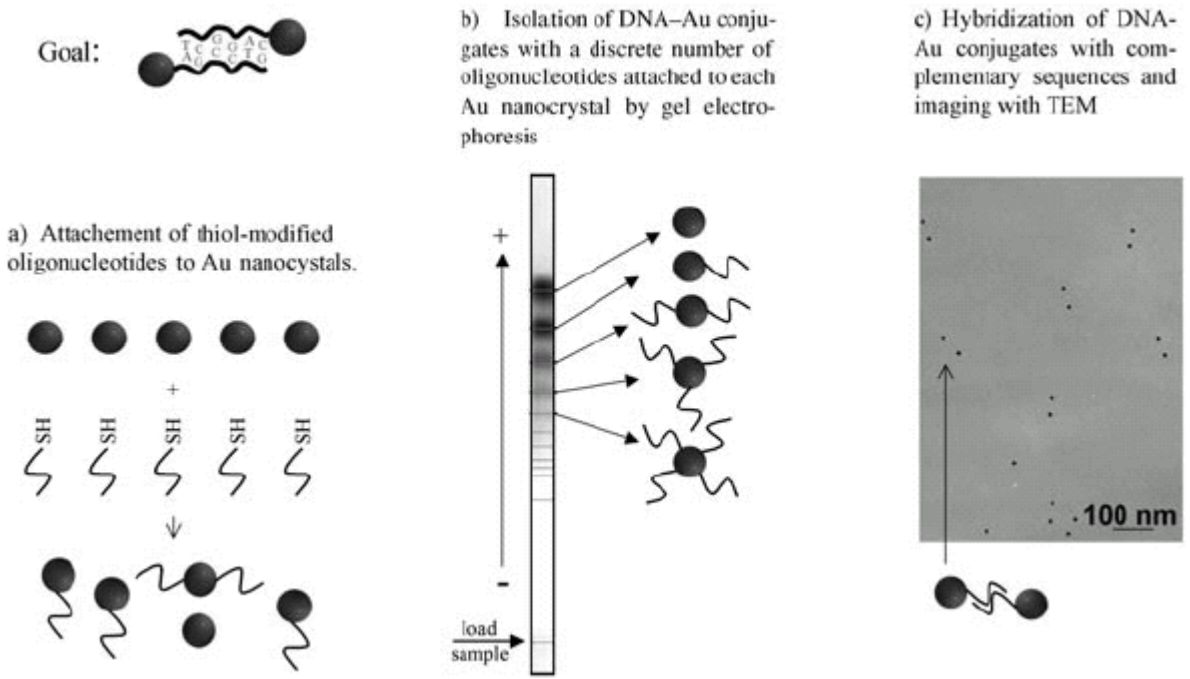

Figure 7. Forming DNA-meditated dimers of Au nanoparticles requires each nanoparticle to be functionalized with one oligonucleotide, with both oligonucleotides being complementary to each other. a) When phosphine- (or citric acid) stabilized Au nanoparticles and thiol-modified oligonucleotides react, DNA binds with its thiol group to the Au surface. However, even for 1:1 mixtures of DNA and Au, Au nanoparticles with more or less than one bound oligonucleotide will result; b) Au nanoparticles with a different number of DNA molecules bound per particle can be sorted by gel electrophoresis (image adapted from ref. [87]). Individual bands of nanoparticles with a discrete number of DNA molecules per particle can be observed and extracted from the gel; c) Au nanoparticles with one DNA molecule can be mixed with another solution of Au nanoparticles modified with a complementary DNA sequence. The single-stranded DNA molecules hybridize to a double strand, thus connecting the Au nanoparticles. The resulting dimers can be observed by TEM imaging (the Au-nanoparticle dimers shown comprise two 10-nm-diameter Au nanocrystals; the DNA molecules cannot be seen by TEM). Image courtesy of D. Zanchet et al.[7]

Alivisatos, A. P.; Johnsson, K. P.; Peng, X.; Wilson, T. E.; Loweth, C. J.; Bruchez, M. P. Jr.; Schultz, P. G. *Nature*, **1996**, *382*, 609-611.

Nanoparticle-based Sensors

selective colorimetric detection system for polynucleotides

thermal transition associated with the color change

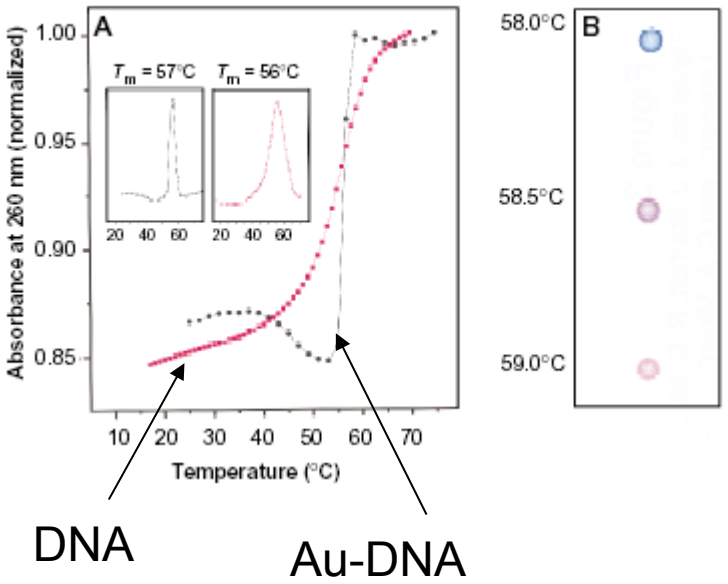

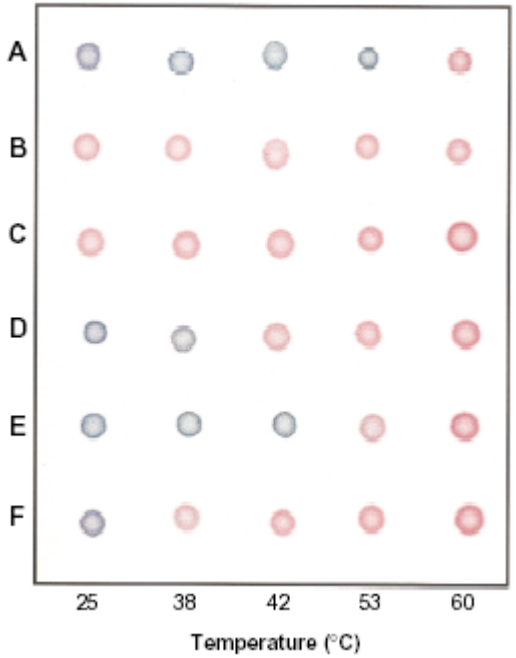

Selective polynucleotide detection for the target probes : (**A**) complementary target; (**B**) no target; (**C**) complementary to one probe; (**D**) a 6-bp deletion; (**E**) a 1-bp mismatch; and (**F**) a 2-bp mismatch. Nanoparticle aggregates were prepared in a 600-μl thin-walled Eppendorf tube by addition of 1 μl of a 6.6μM oligonucleotide target to a mixture containing 50 μl of each probe (0.06 μM final target concentration). The mixture was frozen (5 min) in a bath of dry ice and isopropyl alcohol and allowed to warm to room temperature. Samples were then transferred to a temperature controlled water bath, and 3-μl aliquots were removed at the indicated temperatures and spotted on a C_{18} reverse phase plate.

Elganian, R.; Storhoff, J.J.; Mucic, R. C.; Letsinger, R. L.; Mirkin, C. A. *Science* **1997**, *277*, 1078-1081.

Nanoparticle-based Sensors

selective colorimetric detection system for polynucleotides

λ_{max} 520 nm

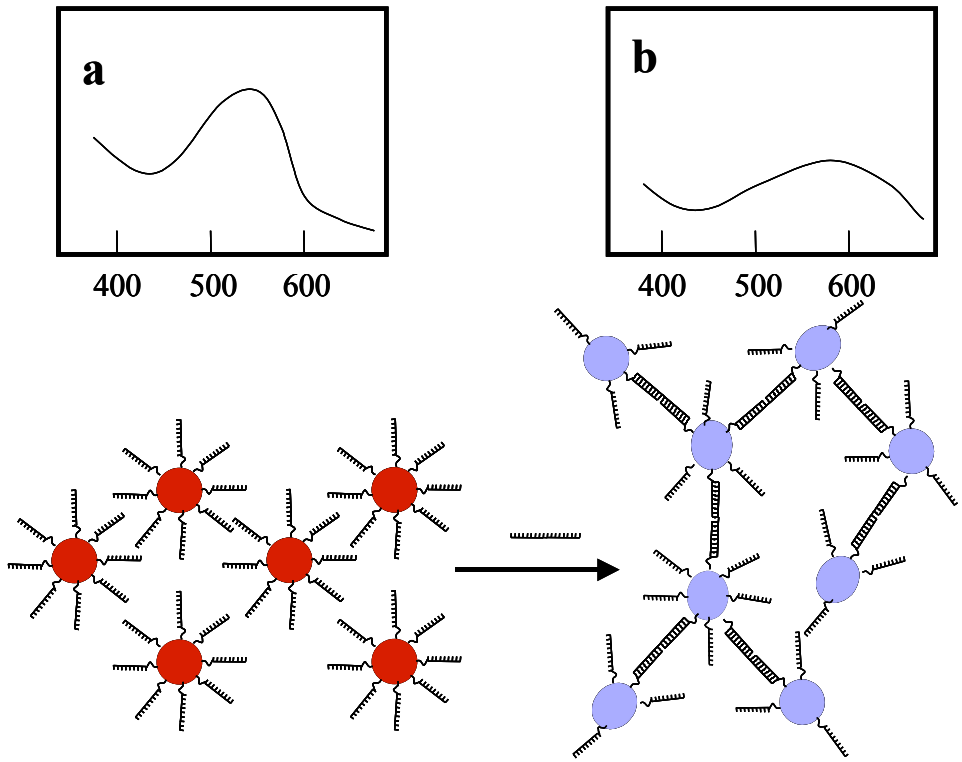

very sensitive: 10 femtomoles of polynucleotide could be detected

Elganian, R.; Storhoff, J.J.; Mucic, R. C.; Letsinger, R. L.; Mirkin, C. A. *Science* **1997**, *277*, 1078-1081.

Nanoparticle-based Sensors

scanometric DNA array detection

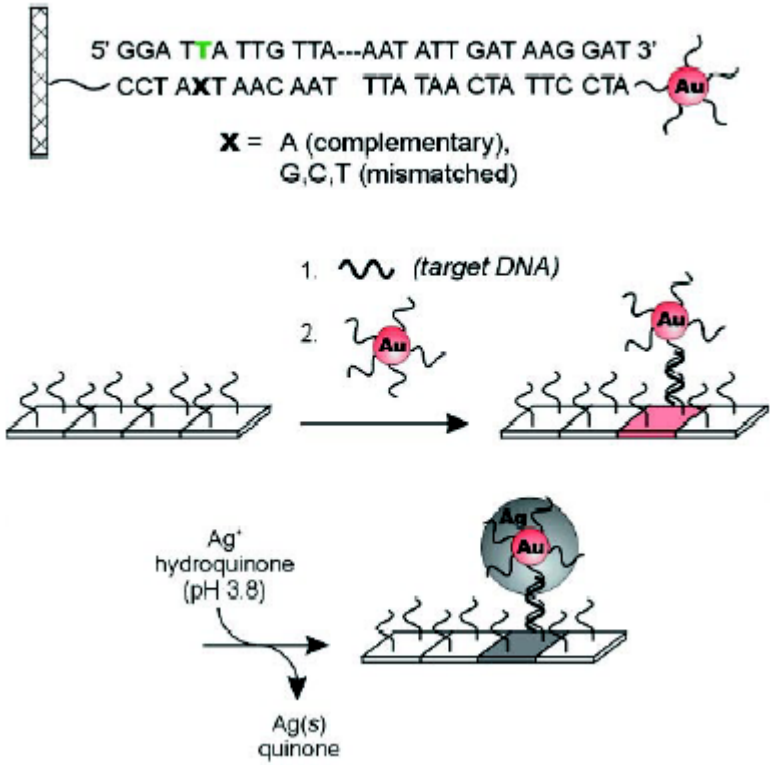

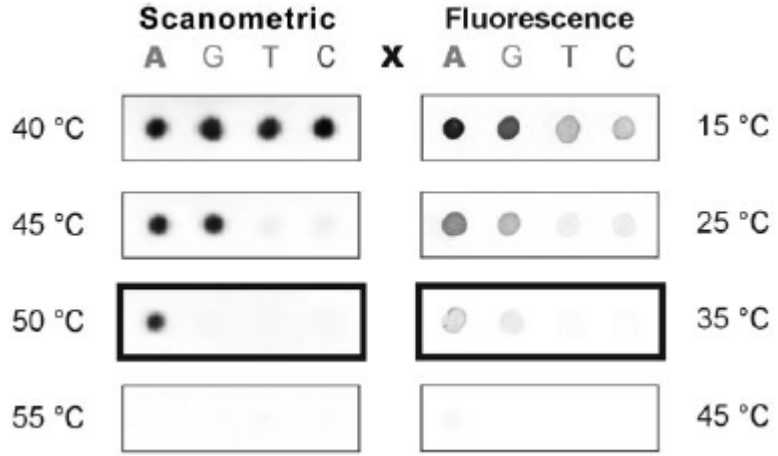

Taton, T. A.; Mirkin, C. A.; Letsinger, R. L. *Science* **2000**, *289*, 1757-1760.

Nanoparticle-based Sensors

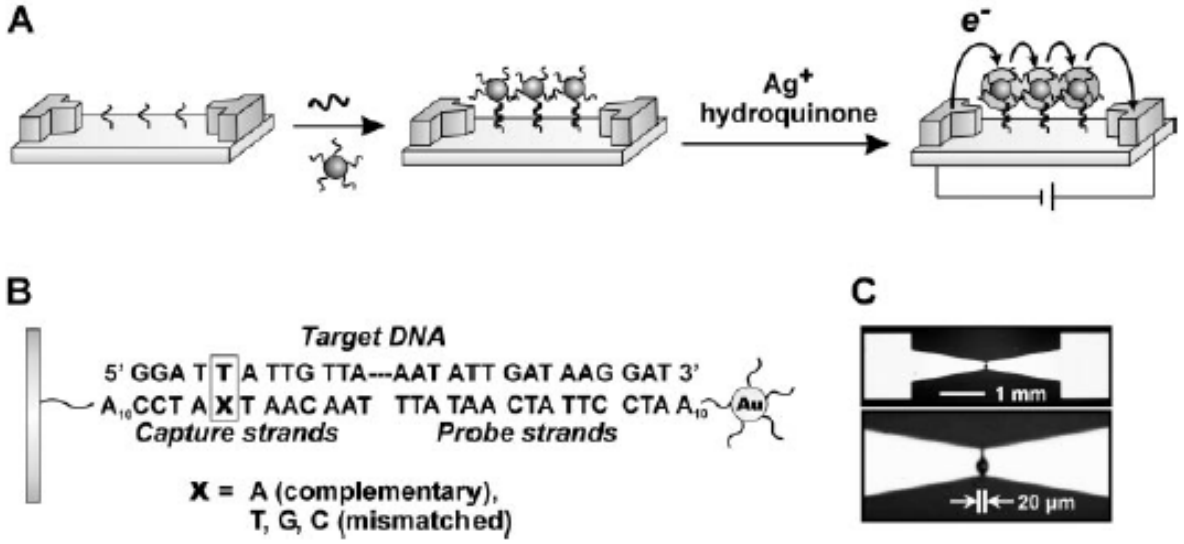

(**A**) Scheme showing concept behind electrical detection of DNA. (**B**) Sequences of capture, target, and probe DNA strands. (**C**) Optical microscope images of the electrodes used in a typical detection experiment. The spot in the electrode gap in the high-magnification image is food dye spotted by a robotic arrayer (GMS 417 Microarrayer, Genetic Microsystems, Woburn, MA).

target DNA was detected at concentrations as low as 500 femtomolar and with a point mutation selectivity factor of ~100,000:1

Park, S. J.; Taton, T. A.; Mirkin, C. A. *Science* **2002**, *295*, 1503-1506.

Gold nanoparticles-based protease assay

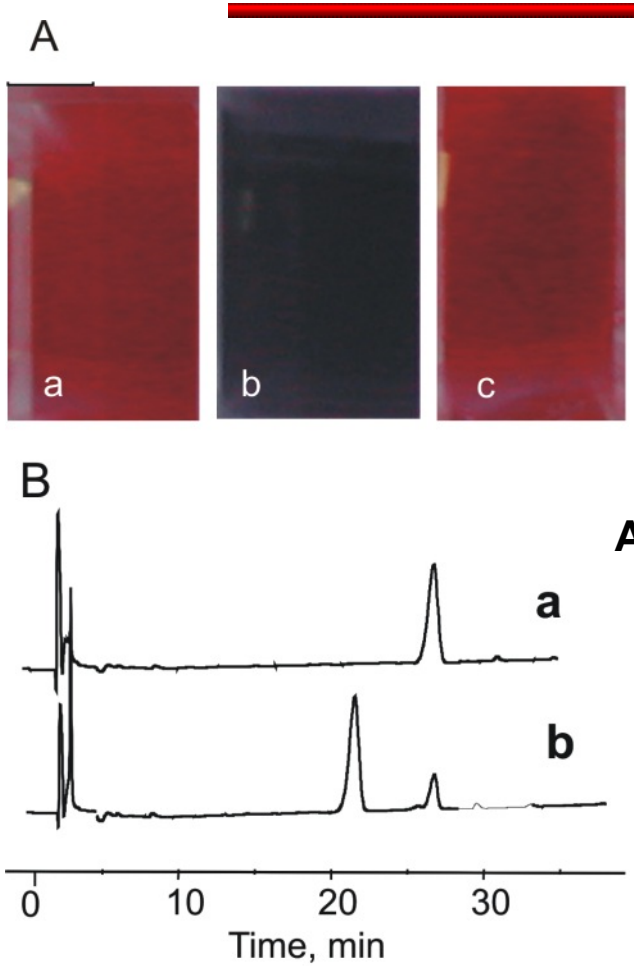

Ac-Cys(S-Ac)-Gly-DPhe-Pro-LArg-Gly-Cys(S-Ac)-OH, 1.

Ac-Cys(S-Ac)-Leu-Arg-Arg-Arg-Arg-Val-Tyr-Pro-Tyr-Pro- nor-Leu-Glu-Leu-Cys(S-Ac)-OH, 2.

Figure 1. A. Color of the gold colloids: (a) untreated solution; (b) 5 min after the addition of **1** ([**1**]=62 nM); (c) 5 min after the addition of **1** ([**1**]final=62 nM) incubated for 90 min with thrombin ([thrombin]=35 nM, [**1**]=62 μM). **B**. RP-HPLC chromatogram of the original peptide **1** (upper trace, a) and after exposition for 60 min to thrombin (lower trace, b). Conditions: [**1**]final=62 μM, [thrombin]= 30 nM, pH=8, 25°C. The peak at 21.5 min corresponds to the fragment Ac-Cys(S-Ac)-Gly-(D)Phe-Pro-Arg-OH.

C. Guarise, L. Pasquato, V. De Filippis, P. Scrimin, *Proc. Natl. Acad. Sci. U.S.A.*, **2006**, *103*, 3978-3982

Gold nanoparticles-based protease assay

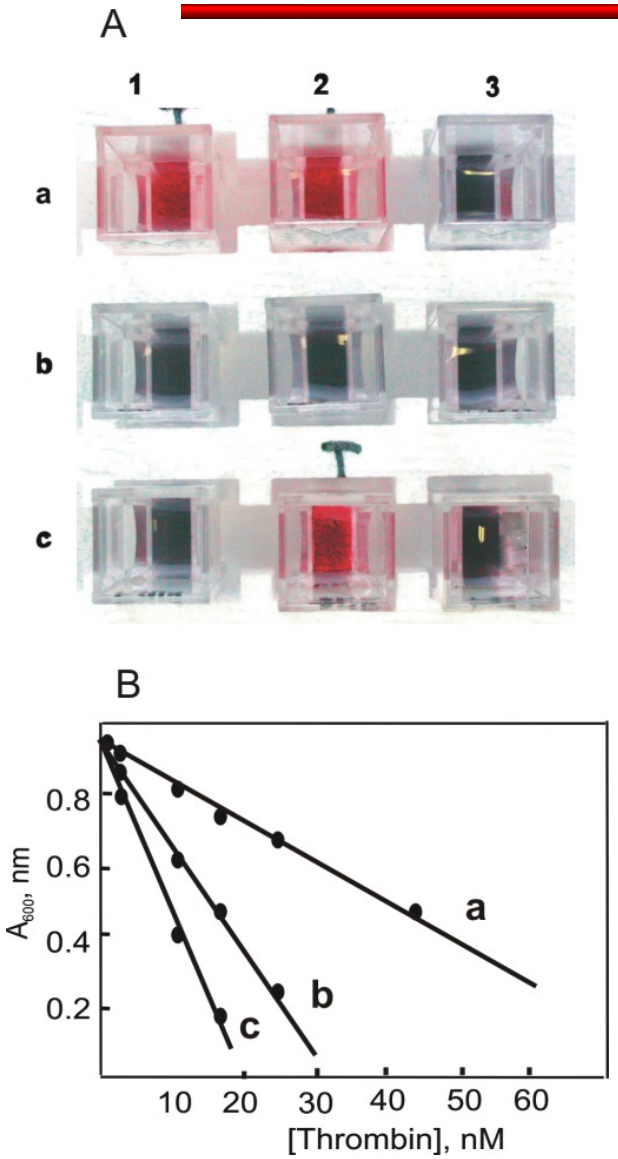

Fig. 3. Thrombin assay. (*A*) Colorimetric test for the presence of thrombin. Each cuvette contained the following enzymes: *a1*, chymotrypsin, plasmin, factor Xa, and thrombin; *a2*, chymotrypsin and thrombin; *a3*, chymotrypsin, plasmin, and factor Xa; *b1*, factor Xa and chymotrypsin; *b2*, chymotrypsin; *b3*, factor Xa; *c1*, none; *c2*, thrombin; *c3*, plasmin. (*B*) Absorbance at 600nmof the gold colloid solution after addition of a solution of peptide **1** ([**1**]final62 nM) exposed to different concentrations of thrombin for 30 min (line a), 60 min (line b), and 90 min (line c) at pH 8 and 25°C.

C. Guarise, L. Pasquato, V. De Filippis, P. Scrimin, *Proc. Natl. Acad. Sci. U.S.A.*, **2006**, *103*, 3978-3982

Gold nanoparticles-based protease assay

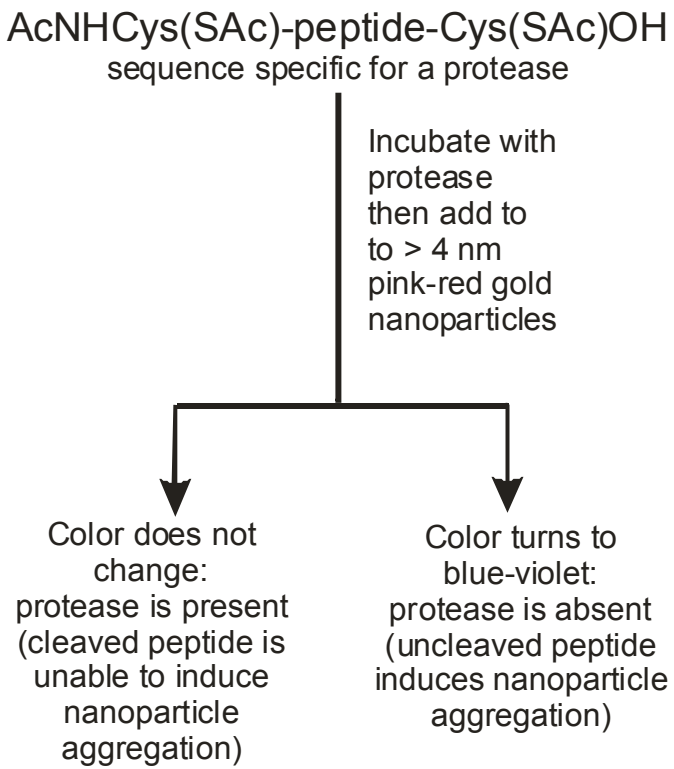

C. Guarise, L. Pasquato, V. De Filippis, P. Scrimin, *Proc. Natl. Acad. Sci. U.S.A.*, **2006**, *103*, 3978-3982

Hybrid Nanoparticle−Liposome Detection of Phospholipase Activity

Daniel Aili†, Morgan Mager†, David Roche and Molly M. Stevens
Nano Letters 2010

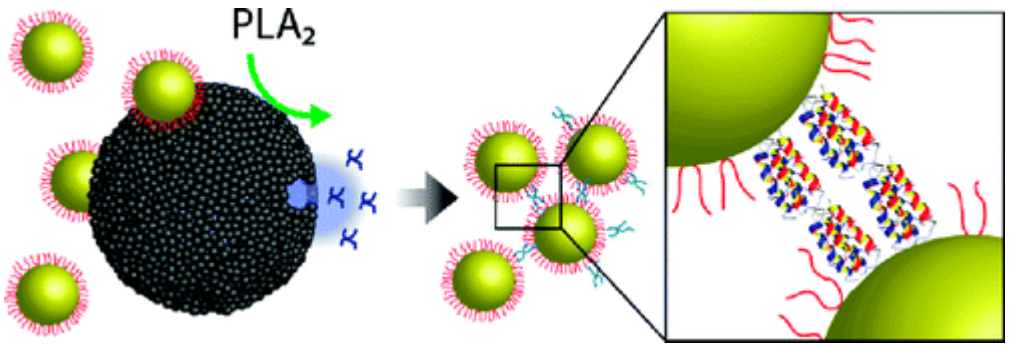

A flexible nanoparticle-based phospholipase (PL) assay is demonstrated in which the enzymatic substrate is decoupled from the nanoparticle surface. Liposomes are loaded with a polypeptide that is designed to heteroassociate with a second polypeptide immobilized on gold nanoparticles. Release of this polypeptide from the liposomes, triggered by PL, induces a folding-dependent nanoparticle bridging aggregation. The colorimetric response from this aggregation enables straightforward and continuous detection of PL in the picomolar range. The speed, specificity, and flexibility of this assay make it appropriate for a range of applications, from point of care diagnostics to high-throughput pharmaceutical screening.

A nanoplasmonic molecular ruler for measuring nuclease activity and DNA footprinting

G. L. LIU, Y. YIN, S. KUNCHAKARRA, B. MUKHERJEE, D. GERION,
S. D. JETT, D. G. BEAR, J. W. GRAY, A. P. ALIVISATOS, L. P. LEE1, F. F.CHEN
nature nanotechnology **2006**, *1*, 47

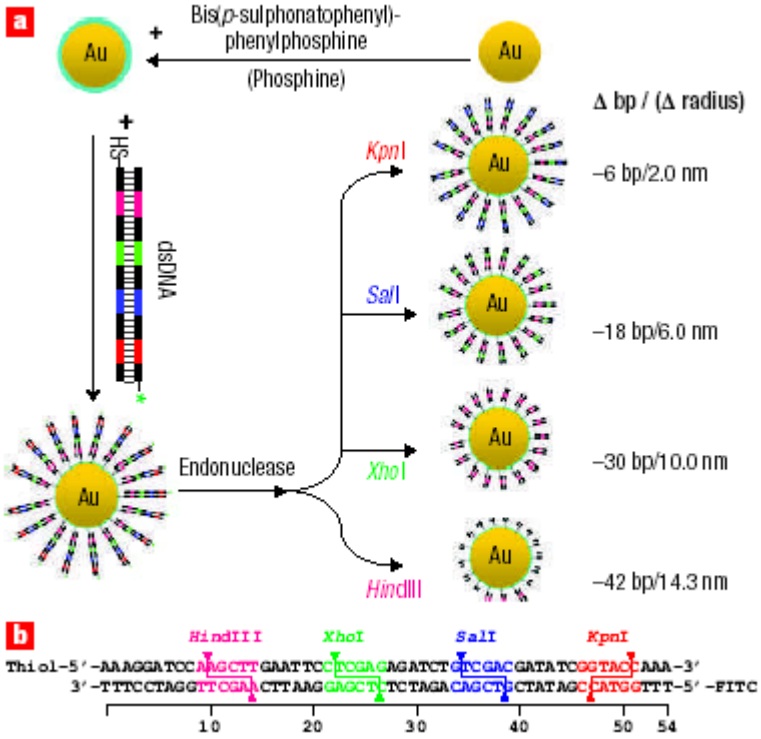

Figure 1. Design of the Au–DNA nanoplasmonic molecular ruler. a, Synthesis process of the Au–DNA nanoconjugate. The 20-nm Au nanoparticle modified with a phosphine surfactant monolayer was enclosed by a layer of synthesized 54-bp dsDNA. A thiol group and the FITC (fluorescein isothiocyanate) fluorophore (as indicated by green star) were synthesized at each end of the dsDNA, respectively. Through the thiol–Au chemistry, the dsDNA was tethered onto the Au nanoparticles. b, The dsDNA contains endonuclease incision sites positioned at 12, 24, 36 and 48 bp from the Au-nanoparticle-tethered end. The fluorescent labelling (FITC) is only for further confirmation of the nuclease reactions, and is not necessary for plasmon resonance measurements.

Organization of simple sub-units in complex structures

…the tools available in supramolecular chemistry

multivalency

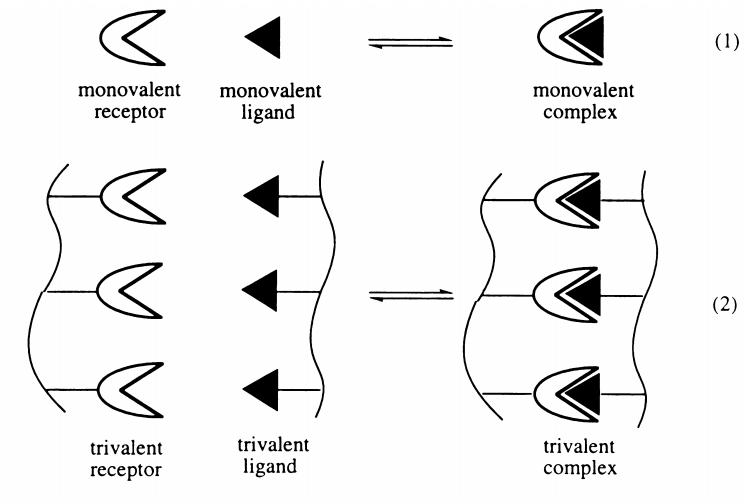

recognition

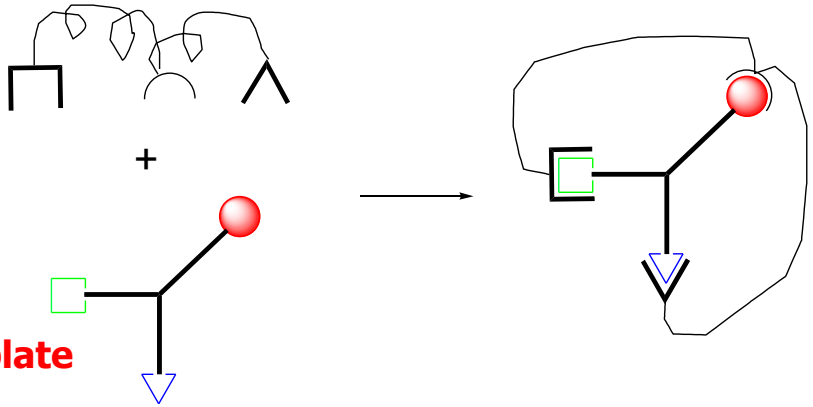

Interactions between groups spatially closed

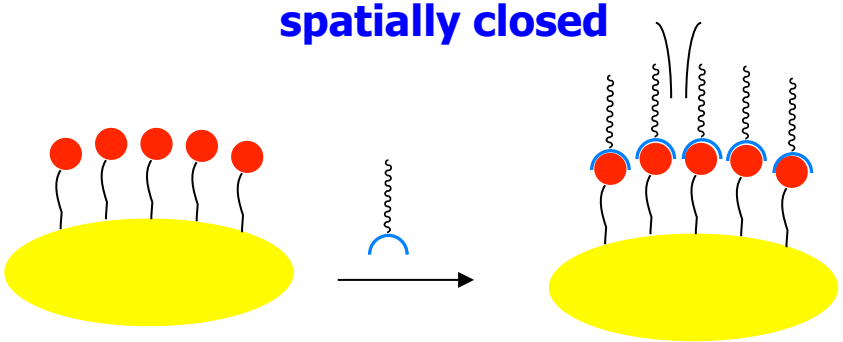

catalytic activity of MPC-C12-TEG-C12-P2-H

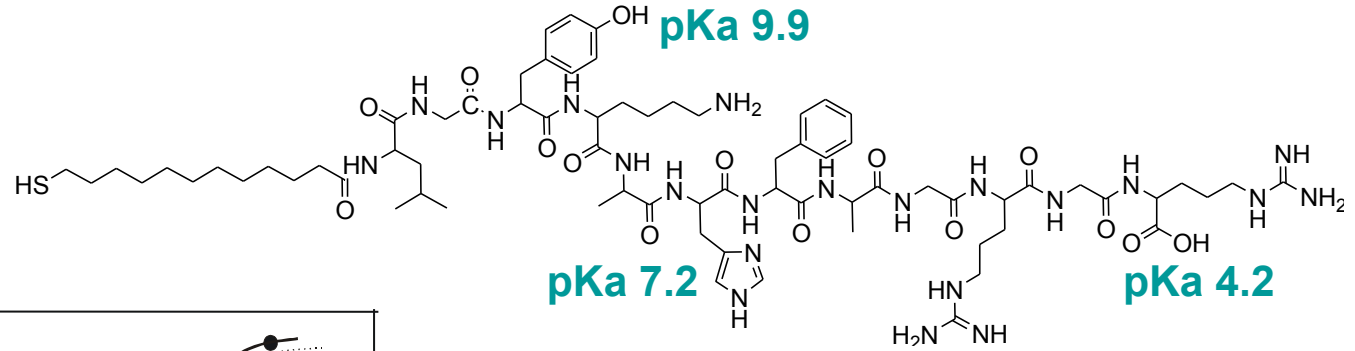

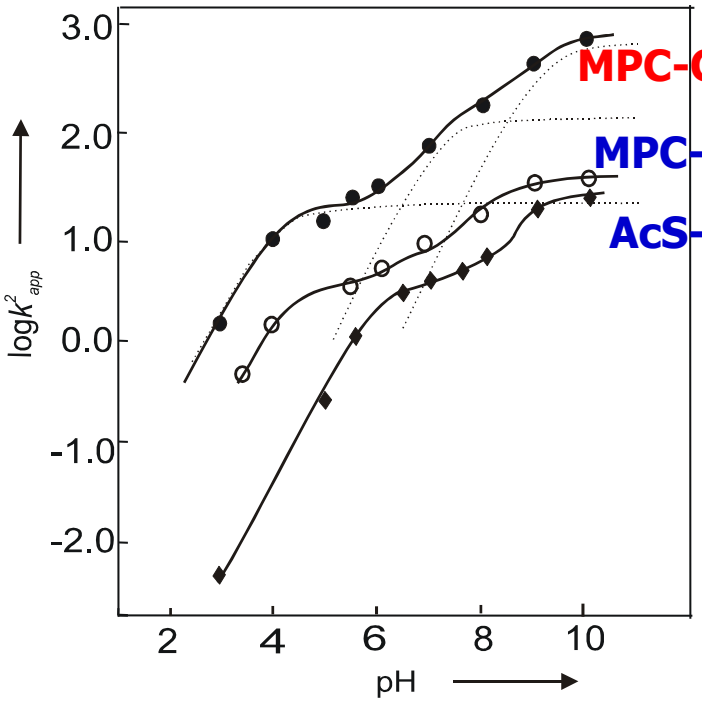

MPC-C12-TEG-C12-P2-H

MPC-C12-TEG-HFOH

AcS-C12-P2-H

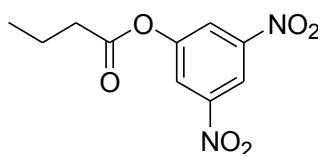

DNPB

cat.

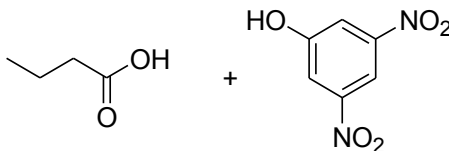

3000-fold rate acceleration (over Ac-C12-HFOH)
500-fold acceleration (over AcS-C12-P2-H)

Log of the apparent second order rate constant against pH for the hydrolysis of DNPB catalyzed by nanoparticles Au-PEP (●) nanoparticles Au-**2** (○), and *S*-acetylated peptide **1** (♦). The solid lines represent the best fits of functions describing the dissociation of residues involved in catalysis with p*K*a values of 4.2, 7.2 and 9.9, in the case of Au-PEP, 4.2 and 8.1 for Au-**2**, and 6.1 and 9.2 for *S*-acetylated **1**. The dotted lines represent the calculated contribution of each species to the solid curve for Au-PEP. Conditions: [catalyst]=4.0×10^{-5} M, [buffer]=10-20 mM, 25°C.

Pengo, P.; Baltzer, L.; Pasquato, L.; Scrimin, P. *Angew. Chem. Int. Ed.* **2007**, *46*, 400-404.

catalytic activity of MPC-C8-TEG-C12-P2-H

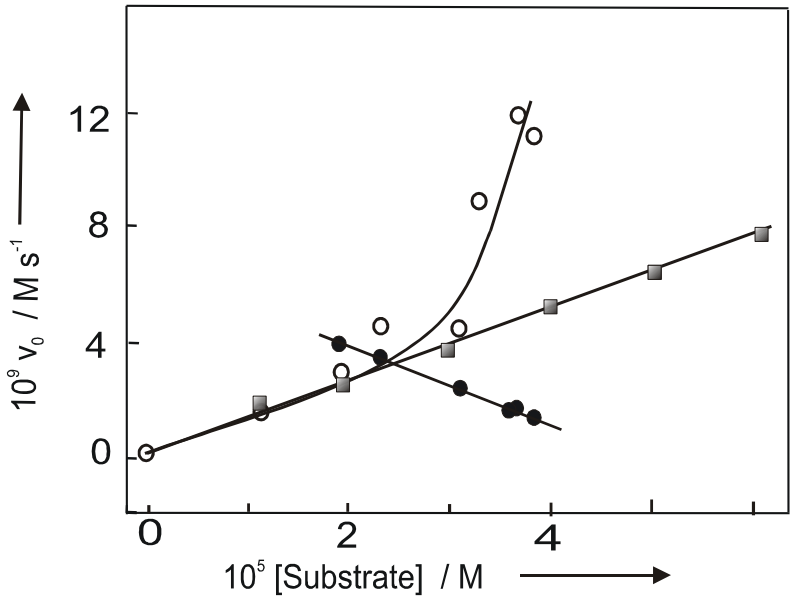

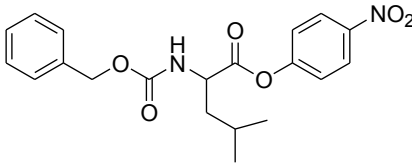

Z-(L)-Leu-ONp

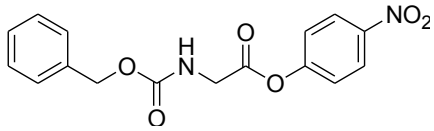

Z-Gly-ONp

DNPB behaves as Z-Gly-ONp

Figure 2. Dependence of the initial rate (M s^{-1}) of intermediate formation (○) and its hydrolysis (●) with Z-Leu-PNP and that of hydrolysis (■) with Z-Gly-PNP upon substrate concentration. Conditions: [**S-C12-P2-OH**]=1.3×10^{-5} M (bound to Au-PEP), pH 7, 25°C.

$$\text{Cat} + \text{S} \underset{k_-}{\overset{k_+}{\rightleftharpoons}} \text{Cat-S} \xrightarrow{k_{cat}} \text{Cat-S'} + \text{P1} \xrightarrow{k_2} \text{Cat} + \text{P2}$$

serine-proteases like

Pengo, P.; Baltzer, L.; Pasquato, L.; Scrimin, P. *Angew. Chem. Int. Ed.* **2007**, *46*, 400-404.

Detection and identification of proteins using nanoparticle–fluorescent polymer ‘chemical nose’ sensors

C.-C. YOU, O. R. MIRANDA, B. GIDER1, P. S. GHOSH, I.-B. KIM,
B. ERDOGAN1, S. A. KROVI, U. H. F. BUNZ, VINCENT M. ROTELLO
nature nanotechnology VOL 2 |MAY 2007 , page 318

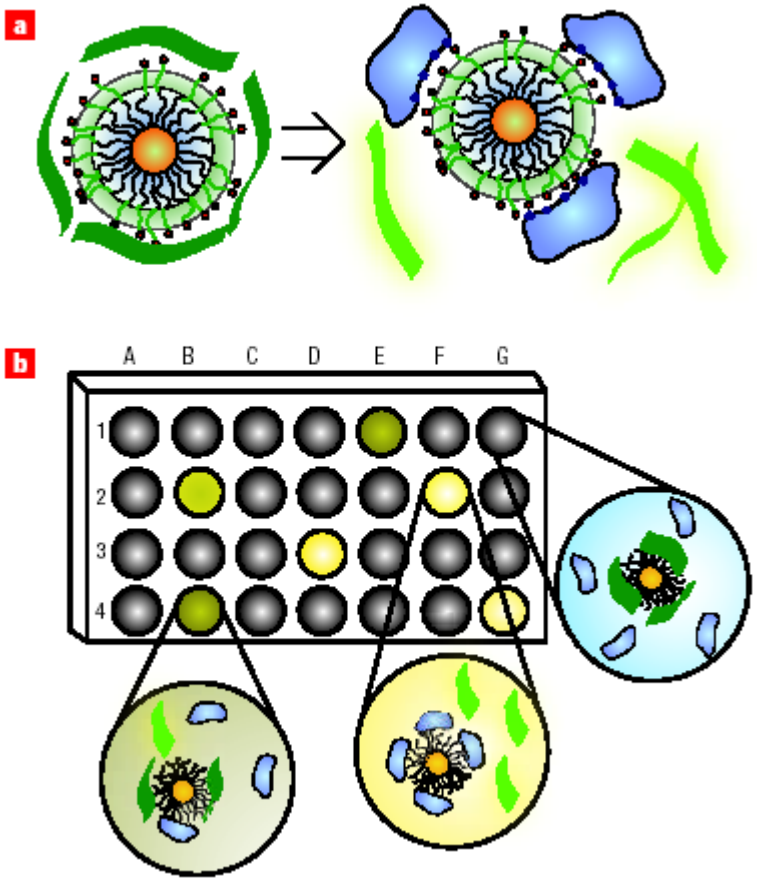

Figure 1 Fluorophore displacement protein sensor array. a, Displacement of quenched fluorescent polymer (dark green strips, fluorescence off; light green strips, fluorescence on) by protein analyte (in blue) with concomitant restoration of fluorescence. The particle monolayers feature a hydrophobic core for stability, an oligo(ethylene glycol) layer for biocompatibility, and surface charged residues for interaction with proteins. **b**, Fluorescence pattern generation through differential release of fluorescent polymers from gold nanoparticles. The wells on the microplate contain different nanoparticle–polymer conjugates, and the addition of protein analytes produces a fingerprint for a given protein.

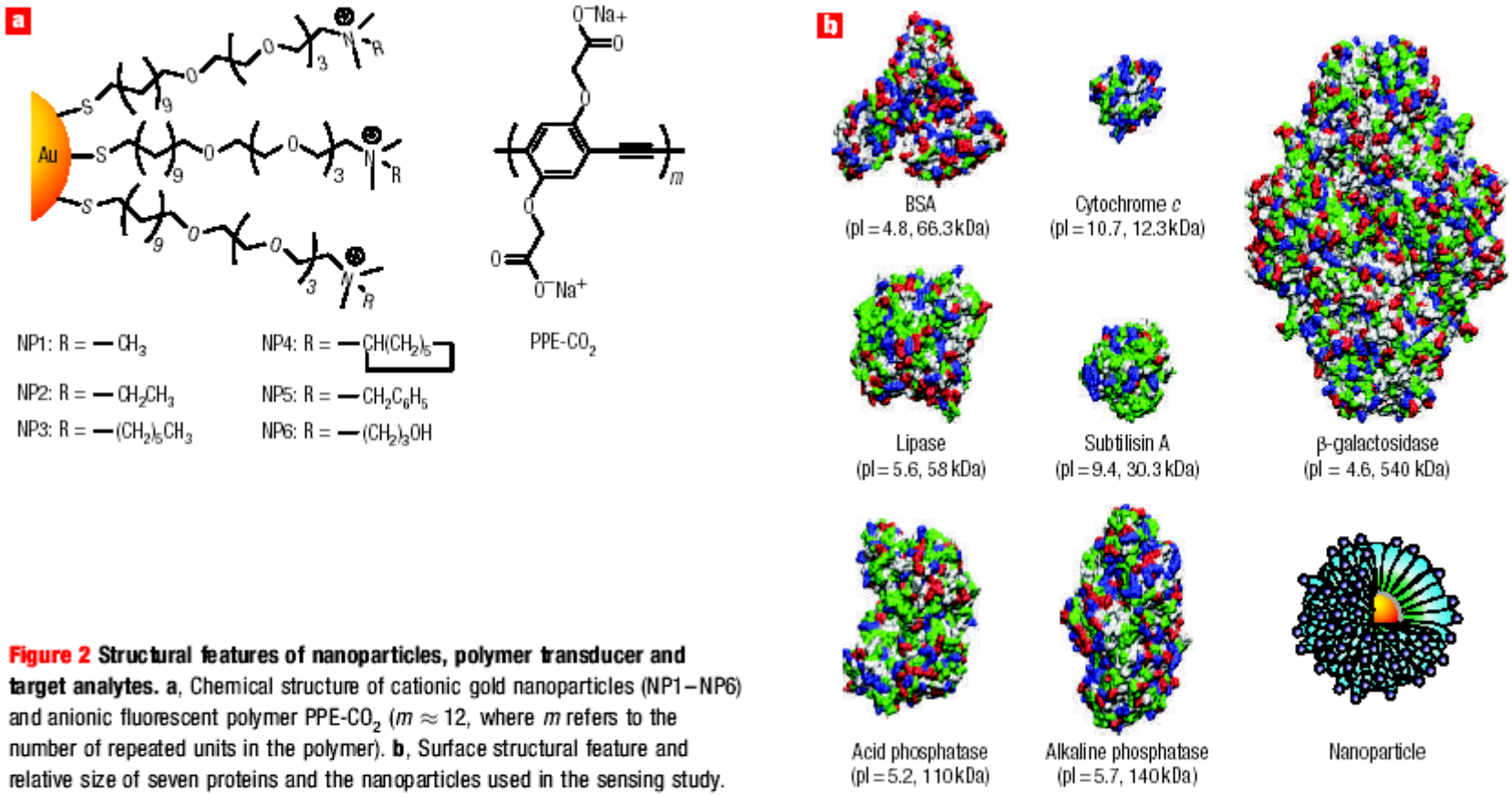

Figure 2 Structural features of nanoparticles, polymer transducer and target analytes. a, Chemical structure of cationic gold nanoparticles (NP1–NP6) and anionic fluorescent polymer PPE-CO_2 ($m \approx 12$, where m refers to the number of repeated units in the polymer). **b**, Surface structural feature and relative size of seven proteins and the nanoparticles used in the sensing study. Colour scheme for the proteins: nonpolar residues (grey), basic residues (blue), acidic residues (red) and polar residues (green).

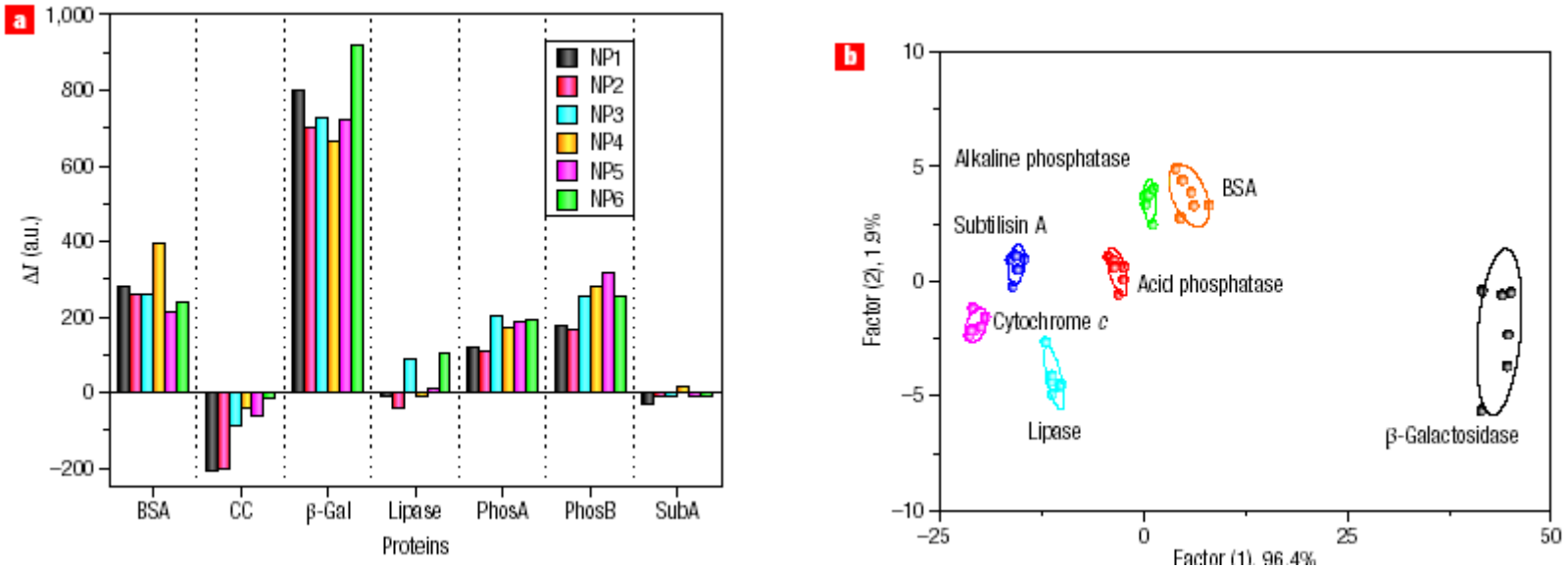

Figure 4 Array-based sensing of protein analytes at 5 μM. a, Fluorescence response (ΔI) patterns of the NP–PPE sensor array (NP1–NP6) against various proteins (CC, cytochrome *c*; β-Gal, β-galactosidase; PhosA, acid phosphatase; PhosB, alkaline phosphatase; SubA, subtilisin A). Each value is an average of six parallel measurements. **b**, Canonical score plot for the first two factors of simplified fluorescence response patterns obtained with NP–PPE assembly arrays against 5 μM proteins. The canonical scores were calculated by LDA for the identification of seven proteins. The 95% confidence ellipses for the individual proteins are also shown.

LDA = linear discriminant analysis

photothermal therapy

travel as far through living tissue as a magnetic field can. "We wanted something that

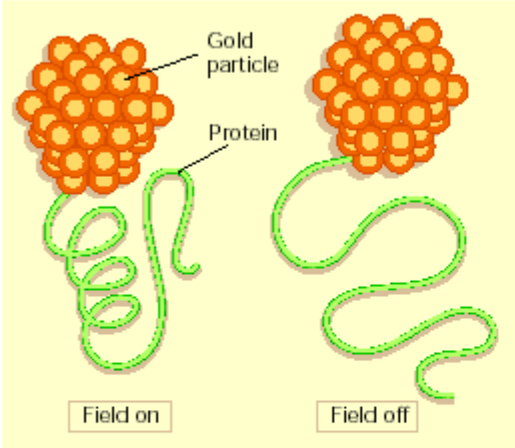

Kimberly Hamad-Schifferli (right) hopes to control proteins by attaching tiny gold particles to them — in a radio field the particle heats up, altering the protein's structure and inactivating it.

'nano' word is over-used and over-hyped," says John Ryan, director of the Nanobiotech-

paced activities of daily life in the cell. And for those in the nanosystems alliance, nanotechnology is the best way to get a grip on the many fleeting processes involved. Alliance member Leroy Hood, a molecular biologist at the Institute for Systems Biology in Seattle, predicts that nanotechnology will reveal as much new information about the cell as did the automated DNA sequencer — a device that he invented. "The combination of microfluidics and nanotechnology," Hood asserts, "will transform how biologists do everything." ■

Catherine Zandonella is a freelance writer in New York.

1. Melosh, N. A. *et al. Science* **300**, 112–115 (2003).
2. Vo-Dinh, T. *J. Cell. Biochem.* **87**, 154–161 (2002).
3. Klarreich, E. *Nature* **413**, 450–452 (2001).
4. Quintana, A. *et al. Pharm. Res.* **19**, 1310–1316 (2002).
5. Hamad-Schifferli, K., Schwartz, J. J., Santos, A. T., Zhang, S. & Jacobson J. M. *Nature* **415**, 152–155 (2002).

Alliance for NanoSystems Biology

www.nanosysbio.org